2010

# Evaluation of Upper Motor Neuron Pathology in Amyotrophic Lateral Sclerosis by Mri;Towards Identifying Noninvasive Biomarkers of the Disease

Venkateswaran Rajagopalan
*Cleveland State University*

# EVALUATION OF UPPER MOTOR NEURON PATHOLOGY IN AMYOTROPHIC LATERAL SCLEROSIS BY MRI: TOWARDS IDENTIFYING NONINVASIVE BIOMARKERS OF THE DISEASE

VENKATESWARAN RAJAGOPALAN

Bachelor of Engineering in Electrical and Electronics Engineering

RVS College of Engineering and Technology

May 2000

Master of Science in Biomedical Engineering

Indian Institute of Technology Madras

June 2003

Submitted in partial fulfillment of requirements for the degree

DOCTOR OF ENGINEERING IN APPLIED BIOMEDICAL ENGINEERING

at the

CLEVELAND STATE UNIVERSITY

July 2010

This Thesis has been approved
for the Department of CHEMICAL AND BIOMEDICAL ENGINEERING
and the College of Graduate Studies by

Thesis/Dissertation Chairperson, Guang H Yue

Department & Date

Erik P Pioro

Department & Date

George P. Chatzimavroudis

Department & Date

Randolph Setser

Department & Date

Andrew B Slifkin

Department & Date

This dissertation is dedicated in loving memory of my grandmother
Smt. Narayani

## ACKNOWLEDGEMENTS

I would like to express my sincere thanks and gratitude to all those who have associated themselves with my research studies, aided me in my investigations, offered their valuable suggestions and made this dissertation possible.

I would like to express my sincere thanks and gratitude to Dr. Erik P Pioro and Dr. Guang H Yue, my advisors for first introducing me into this work and motivating me during difficulties and enabling me to a perfect finish. Their pleasant nature and carefree attitude put me at ease and I was able to discuss even my wildest ideas with them, which has proved to be useful in the long run. I would like to express my sincere thanks and gratitude to Dr. Erik P. Pioro for sparing his valuable time and readiness for discussing the problem and results at any time despite his busy clinical appointments. His enlightening discussions and thought provoking suggestions helped me to provide a definite form to thesis.

I would like to express my sincere thanks and gratitude to Dr. Jacqueline Chen, Dr. Mark J Lowe for their suggestions and help during the course of the research.

I would like to express my sincere thanks and gratitude to Dr. George P Chatzimavroudis, Dr. Randolph Setser and Dr. Andrew B Slifkin my thesis committee members for advice and constructive criticism during the review of the progress of research.

My sincere and deepest thanks to two wonderful people Ms Becky Laird and Ms Darlene Montgomery in Chemical and Biomedical Engineering Department at CSU for their support and who took care of all my problems thereby, enabling me to concentrate

on my research.

I would like to take this opportunity to express my sincere thanks and gratitude to all my teachers from kindergarden till PhD especially Prof. Sivaramakrishnan, Mr. Murugan, Mr. Balaji Prasad, Dr. Venkatesh Balasubramaniam, Mrs. Amudha and Dr. Pioro and Dr.Yue who not only supported and motivated me but also were an inspiration to me.

My thanks to Dr.Vlodek in CCF and my lab mates, Vinoth, Luduan, Tina, Tony, Alex, Mehmed and Yin for providing nice working atmosphere.

Many thanks to my friends Didier, Phanikiran, Dr. Anup, Vijayamohan, Prasath, Ellie, Serge, Shiva,Sonal, Amit, Pinaki, Navneeth, Ganesh, Bharat and Atul for their support and sharing many lighter moments.

I would be failing on my part if I do not acknowledge the love, affection, encouragement inspiration and moral support given by my parents, grandmother, sister and other family members who have been behind me in all stages of my life and are the sole reason for my achievements.

EVALUATION OF UPPER MOTOR NEURON PATHOLOGY IN AMYOTROPHIC LATERAL SCLEROSIS BY MRI: TOWARDS IDENTIFYING NONINVASIVE BIOMARKERS OF THE DISEASE

VENKATESWARAN RAJAGOPALAN

## ABSTRACT

Amyotrophic lateral sclerosis (ALS) is the commonest adult motor neuron disease (MND) which causes progressive muscle paralysis and death usually within 5 years of symptom onset. As a result, only ~30,000 individuals in the United States are afflicted at any one time even though 5,000 or more individuals are diagnosed yearly. The diagnosis of ALS requires evidence of degeneration in upper motor neurons (UMNs) in the brain and in lower motor neurons (LMNs) that exit the brainstem and spinal cord to innervate skeletal muscles. Diagnosis can be incorrect or delayed when disease is early or atypical because non-invasive objective tests of UMN involvement do not exist, unlike electromyography to assess the LMN. Although magnetic resonance imaging (MRI) of brain and spinal cord is used primarily to identify conditions which mimic ALS, novel MRI sequences and post-processing techniques can identify macroscopic and even sub-macroscopic changes in ALS brain related to neuronoaxonal degeneration (e.g., in corticospinal motor tracts). MRI-based techniques like diffusion tensor imaging (DTI) and proton magnetic resonance spectroscopy ($^{1}$H-MRS), as well as nuclear medicine modalities like positron emission tomography (PET) and single photon emission

tomography (SPECT) are being used to study brains of patients with ALS. Many previous MRI studies of ALS brain are limited either in methodology or information obtained being primarily qualitative, i.e. changes visible to the naked eye (macroscopic). This study employed both routine and novel MRI sequences to objectively assess gray and white matter pathology of the brain in ALS patients, including T2 relaxometry, DTI, and voxel based morphometry (VBM) of 3D high resolution T1-weighted images. DTI metrics showed significant ($p<0.05$) changes in rostral extent of corticospinal tract (CST) in ALS patients with predominantly UMN symptoms and signs, and the ALS-dementia patients, whereas more caudal involvement was observed in ALS patients with classic findings of UMN and LMN dysfunction. Significant ($p<0.05$) grey matter volume and cortical thickness reductions were observed only in the ALS dementia group when compared to controls, which suggests that neurodegeneration might begin as a neuronopathy in these patients. Preserved grey matter volume and cortical thickness in other ALS patients suggests a dying back axonopathy and warrants further study. To our knowledge this is the first study in a large number of ALS patients categorized into different subgroups based on their clinical presentation. Future comparisons of brain MRI and post-mortem histopathology in the same patient will allow radiopathologic correlation of tissue pathology underlying the radiographic changes, including CST hyperintensity. These may reveal differences in pathogenic mechanisms causing ALS which could respond differently to novel pharmacotherapies.

# TABLE OF CONTENTS

Page

# LIST OF TABLES

# LIST OF FIGURES

Figure

# LIST OF ABBREVIATIONS

ALS = Amyotrophic lateral sclerosis

MND = Motor neuron disease

NIH = National institutes of health

MRI = Magnetic resonance imaging

CST = Corticospinal tract

UMNs = Upper motor neurons

LMNs = Lower motor neurons

WM = White matter

GM = Grey matter

SE = Spin echo

FSE = Fast spin echo

CPMG = Carr-Purcell-Meiboom-Gill

EMG = Electromyography

CNS = Central nervous system

DTI = Diffusion tensor imaging

EPI = Echo planar imaging

MPRAGE = Magnetization prepared rapid gradient echo

FA = Fractional anisotropy

ROI = Region of interest

MR = Magnetic resonance

TR = Repetition time

TE = Echo time

T2-w = T2-weighted

T1-w = T1-weighted

FTD =Frontotemporal dementia

SS-EPI=Single shot echo planar imaging

CP= Cerebral peduncle

IC= Internal capsule

LV= Top of the lateral ventricle

MC =Subcortical motor cortex

ANOVA= Analysis of variance

DW= Diffusion weighted

H-MRS = Proton magnetic resonance spectroscopy

PET = Positron emission tomography

SPECT = Single photon emission tomography

CT= Computed tomography

fMRI =Functional MRI

PNS = Peripheral nervous system

FLAIR = Fluid attenuated inversion recovery

MTR = Magnetization transfer ratio

RF = Radiofrequency

FA = Fractional anisotropy

MD = Mean diffusivity

VBM = Voxel-based morphometry

ROI = Region of interest

SNR = Signal to noise ratio

Westin's CP = Planar anisotropy

Westin's CL = Tubular anisotropy

RA = Relative anisotropy

MD = Mean diffusivity

FACT = Fiber assignment by continuous tracking

FWHM = Full-width half-maximum

GLM = General linear model ()

FDR = False discovery rate

GRF = Gaussian random field

GM-WM =Grey –white matter

GM-CSF = Grey matter-cerebrospinal fluid

# CHAPTER I

# INTRODUCTION TO AMYOTROPHIC LATERAL SCLEROSIS

## 1.1 Amyotrophic Lateral Sclerosis (ALS)

According to the National Institute of Neurological Disorders and Stroke (at the NIH) at least 30,000 Americans[1] are afflicted with ALS and approximately 5,000 new cases are diagnosed annually. The term ALS is derived from 'amyotrophic' refering to muscle atrophy or weakness which signifies disease of the lower motor neuron (LMN) and 'lateral sclerosis' refering to scarring or gliosis of the lateral columns of the spinal cord, which indicates degeneration of the corticospinal tract portion of the upper motor neuron (UMN) [2]. ALS is the commonest adult motor neuron disease (MND) that causes progressive degeneration of UMNs, which arise in the cerebral cortex [3] and of LMNs, which arise in the brainstem and spinal cord. This results in weakness, atrophy and spasticity of skeletal muscles involved in limb movement, speech, swallowing, and breathing. The disease is sporadic in ~90% of cases and familial in ~10% [2, 3]. ALS affects individuals of all races in all geographic areas equally except for some minor exceptions like in Western Pacific where the prevalence is 50 times higher than elsewhere [2, 3]. The

peak age of onset is between 50 and 70 years, with increasing age being the most important risk factor for developing ALS. In addition, patients developing ALS younger than 41 years tend to survive longer than those with onset older than 60 years [3]. Males are affected 1.5 to 2.0 times more often than females, although this reaches unity (1:1) over 65 years of age [3]. Average survival after the onset of ALS symptoms is ~3 years with mean disease duration reported to be between 31 and 43 months[3]. The cause of ALS and its site of origin within the nervous system are unknown and it is universally fatal.

## 1.2 Diagnosis

ALS is relatively easy to diagnose when advanced or its fully developed classic form with combined UMN and LMN dysfunction, although there are exceptions to this [4]. Diagnosis of ALS may be difficult and even be missed a) when atypical features occur, b) during certain stages of the disease when UMN or LMN features predominate, c) because a number of diseases can mimic ALS, including multiple sclerosis, radiculomyelopathy, multifocal motor neuropathy with conduction block, myasthenia gravis, and myopathy[3], and d) because no single test definitively diagnoses ALS, and diseases that mimic it need to be excluded.

All this results in diagnostic errors with some reporting only approximately 60% of ALS patients to be diagnosed correctly on their initial evaluation[3]. At present, diagnosis is based on consistent clinical features, evidence of disease progression, and laboratory investigations (e.g., blood tests, electromyography, and neuroimaging)

excluding conditions which resemble or mimic ALS, as mentioned above [5]. As a result, the delay between symptom onset and definitive diagnosis of ALS averages 12 months. Considering 80% of patients survive only 3-5 years from onset of symptoms [2], shortening the time to diagnosis is imperative. There is great interest in identifying biomarkers of ALS which could allow earlier diagnosis, identification of disease subtypes (which exist phenotypically) and monitoring of disease progression to assess efficacy of pharmacotherapies.

Based on the World Federation of Neurology El Escorial criteria [6], ALS is diagnosed only when there is evidence of both UMN and LMN dysfunction in the absence of other mimicking pathologies. This may be complicated in earlier stages or atypical forms of disease when UMN or LMN changes predominate rather than both motor neuron pools showing clinical dysfunction. Electromyography (EMG) provides an objective measure of LMN involvement even when it is not obvious clinically, but no equivalent exists for assessment of UMN dysfunction [7, 8]. On the other hand, prominent LMN changes like muscle atrophy, hypotonia, and hyporeflexia can mask coexistent UMN signs arising from degeneration of cortical motor neurons and their projections. Novel applications of neuroimaging as a noninvasive objective measure of UMN involvement could assist in such diagnosis as well as provide insights into disease pathogenesis and progression.

Presently, neuroimaging of brain and spinal cord of patients evaluated for ALS is used primarily to exclude pathologies that can mimic disease, such as strokes, tumors,

inflammation, demyelination, and compression [3]. Conventional magnetic resonance imaging (cMRI) is the commonest imaging modality used for these purposes now. Special MRI applications like diffusion tensor imaging (DTI), proton magnetic resonance spectroscopy ($^{1}$H-MRS), and nuclear medicine techniques like positron emission tomography (PET) and single photon emission tomography (SPECT) are increasingly being used to identify changes potentially specific to ALS [3, 9].

## 1.3 Neuroanatomy

For technical reasons, the UMNs in the brain are most accessible to MRI techniques that may reveal changes specific to ALS. A general understanding of the neuronal regions and tracts commonly affected in ALS is necessary to analyze and interpret the MRI changes.

Cortical UMNs which project to lower brainstem spinal cord LMNs are localized primarily in layer V of the precentral gyrus (Broca's area 4). The axons of all corticomotoneurons descend through the subcortical white matter through the corona radiata and centrum semiovale in a somatotopic orientation before entering the internal capsule and brainstem. Motor axons arising from cortical neurons in the far lateral hemisphere that travel within the corticobulbar tract, pass through the genu of the internal capsule to finally terminate on motor nuclei in dorsal regions of the midbrain, pons or medulla. In contrast, axons arising from more parasagittally located corticomotoneurons and traveling in the corticospinal tract (CST) pass through the posterior limb of the internal capsule to enter the brainstem. These CST fibers subsequently pass sequentially

through the cerebral peduncle of the midbrain, basis pontis, and finally pyramidal tract of the medulla prior to decussating at the cervicomedullary junction of the upper cervical spinal cord [3]. Pictorial representations of corticobulbar and corticospinal tracts are shown in Figures 1 and 2. Both of these central motor axon tracts degenerate in ALS to varying degrees depending on the distribution of disease.

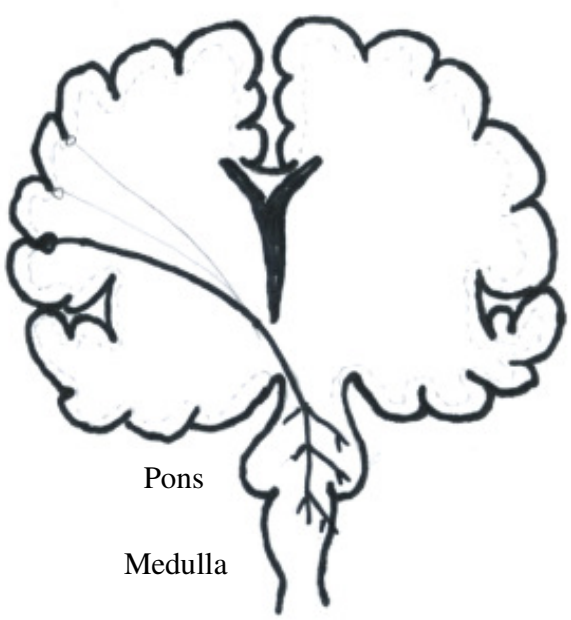


**Figure 1: Pictorial diagram of Corticobulbar tract.**

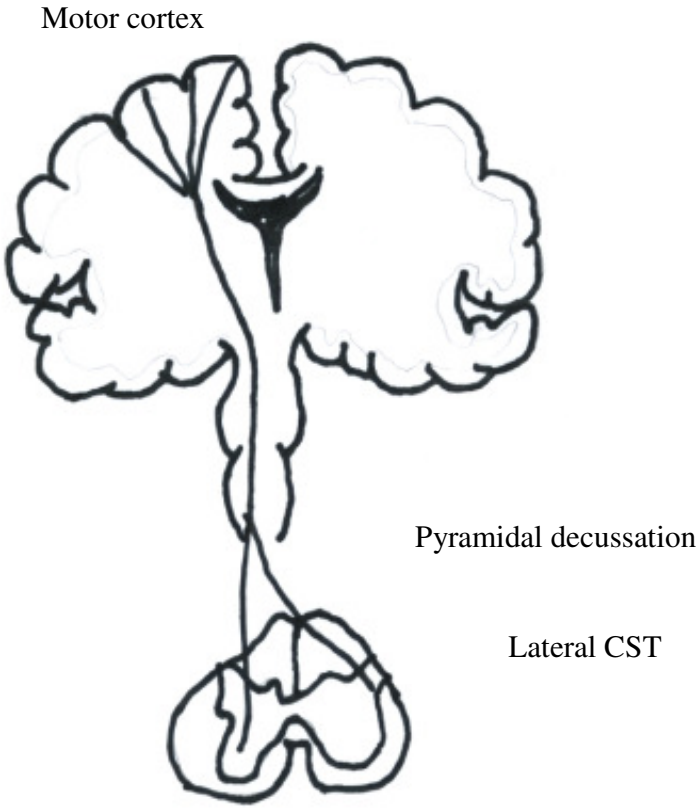


**Figure 2: Pictorial diagram of corticospinal tract.**

Typical clinical features when UMNs of the *corticobulbar* pathway degenerate include slurring of speech (dysarthria), swallowing difficulty (dysphagia), facial weakness, and spasticity (increased jaw jerk, facial reflexes, hyperactive gag), as well as pseudobulbar affect (pathologic laughter and crying). When *corticospinal* pathway UMNs are affected, typical clinical features include limb spasticity causing loss of finger dexterity and gait instability, limb and trunk weakness, and pathologically increased stretch reflexes [3].

## 1.4 Neuroimaging in ALS

Among the different neuroimaging modalities available today, MRI is preferred because it is noninvasive and can provide different contrasts between tissues types depending on the sequences used. This allows detection of abnormalities in ALS that are not detected by other modalities such as computed tomography (CT) [3]. Continued improvements in MRI hardware (e.g. higher field strength magnets) and development of novel sequences and post-processing techniques have resulted not only in life-like images but also means to quantify abnormalities of structure and function. Examples of novel MRI techniques being used to identify structural and even functional brain pathology in ALS include diffusion tensor imaging (DTI)[10] and functional MRI (fMRI)[11] developed in the 1990's.

## 1.5 Project Aim

The etiology of ALS and its site of origin within the central nervous system (CNS) are unknown. By definition, the diagnosis of ALS is based on identifying motor neuron degeneration in both the CNS and peripheral nervous system (PNS), which can also be termed the upper motor neuron (UMN) and lower motor neuron (LMN), respectively. However, whether ALS neurodegeneration begins in the CNS or PNS is debated. In reference to a CNS (or UMN) origin, where degeneration begins is also unknown. Theoretically, it can begin anywhere along the rostrocaudal extent of the motor neuron pathway: in the motor neuron cell body (perikaryon) located in the cerebral cortex gray matter, as a *neuronopathy*, or along the motor axon in the subcortical white matter, as an *axonopathy* as shown in figure 3 below. If ALS is a neuronopathy, degeneration will proceed in an anterograde (proximal to distal or rostral to caudal) fashion with axon pathways affected later; if it is an axonopathy, degeneration will be retrograde (distal to proximal or caudal to rostral) with the perikaryon affected later. Based on preliminary data, the author hypothesizes that classic and UMN–predominant ALS is predominantly a dying back axonopathy with retrograde degeneration of the perikaryon. This is in contrast to patients with ALS and frontotemporal dementia (FTD) in whom the author hypothesizes neurodegeneration to begin in the neocortex (as a neuronopathy) with anterograde degeneration of the UMN. By testing these hypotheses, this study aims to identify biomarkers of the disease process which may help in making early diagnoses and provide insights into pathogenic mechanisms.

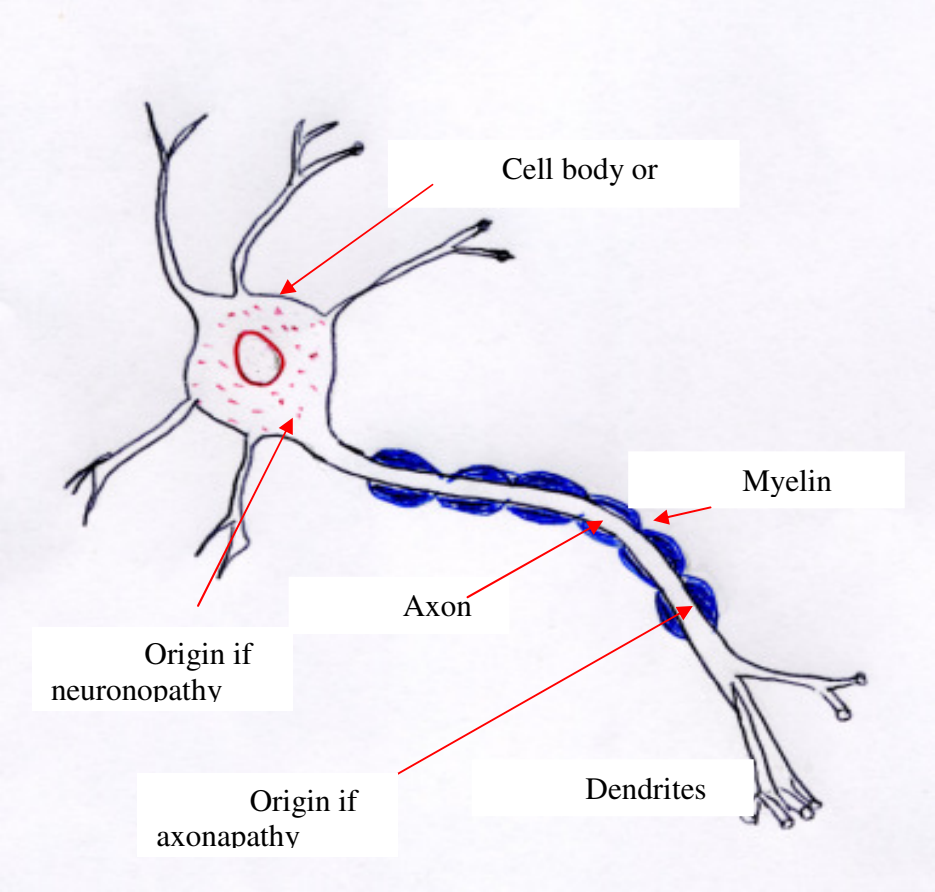


**Figure 3: Schematic of neuronopathy and axonopathy locations in a neuron**

Even though ALS patients have clinical evidence of both UMN and LMN dysfunction, a large percentage of patients begin with UMN abnormalities and subsequently develop LMN signs. It is observed that some patients with predominantly UMN signs have bilateral CST hyperintensities visible on routine T2, proton density, and FLAIR images, while others do not, even though both groups have comparable degrees of clinical UMN dysfunction and duration of disease. The explanation for this difference

in the presence or absence of CST hyperintensities is unknown. It is hypothesized that in UMN-predominant ALS patients without CST hyperintensities, the UMN degeneration is: (1) below the threshold of detection by routine MRI but still predominantly axonal, (2) arising in the cerebral cortex (as a neuronopathy) or (3) arising extracranially in the spinal cord (as an axonopathy).

The above paragraphs suggests that pathological mechanisms of ALS may be different in ALS patients with predominant UMN signs with and without CST hyperintensity and those of classic ALS and ALS with dementia. For instance clinical signs indicate more caudal onset of neurodegeneration (e.g. spinal cord) in classic ALS patients when compared with UMN predominant or in ALS dementia patients. In order to gain better insight into the pathophysiological mechanisms of ALS disease process it is imperative to categorize ALS patients. Therefore in this study ALS patients were categorized based on their clinical symptoms and clinical evaluation of their conventional MR images; 1) ALS patients with predominant UMN signs when compared to LMN signs (based on their clinical evaluation) and in addition showed hyperintense signal along CST (based on their conventional T2 and PD weighted images), 2) ALS patients with predominant UMN signs when compared to LMN signs (based on their clinical evaluation) without any hyperintense signal along the CST (based on their conventional T2 and PD weighted images), 3) ALS patients with classic features i.e. no predominance in either UMN and LMN signs (based on their clinical evaluation) and 4) ALS patients with dementia (based on their clinical evaluation, conventional MR images and PET scan).

As shown in figure 4 below, T2 relaxometry and diffusion tensor imaging (DTI) will be used to interrogate axonal integrity within the corticospinal tract (CST), the major descending white matter motor tract and T1 imaging to examine volume (using voxel based morphometry, VBM) and thickness of the cerebral cortex as measures of neuronal integrity. These results will be compared to ALS patients with typical combined UMN and LMN signs, ALS patients with FTD, and neurologic control patients without ALS or UMN deficits.

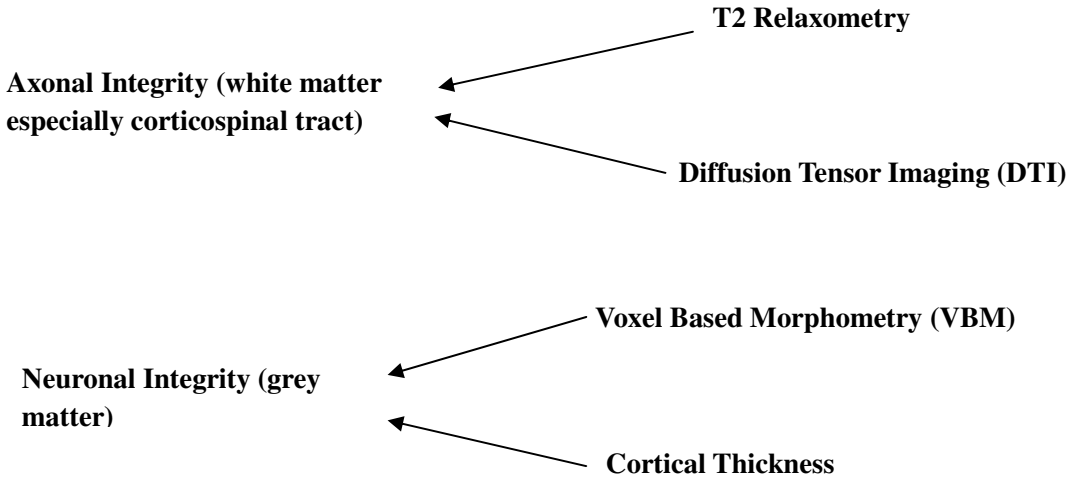


**Figure 4: MR imaging techniques to investigate axonal and neuronal integrity in ALS**

Chapter II discusses quantitative T2 relaxometry technique employed in investigating axonal integrity within CST in UMN predominant ALS patients with and without CST hyperintensity.

In Chapter III a novel non invasive modality called diffusion tensor imaging based on anisotropic diffusion property of water molecule in various neuronal fiber tracts was employed to investigate axonal integrity of CST in ALS patients. The main advantage of this technique over other conventional quantitative techniques is its ability to discern different neuronal fiber tracts within WM structures which otherwise appear homogeneous (conventional T1 or T2 weighted images). Diffusion tensor metrics was used to determine whether the presence or absence of CST hyperintensities in UMN-predominant ALS patients results from (1) divergent pathologies in subcortical axons (if both groups show similar changes) or (2) degeneration of the perikaryon in motor cortex or extracranial CST (if differences are found between groups). These results were then compared to ALS patients with typical combined UMN and LMN signs, ALS patients with FTD, and neurologic control patients without ALS.

Chapter IV discusses assessment of neuronal integrity in ALS patients using high resolution T1 weighted images. Quantitative measurements techniques such as voxel based morphometry and cortical thickness were employed to assess grey matter volume changes in ALS dementia patients for evidence of cortical atrophy. These results were then compared with ALS patients with typical (combined UMN and LMN signs), ALS patients with predominant UMN signs and neurologic control patients without ALS.

## 1.6 References


**1.** Amyotrophic Lateral Sclerosis in Veterans: Review of the Scientific Literature 2006.

**2.** Rowland LP, Shneider NA. Amyotrophic lateral sclerosis. N Engl J Med. May 31 2001;344(22):1688-1700.

**3.** Mitusmoto H, Chad D, Pioro EP. Amyotrophic Lateral Sclerosis Vol 49 Philadelphia: Oxford University Press; 1998.

**4.** Brooks BR. Diagnostic dilemmas in amyotrophic lateral sclerosis. *J Neurol Sci.* Jun 1999;165 Suppl 1:S1-9.

**5.** Shook SJ, Pioro EP. Racing against the clock: recognizing, differentiating, diagnosing, and referring the amyotrophic lateral sclerosis patient. Ann Neurol. Jan 2009;65 Suppl 1:S10-16.

**6.** Brooks BR, Miller RG, Swash M,

et al. El Escorial revisited: revised criteria for the diagnosis of amyotrophic lateral sclerosis. Amyotroph Lateral Scler Other Motor Neuron Disord. Dec 2000;1(5):293-299.

**7.** Abe O, Yamada H, Masutani Y, et al. Amyotrophic lateral sclerosis: diffusion tensor tractography and voxel-based analysis. NMR Biomed. Oct 2004;17(6):411-416.

**8.** Hong YH, Lee KW, Sung JJ, Chang KH, et al. Diffusion tensor MRI as a diagnostic tool of upper motor neuron involvement in amyotrophic lateral sclerosis. J Neurol Sci. Dec 15 2004;227(1):73-78.

**9.** Pioro EP, ed. Neuroimaging in ALS and ALS with Frontotemporal Dementia In: Dementia and Motor Neuron Disease; 2006. Strong M, ed.

**10.** Blain CR, Williams VC, Johnston C, et al. A longitudinal study of diffusion tensor MRI in ALS. Amyotroph Lateral Scler. Dec 2007;8(6):348-355.

**11.** Brooks BR, Bushara K, Khan A, et al. Functional magnetic resonance imaging (fMRI) clinical studies in ALS--paradigms, problems and promises. Amyotroph Lateral Scler Other Motor Neuron Disord. Jun 2000;1 Suppl 2:S23-32.

# CHAPTER II

# T2 RELAXOMETRY IN ALS

## 2.1 Introduction

Routine MRI studies using T2 weighted (T2-w), proton-density, and fluid attenuated inversion recovery (FLAIR) weighted images occasionally identify hyperintense signal along the CST [1] in a ALS patient as shown in Figure 5.

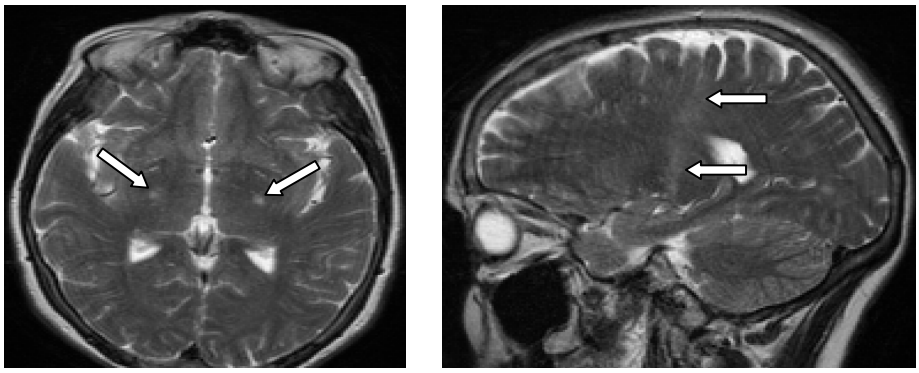

**Figure 5: Routine MR imaging, T2-weighted axial (left) and sagittal (right) MR brain images show corticospinal tract hyperintensity (arrows) in a UMN-predominant ALS patient**

Previous studies[1] have demonstrated this change in 17% to 67% (median 40%) of ALS patients although a preliminary analysis at the Cleveland Clinic found this change in ~31% of ALS patients. Based on one radiologic-pathologic study, such hyperintensity represents demyelination and wallerian degeneration of the descending CST fibers[2]. Such CST hyperintensity occurs in some but not all patients with very prominent UMN findings[3] .

Most previous MRI studies of ALS brain have described qualitative changes i.e. relying on visual evaluation of disease related abnormalities[4]. Such qualitative evaluation depends greatly on several factors, including: quality of the MR image (e.g. signal to noise ratio, SNR), limits of visual detectability, the interpreter's experience and image reproducibility. These limitations can be minimized if the MR images can be quantitatively assessed. Some such quantitative MR image sequences which are currently employed in diagnosis of neurological diseases are magnetization transfer ratio (MTR), T2 relaxometry, DTI and T1-w volumetric imaging. The first study will focus on T2 relaxometry as quantitative measures of ALS brain pathology.

The premise of T2 relaxometry is the quantitative comparison of T2 relaxation times obtained from tissues which have different densities either normally (e.g., gray matter vs white matter) or because of pathology (e.g. motor fibers either healthy or undergoing wallerian degeneration). The basis of proton-based MR imaging is, in sequential order, the alignment of body protons ($^1H$) in a static magnetic field ($B_0$), the perturbation of this alignment by the application of a radiofrequency (RF) pulse

perpendicular to the direction of $B_0$, the excitation of protons whose frequencies are in resonance with the RF field, and the return to steady state (equilibrium) of the protons by emission of this acquired energy. Body protons transfer this energy in two ways: (1) spin lattice relaxation when energy is emitted to their neighboring lattice due to mechanical motion and vibration; (2) spin-spin interaction when energy is transferred between closely adjacent protons. This latter process is known as T2 relaxation. In solids, where protons are more tightly packed and spin-spin relaxation is increased, T2 time will be short. In contrast, in liquids where protons are farther apart and spin-spin relaxation is decreased, T2 time will be long[5] . Differences in T2 relaxation times may reflect structural changes arising from disease; for example, edema results in a prolonged T2 relaxation time as more fluid accumulates.

Previous studies[6, 7] of T2 relaxometry in ALS used dual echo sequences because of clinical scanning time constraints and protocol simplicity. However, dual echo sequences are limited by inadequate sampling of the T2 decay curve[8] , dependency on echo sampling intervals[9, 10], poor signal to noise ratio[8, 11] . Many T2 relaxometry studies[12, 13] have employed fast spin echo (FSE) dual-echo sequence to measure T2 relaxation times. However, FSE sequence is prone to high spatial frequency effects. High spatial frequency effects occurs due to contrast averaging i.e. only the echo corresponding to effective TEs forms the center of the k-space, and the remaining echoes in the turbo factor or echo train length occupy other slabs of the k-space, resulting in a T2 contrast that will have some dependence on spatial frequency[13]. The concern here was that the use of data from a dual echo FSE sequence to measure T2 via the typical monoexponential fit

method would not accurately measure T2 relaxation time in all brain regions i.e. the signal in regions of high spatial frequency will correspond to a temporal evolution different than the "effective" echo time used in the fit. Thus, some error will occur depending on the spatial frequency characteristics of the brain region of interest. On the other hand, for a SE sequence, all signal is measured at approximately the same time and there will be no spatial frequency-dependence. The multiple-echo SE sequence will more properly measure T2 relaxation time in all regions regardless of spatial characteristics.

## 2.2 Aim

The aim of this study is to evaluate the accuracy of T2 relaxation times along the CST and whole brain white and grey matter structures derived from dual-echo FSE sequences relative to multiple-echo SE sequences. If the error values along CST are found to be within acceptable limits (< 10%) then T2 relaxation values measured using the dual-echo FSE sequence will be used to evaluate pathophysiology of ALS.

## 2.3 Hypothesis

It is hypothesized that errors of T2 relaxation times based on dual echo FSE sequence would be large in high spatial frequency regions (i.e. at brain structure edges), but small in low spatial frequency regions such as the CST.

If the above hypothesis is true, then T2 values from dual echo FSE sequence will be used to investigate the following hypotheses. It is hypothesized that in UMN-predominant ALS patients without CST hyperintensities, UMN degeneration is either: (1)

below the threshold of detection by routine MRI but still predominantly axonal, (2) arising in the cerebral cortex (as a neuronopathy) or (3) arising extracranially in the spinal cord (as an axonopathy).

## 2.4 Methods

### 2.4.1 Image sequences

Clinically obtained MRI data and storage of de-identified images was approved by our local Institutional Review Board as part of the "Neuroimaging Registry/Database for CNS Analysis in Patients with Motor Neuron Disease". Both dual-echo FSE and multiple-echo SE images were acquired axially in 9 subjects (8 ALS patients and 1 control) aged 49 to 84 (63±11.7, mean±SD) years on a 1.5 T MRI scanner (Siemens Symphony, Erlangen, Germany). Dual-echo FSE imaging parameters were: number of slices = 40, contiguous, slice thickness = 4 mm, in-plane resolution = 0.9×0.9 mm; pulse sequence parameters were: TR = 3900 ms, TE = 26 ms and 104 ms, echo train length or turbo factor = 7, and number of averages = 1; total scan time = 3.5 minutes. Multiple-echo spin echo imaging parameters were: number of echoes =16, number of slices = 8, covering the upper half of the brain, slice thickness = 4 mm, slice gap = 4 mm, in-plane resolution = 1.3×0.9 mm; pulse sequence parameters were: TR = 3900 ms, 16 TEs ranging from 22-352 ms, number of averages = 1; total scan time = 7.5 minutes. A high resolution 3D T1-w MPRAGE sequence provided good grey-white matter contrast [14]. MPRAGE imaging parameters were: number of slices = 160, contiguous, slice thickness = 1 mm, in-plane resolution = 0.9×0.9 mm; pulse sequence parameters were: TR = 1970 ms, TE = 4.38 ms, number of averages = 1, flip angle =$10^{o}$, TI =1100 ms and scan time =

6.45 minutes. DTI was also performed using EPI sequence along 12 diffusion weighted (b = 1000 s/mm$^2$) directions and one $b_0$ = 0 s/mm$^2$ for identification of CST. Imaging parameters were: 30 slices, 4 mm thick, with 1.9×1.9 mm in-plane resolution; pulse sequence parameters were: TR = 6000 ms, TE = 121 ms, EPI factor = 128, number of averages = 6 and scan time = 7.54 minutes. Because EPI-based DTI data is geometrically distorted by susceptibility artifact at bone-air-tissue interfaces, gradient-echo sequence field map images were acquired. Field map imaging parameters were: number of slices = 30, slice thickness = 4 mm, slice gap = 4 mm, TR=500 msec, TEs = 6.11 and 10.87 msec.

### 2.4.2 Data processing

Relaxation of signal intensity after a spin echo pulse sequence is given by equation 1[5].

Signal (S)

$$S = M_0(1 - e^{-TR/T1})e^{-TE/T2} \quad \text{.....1}$$

Where $M_0$ is proton density, $T_1$ and $T_2$ are longitudinal and transverse relaxation times.TR timing was set long enough in the imaging protocol to exclude T1 effects[14] . T2 relaxation times are then estimated by assuming a mono exponential decay model which is as given in equations 2 below.

$$S = S_0 e^{-TE/T2} \quad \text{..... 2}$$

$S_0$ being a parameter of no interest, the images are then log transformed and the final equation which is used to calculate T2 map is given in equation 3 below.

$$T2 = \frac{TE_2 - TE_1}{\ln \frac{S_1}{S_2}} \quad \text{..... 3}$$

$TE_2$ and $TE_1$ are the echo timings, and $S_1$ and $S_2$ are the image signal intensities at the two echo time points, respectively.

Using the above equation, T2 relaxation times are calculated for every voxel resulting in a T2 map. Since only mono-exponential fit is possible with the FSE sequence the SE data were fitted with the same mono-exponential model. All SE images were linearized by log transformation and a linear least square fit was used to estimate the T2 decay curve using all sixteen echos. A percentage error map was then calculated from the T2 maps obtained from SE and FSE sequences, as given in equation 4 below.

$$Percentage\ error = \frac{|T2\_FSE - T2\_SE|}{T2\_SE} \times 100 \quad \text{.....4}$$

### 2.4.3 Regional T2 relaxation values

Two approaches were taken to validate T2 relaxation times derived from FSE sequences compared to SE sequences. The first was to assess error values of T2 relaxation times along the CST in ALS patients. DTI was used to generate tractography maps identifying exact location of each patient's CST. The second was to assess T2 relaxation time error across whole brain GM and WM structures.

#### 2.4.3.1 CST T2 relaxation time error values

T2 relaxation time error values were calculated along the CST in the following manner: (a) CSTs are reconstructed from the patient's own DTI images after correction of field distortion by using FUGUE from FSL (http://www.fmrib.ox.ac.uk/fsl/)[15, 16]. (b) Undistorted DTI images are processed using DTI Studio open software (https://www.mristudio.org/)[17]) to estimate diffusion tensor matrix for each element in the

voxel is calculated based on multivariate linear least square fit, and the obtained tensor matrix is diagonalized to derive eigenvalues and eigenvectors. (c) Virtual neuronal fibers are reconstructed using the fiber assignment by continuous tracking (FACT) algorithm [17], which is described in detail elsewhere[18]. The tracking parameters used were: termination FA threshold value = 0.2 [21] and bending angle threshold = 41°.

After these preliminary processing steps, CST fiber tracts were reconstructed after Wakana et al[19] by placing one region of interest (ROI) caudally in the cerebral peduncle and another rostrally just below the primary motor cortex. Subsequently, a map of CST tracts was obtained and DTI images were registered to T2-w images by co-registering b=0 images with T2-w images using an affine transformation (FLIRT from FSL)[20]. Finally, the transformation matrix was applied to the CST tracts and a CST mask image was created in order to superimpose them over the calculated error maps as shown in figure. 6. Compared to manually tracing the ROI, we found that this tractography-based method gives more accurate identification of the CST, is highly reproducible as it is free of operator bias, and is less time intensive. T2 relaxation error values (percentage error as given in equation 4) were obtained along the intracranial CST, percentage error values were plotted as histograms for left and right CST separately as shown in figures 7) and 8) and the mode values of the peak of the histograms were measured as error value in each and every subject and are given in Table I

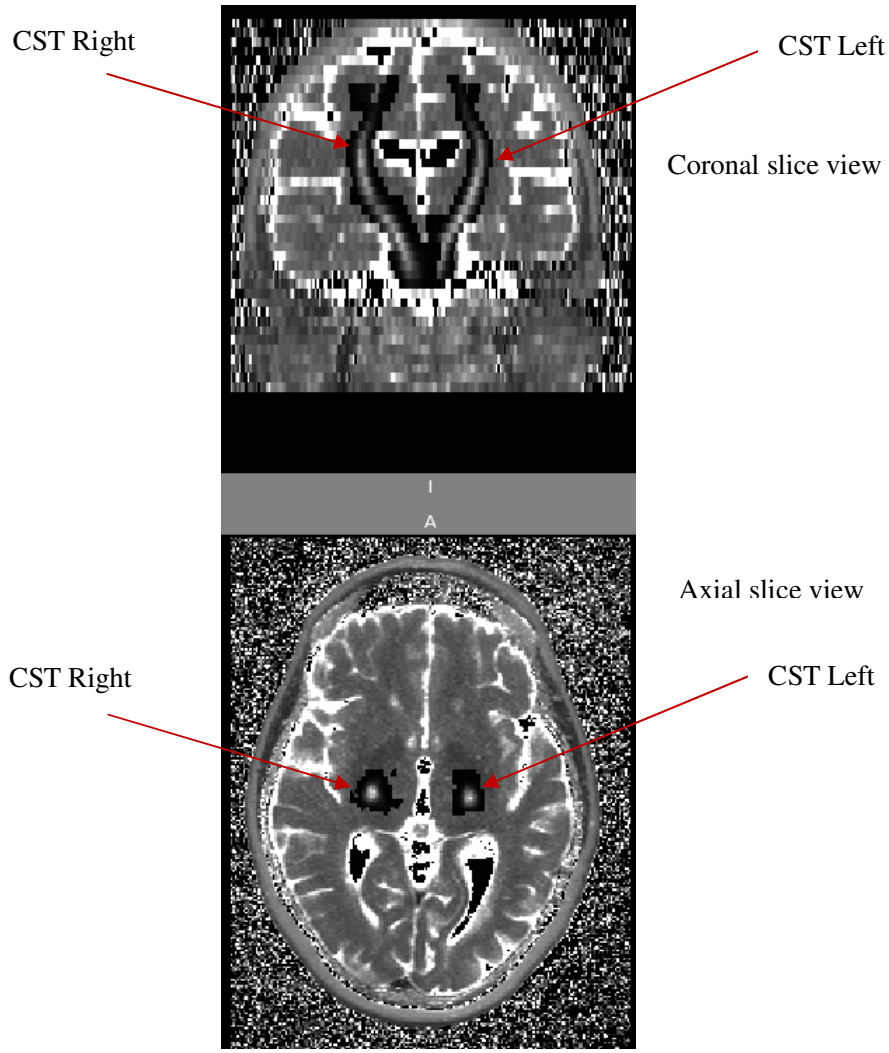


**Figure 6: CST tracts superimposed on T2 relaxation map in one of our ALS patients**

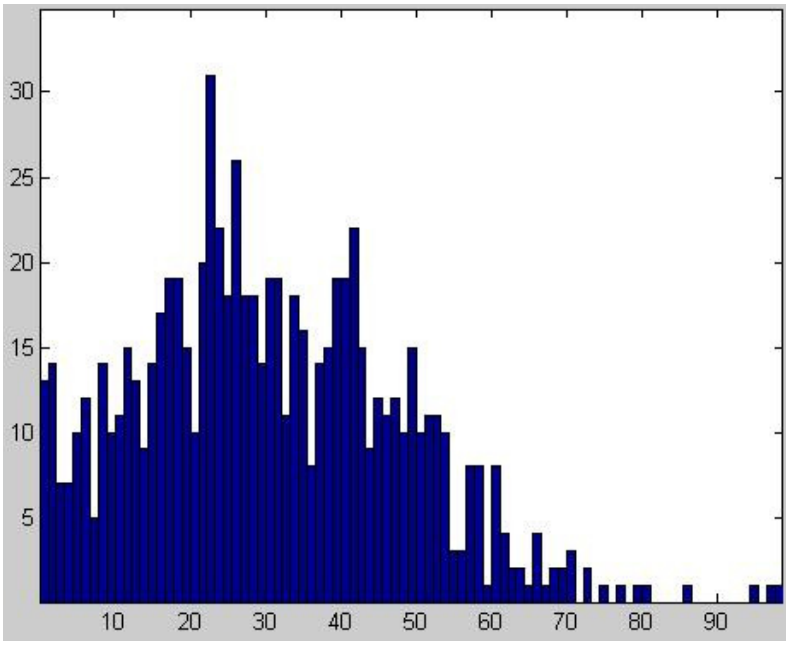


**Figure 7: Histogram of absolute percentage error values along left CST in one of our subjects**

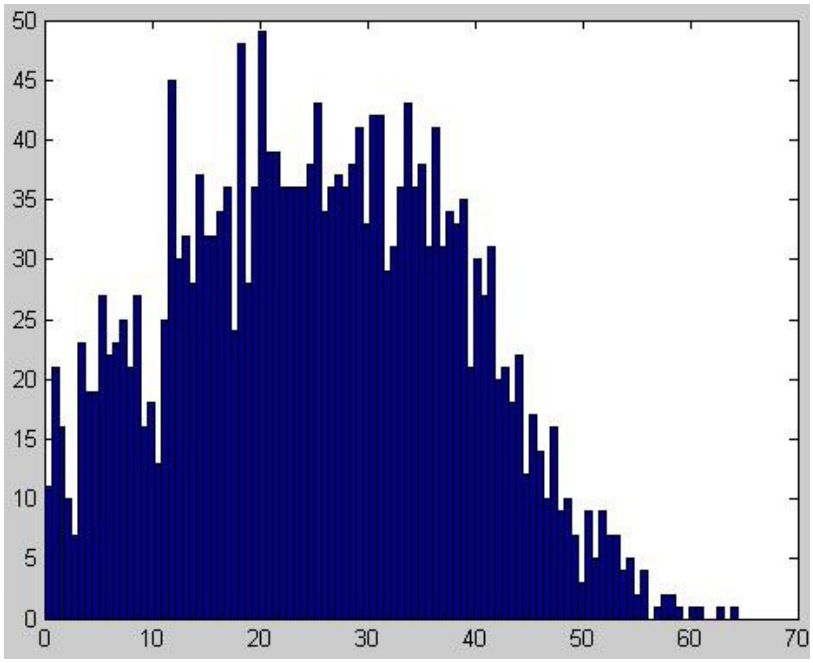


**Figure 8: Histogram of absolute percentage error values along right CST in one of our subjects**

#### 2.4.3.2 Whole brain T2 relaxation time error values

All image processing was done with FSL open software (http://www.fmrib.ox.ac.uk/fsl/)[16]. GM and WM segmentation was performed on T1-w MPRAGE images because they provide good grey-white contrast. T2 relaxation time error maps were calculated from whole brain WM and GM structures in the following manner: (a) Brain and non-brain structures were extracted using BET[21], and the extracted brain image was segmented into WM, GM and CSF probability maps using FAST[22] . (b) Affine registration was used to register T1-w images to T2-w images using FLIRT[20, 23] . (c) The transformation matrix was then applied to WM and GM maps. (d) A binary mask of WM and GM was created by setting a threshold value of P> 0.75 to eliminate any misclassified WM, GM or CSF tissues. (e) WM and GM masks were then multiplied with the percentage error map to obtain whole brain GM and WM error values as shown in figure 9 a) and b). Processing steps from a) to d) was pictorially represented in figure 10 below. Error values of T2 relaxation times in GM and WM structures were then plotted as histograms. Figure 11 a) and b) shows typical histogram of WM and GM error values in one of our subjects .Mode values of the peak of the histograms were measured as error value in each and every subject and are given in Table II..

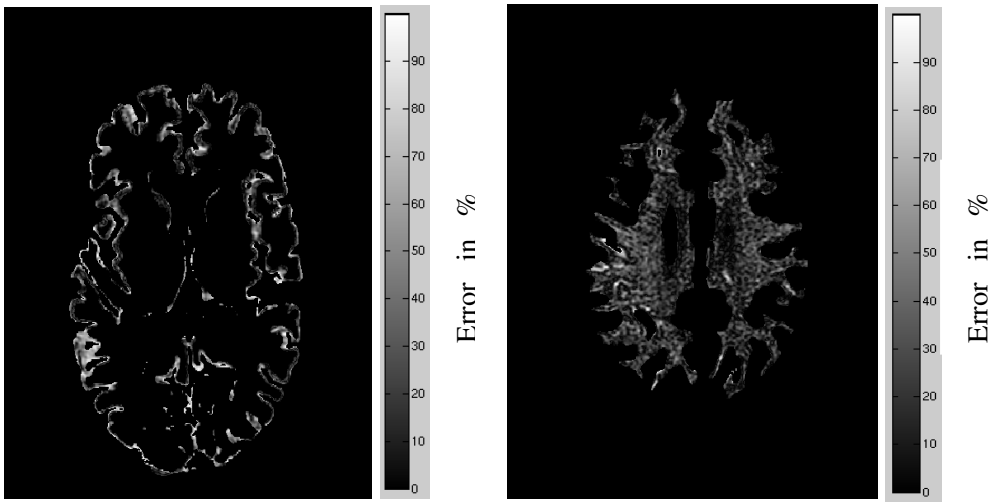


a.) b)

**Figure 9: MR images of Grey matter a)and White matter b) absolute percentage error maps in one of our subjects**

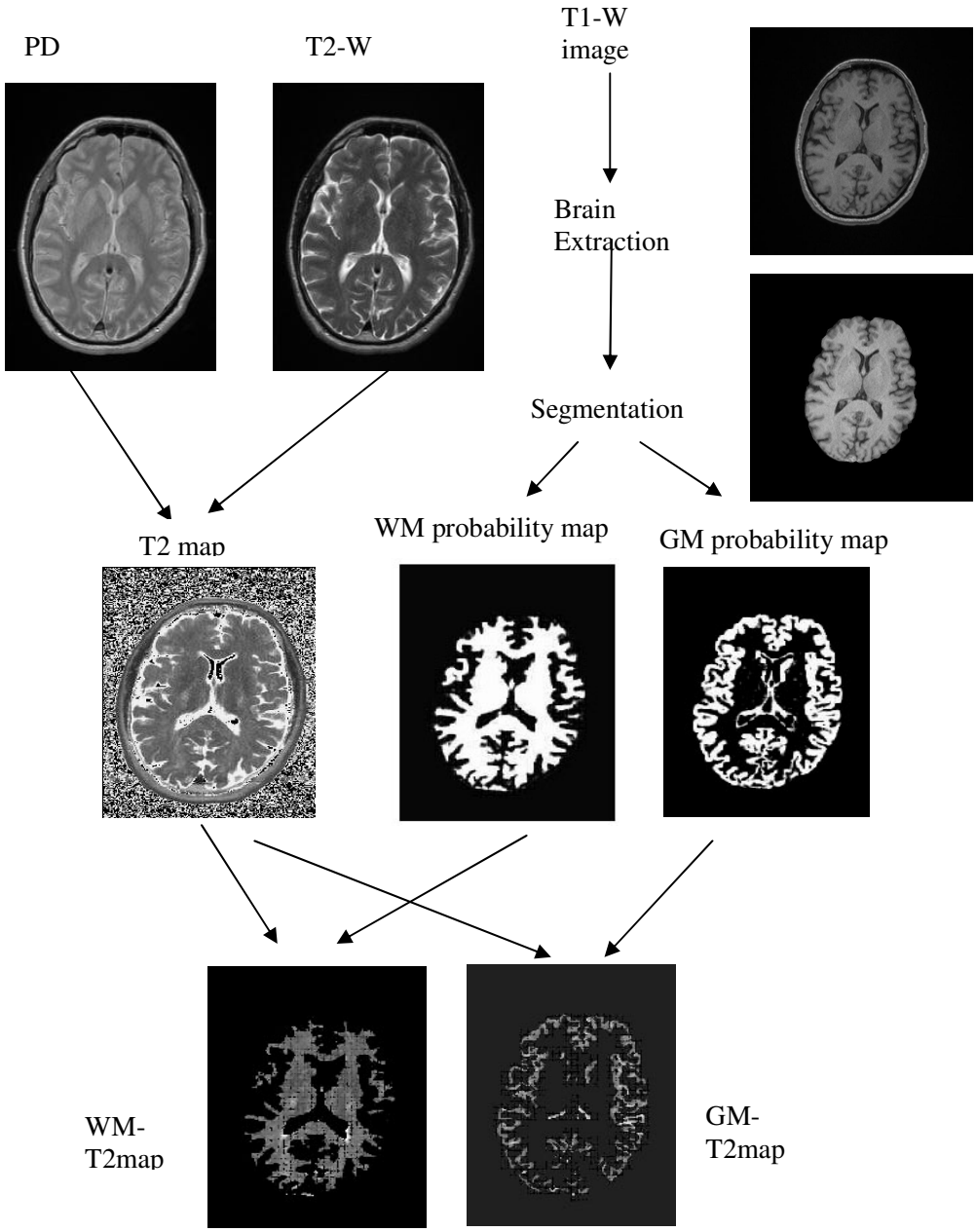


**Figure 10: Pictorial representation of processing steps for whole brain approach**

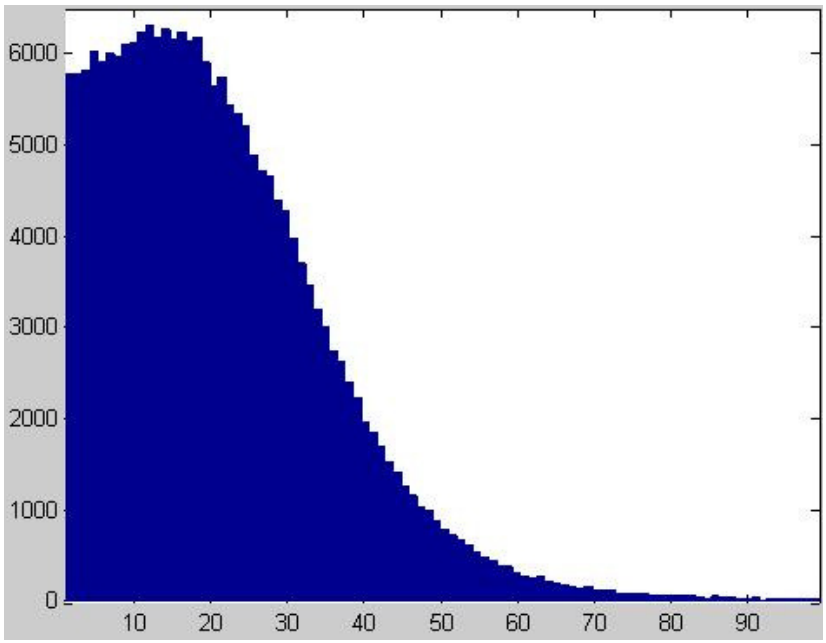


a)

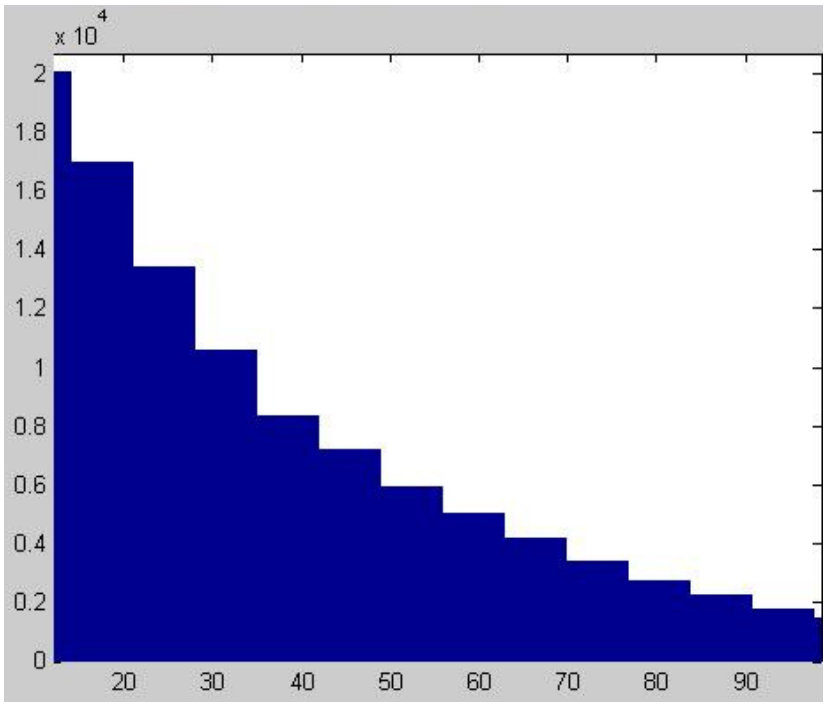


b)

**Figure 11: Histogram of whole brain absolute percentage error values of a) white matter b) grey matter structures in one of our subjects**

## 2.5 Results

T2 relaxation value errors calculated from FSE vs. SE sequences in all 9 brains are shown for the CST (Table I), and for whole brain WM and GM structures (Table II). In the CST, error values were >10% in all subjects and >20% in 6 of 9 subjects (Table I). This was surprising since we had initially hypothesized that T2 relaxation value errors in the CST would not be high (>10%) since this region should normally not have high spatial frequency characteristics. Large errors would be expected only in brain regions with high spatial frequency because FSE sequences have pronounced high spatial frequency effects. On the other hand, whole brain GM and WM regions generally had low error values (<10%), although 6 subjects had error values slightly >10% in WM regions (Table II). Overall, WM and GM T2 relaxation values were similar between FSE and SE derived sequences suggesting a greater proportion of low vs. high spatial frequency regions in whole brain. Also unexpected was the lowest percent error occurring in the GM fraction considering the cortical surface would be expected to exert high spatial frequency effects.

**Table I: Mode values of absolute percentage error in T2 Relaxation Times along Right and Left Corticospinal Tracts measured from histogram in all the subjects**

| Subject | Mode values of absolute percentage error | |
|---|---|---|
| | Left CST | Right CST |
| 1 | 15.56 | 19.67 |
| 2 | 18.16 | 19.14 |
| 3 | 26.53 | 18.55 |
| 4 | 21.55 | 22.53 |
| 5 | 22.58 | 18.51 |
| 6 | 23.5 | 24.63 |
| 7 | 23.64 | 9.58 |
| 8 | 18.84 | 23.76 |
| 9 | 30.63 | 20.02 |
| Mean | 22.33 | 19.59 |
| SD | 4.55 | 4.39 |

SD- Standard deviation

**Table II: Mode values of absolute percentage error in T2 Relaxation Times in whole brain gray and white matter structures measured from histogram in all the subjects**

| Subject | % Error | |
|---|---|---|
| | WM | GM |
| 1 | 12.5 | 4.5 |
| 2 | 15.5 | 2.5 |
| 3 | 12.5 | 1.5 |
| 4 | 16.5 | 3.5 |
| 5 | 2.5 | 3.5 |
| 6 | 8.5 | 1.5 |
| 7 | 8.5 | 47.5 |
| 8 | 13.5 | 2.5 |
| 9 | 16.5 | 38.5 |
| Mean | 11.83 | 11.72 |
| SD | 4.60 | 17.90 |

SD- Standard deviation

## 2.6 Discussion

T2 relaxometry studies in ALS by Hofmann et al.[6], and Tanabe et al.,[7] used a dual-echo SE sequence to measure relaxation times along the CST of patients and control

subjects but failed to detect significant differences between groups. Reasons for this may include small sample size [7], manual ROI identification of the CST region [6, 7] and different MR sequence parameters such as TEs 30 ms and 100 ms [6] vs. 20 ms and 80 ms [7]. Another reason may be the inherent error caused by dual-echo sequences in measuring T2 relaxation time, as demonstrated in an earlier single slice study by Whittall et al.[10] They found that T2 values were underestimated with a dual-echo sequence using a monoexponential fit when compared to a 32-echo CPMG sequence using multiexponential fit, which produced more accurate relaxation times[10]. Even though 32-echo single slice studies are considered to be the gold standard for accuracy of T2 relaxation times, limiting measurements to a single slice because of time constraints may miss important information as ALS pathology may be located in other regions.

Duncan et al [9] showed that dual-echo FSE sequences are less accurate when compared to dual-echo SE sequences. The large error in T2 relaxation values derived from FSE sequences along the CST brings into question the validity of results in studies using this technique. This is even more important when longitudinal measures are performed because the significance of changes detected over time may not be valid. Especially in diseases like ALS, it is imperative to have a robust measure of T2 relaxation times where longitudinal studies are vital not only to study effects of disease progression but also to assess the effects of potential disease modifying agents.

Undoubtedly, the main drawback to obtaining multiple-echo SE sequences is the increased scanning time; in our study, acquiring 16 echoes over 8 slices (with 4 mm slice

gap) took 8 minutes whereas acquiring 40 contiguous slices with a FSE sequence took only 3.5 minutes. In clinical scanning protocols, this is a major consideration since other sequences are also acquired, such as MPRAGE images and DTI, as in our study. The patient's ability to remain motionless in the scanner is also limited, especially when dementia or other co-morbidities exist. This may be the reason why many T2 relaxometry studies of patients with Huntington's disease [13], epilepsy [12, 24], and multiple sclerosis[25] have used FSE sequences. The increasing use of ultra-high field strength magnets (e.g., 3T and higher) and the development of novel scanning sequences will likely overcome the time limitations of multi-echo sequences.

Finally, the Carr-Purcell-Meiboom-Gill (CPMG) sequence is generally accepted as a more accurate way to measure T2 with MRI. Future work should include the use of the CPMG sequence to understand issues related to *in vivo* T2 measurements for clinical studies.

## 2.7 Conclusion

The results clearly demonstrates that T2 relaxation times obtained using dual-echo FSE sequences are not as accurate as values estimated from data acquired using multiple-echo SE sequences. Therefore, T2 relaxometry based on dual-echo FSE sequence will not be used further to investigate the changes in ALS patients. Based on above findings it is recommended that future T2 relaxometry studies employ multi-echo SE sequences or CPMG for accurate and reliable results.

## 2.8 Limitations and Future Scope

The percentage error estimation method adopted in this study may raise concerns about the level of acceptable error i.e. ~10%. To overcome the above the drawback student t-test map can be obtained in order to determine significant difference between the T2 relaxation maps of dual echo FSE and multiple echo SE sequences.

Low percentage error values seen in whole brain grey matter structures suggest that T2 relaxation time measured using dual echo FSE sequence can be used to investigate changes in grey matter structures. Future studies can be directed along this line.

In the next chapter our second study using novel non invasive modality called diffusion tensor imaging (based on anisotropic diffusion property of water molecule in various neuronal fiber tracts) was employed to investigate axonal integrity of CST in ALS patients. The main advantage of this technique over other conventional quantitative techniques is its ability to discern different neuronal fiber tracts within WM structures which otherwise appear homogeneous in conventional MR images (e.g. T1 or T2 weighted images). Diffusion tensor metrics was used to evaluate pathophysiological changes in ALS patients when compared to controls.

## 2.9 References


**1.** Pioro EP, ed. Neuroimaging in ALS and ALS with Frontotemporal Dementia In: Dementia and Motor Neuron Disease; 2006. Strong M, ed.

**2.** Yagishita A, Nakano I, Oda M, et al. Location of the corticospinal tract in the internal capsule at MR imaging. *Radiology.* May 1994;191(2):455-460.

**3.** Matte G P, Pioro E. Clinical features and natural history in ALS patients with upper motor neuron abnormalities on conventional brain MRI. *Neurology.* 2010;74(A216).

**4.** Mitusmoto H Chad DA, Pioro EP. Amyotrophic Lateral Sclerosis Vol 49 Philadelphia: Oxford University Press; 1998.

**5.** Hashemi RH, Bradley WG Jr, Christopher LJ. MRI The Basics. USA: Lippincott Williams and Wilkins; 2004.

**6.** Hofmann E, Ochs G, Pelzl A, et al. The corticospinal tract in amyotrophic lateral sclerosis: an MRI study. *Neuroradiology.* Feb 1998;40(2):71-75.

**7.** Tanabe JL, Vermathen M, Miller R,et al. Reduced MTR in the corticospinal tract and normal T2 in amyotrophic lateral sclerosis. *Magn Reson Imaging*. Dec 1998;16(10):1163-1169.

**8.** Poon CS, Henkelman RM. Practical T2 quantitation for clinical applications. *J Magn Reson Imaging.* Sep-Oct 1992;2(5):541-553.

**9.** Duncan JS, Bartlett P, Barker GJ. Technique for measuring hippocampal T2 relaxation time. *AJNR Am J Neuroradiol.* Nov-Dec 1996;17(10):1805-1810.

**10.** Whittall KP, MacKay AL, Li DK. Are mono-exponential fits to a few echoes

sufficient to determine T2 relaxation for in vivo human brain? *Magn Reson Med.* Jun 1999;41(6):1255-1257.

**11.** Jack CR, Jr. Hippocampal T2 relaxometry in epilepsy: past, present, and future. *AJNR Am J Neuroradiol.* Nov-Dec 1996;17(10):1811-1814.

**12.** Coan AC, Bonilha L, Morgan PS,et al. T2-weighted and T2 relaxometry images in patients with medial temporal lobe epilepsy. *J Neuroimaging.* Jul 2006;16(3):260-265.

**13.** Vymazal J, Klempir J, Jech R, et al. MR relaxometry in Huntington's disease: correlation between imaging, genetic and clinical parameters. *J Neurol Sci.* Dec 15 2007;263(1-2):20-25.

**14.** Carneiro AAO, Vilela GR, de Araujo DB, et al. MRI Relaxometry: Methods and Applications. *Brazilian Journal of Physics.* 2006;36:9-15.

**15.** Jenkinson M. Fast, automated, N-dimensional phase-unwrapping algorithm. *Magn Reson Med.* Jan 2003;49(1):193-197.

**16.** Smith SM, Jenkinson M, Woolrich MW, et al. Advances in functional and structural MR image analysis and implementation as FSL. *Neuroimage.* 2004;23 Suppl 1:S208-219.

**17.** Jiang H, van Zijl PC, Kim J,et al. DtiStudio: resource program for diffusion tensor computation and fiber bundle tracking. *Comput Methods Programs Biomed.* Feb 2006;81(2):106-116.

**18.** Mori S, Crain BJ, Chacko VP, et al. Three-dimensional tracking of axonal projections in the brain by magnetic resonance imaging. *Ann Neurol.* Feb 1999;45(2):265-269.

**19.** Wakana S, Caprihan A, Panzenboeck MM, et al. Reproducibility of quantitative tractography methods applied to cerebral white matter. *Neuroimage.* Jul 1 2007;36(3):630-644.

**20.** Jenkinson M, Smith S. A global optimisation method for robust affine registration of brain images. *Med Image Anal.* Jun 2001;5(2):143-156.

**21.** Smith SM. Fast robust automated brain extraction. *Hum Brain Mapp.* Nov 2002;17(3):143-155.

**22.** Zhang Y, Brady M, Smith S. Segmentation of brain MR images through a hidden Markov random field model and the expectation-maximization algorithm. *IEEE Trans Med Imaging.* Jan 2001;20(1):45-57.

**23.** Jenkinson M, Bannister P R, Brady J M et al. Improved optimisation for the robust and accurate linear registration and motion correction of brain images. *NeuroImage.* 2002;17:825-841.

**24.** Okujava M, Schulz R, Ebner A, et al. Measurement of temporal lobe T2 relaxation times using a routine diagnostic MR imaging protocol in epilepsy. *Epilepsy Res.* Jan 2002;48(1-2):131-142.

**25.** Neema M, Goldberg-Zimring D, Guss ZD, et al. 3 T MRI relaxometry detects T2 prolongation in the cerebral normal-appearing white matter in multiple sclerosis. *Neuroimage.* Jul 1 2009;46(3):633-641.

# CHAPTER III

# DIFFUSION TENSOR IMAGING IN ALS

## 3.1 Introduction

Onset of a disease is accompanied by pathologic changes initially at the microscopic level, before becoming evident macroscopically. Detecting such changes as early as possible is best for purposes of diagnosis and treatment of any disease process. Unlike other conventional MR techniques, diffusion tensor imaging (DTI) is based on diffusion of water molecules at the microscopic level. DTI's efficacy and power in providing this microscopic information non-invasively enabled clinicians and researchers to study ALS along the line of multiple sclerosis[1, 2] and other motor neuron disease (MNDs)[3, 4]. As mentioned in section 1.5 of chapter 1, DTI is an appropriate tool to study axonopathy in MNDs.

DTI is a relatively recently described modality based on the freedom with which water molecules (protons) move randomly within tissue[5] . Because DTI is based on this microscopic level event, it is unique among MR modalities and has the potential of

detecting tissue pathology at near sub-macroscopic levels. Identifying tissue pathology by MRI before it has progressed significantly has several advantages, including more timely diagnosis and earlier therapeutic intervention. In a progressive neurodegenerative disease like ALS, DTI may non-invasively detect pathologic changes which are still at or near microscopic levels. In addition, because most nerve fiber tracts are compact bundles of myelinated motor axons oriented in parallel (e.g., CST or ascending tracts), their DTI characteristics will be different whether healthy (intact) or undergoing degeneration (disrupted).

Highly coherent structures like axon bundles do not allow protons (of water molecules) to diffuse freely in all directions, isotropically. Rather, they restrict protons to move primarily in one direction (along their length), anisotropically; densely packed fiber bundles therefore normally possess high anisotropy and their disruption results in decreased anisotropy. By measuring the magnitude of proton diffusion in multiple directions, fiber (and tract) orientation can be determined[6]. However, in order to determine directionality of highly convoluted or irregular fiber tracts without scanning in an excessive number of directions, a tensor model based on a limited number of diffusion direction measurements was developed[6]. This is the origin of the term diffusion tensor imaging (DTI) and figure 12 below shows how diffusion information is encoded in the tensor matrix.

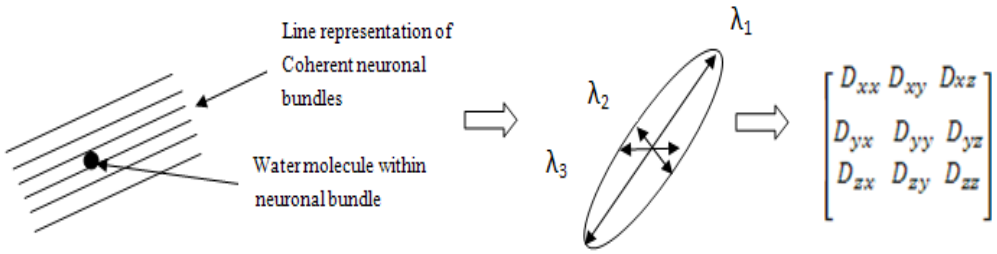


**Figure 12: Representation of water diffusion becoming anisotropic in the presence of compact tissues and how that information is encoded in diffusion tensor matrix.**

The diffusion tensor matrix obtained from diffusion data contains both scalar and vectorial measures. Scalar diffusion measures, i.e., fractional anisotropy (FA) and mean diffusivity (MD), are widely employed because they are vector invariant (independent of the direction of measurement) and provide quantitative information[7]. The most widely evaluated scalar parameters in ALS are MD and FA given in equations 1 and 2 below. FA represents the amount of anisotropy in the diffusion tensor [8] which is increased by fiber tract coherence and integrity and reduced by demyelination or degeneration. MD represents proton diffusion within one or more voxels (region)[8] which decreases as water molecules are more restricted in movement.

$$MD = \frac{(\lambda_1 + \lambda_2 + \lambda_3)}{3} \qquad \text{.....(1)}$$

$$FA = \sqrt{\frac{1}{2}} \frac{\sqrt{(\lambda_1 - \lambda_2)^2 + (\lambda_2 - \lambda_3)^2 + (\lambda_3 - \lambda_1)^2}}{\sqrt{\lambda_1^{\,2} + \lambda_2^{\,2} + \lambda_3^{\,2}}}$$

.....(2)

Conventional MRI and DTI produce significantly different images, as shown in figure 13 below. In conventional T1-w MRI, white and gray matter is visually distinguishable because of contrast differences but white matter myelin appears mostly homogeneous (Fig. 13a). In DTI, the directionality of fiber orientation in white matter produces contrast differences and provides additional tract information (Fig. 13b) [6] . An elegant extension of DTI is tractography, in which fiber tracts can be reconstructed in three dimensions based on vector information from the tensor matrix (Fig. 13c).

a) b)

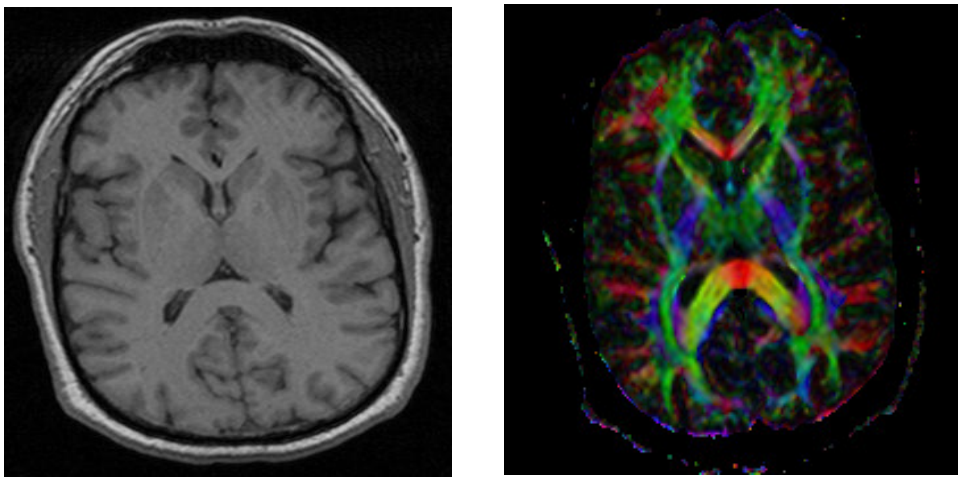

c)

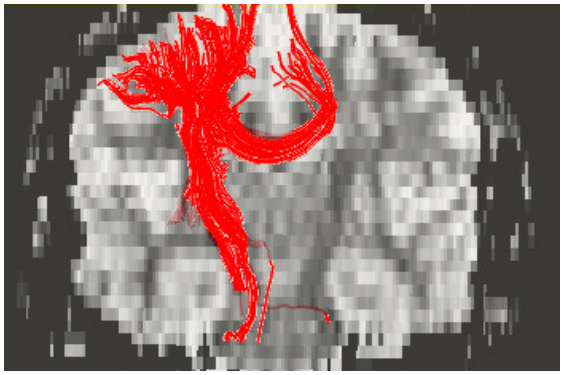

**Figure 13: Brain MRI of one of our ALS subjects showing: a) T1 weighted image, b) DTI FA color map based on vector information (i) red color for left-right orientation, (ii) green for antero-posterior direction and (iii) blue for rostrocaudal orientation; and c)CST neuronal tracts reconstructed based on DTI tractography**

As can be seen from the previous paragraphs that DTI images are not only more informative when compared to conventional MRI scans but also have the ability to detect microscopic changes occurring at very early stages of the disease process. This will

enable the detection of pathologic changes at a much earlier stage and potentially before the disease advances to an irreversible state. Furthermore, the tractography feature of DTI will enable not only reconstruction of virtual neuronal fiber tracts which are affected by the disease process but also identification of newer fiber tracts which might be prone to ALS degeneration.

Previous DTI studies in ALS employed two different approaches in assessing fiber tract integrity: ROI-based and voxel-based morphometry (VBM). The ROI-based approach is hypothesis directed and is best suited when there is *a priori* knowledge about regions that are affected by the disease process. On the other hand, the VBM based approach assumes no prior knowledge about the regions affected by the disease process and is therefore an exploratory one.

### 3.1.1 ROI-based approach

Many DTI studies in ALS have used ROI based identification of the CST at various levels to compare FA and MD values between patients and control subjects. Most of these studies revealed reduced FA and increased MD in the posterior limb of the internal capsule in ALS patients compared to controls[7-10]. Hong et al[11] used *trace* information (which is the sum of diagonal elements of the eigen values of the DTI matrix) to overcome errors introduced by partial volume effects when manually tracing CST in the medullary pyramids. On the other hand, Schimrigk et al[10] used a probability mixture model which would overcome some but not all drawbacks of the ROI based approach.

The advantage of this model is that it is independent of the resolution of the data and by dividing the voxels within the ROI into a) pure fibers class, b) pure background class and c) a partial volume class of both fiber and background class reduces not only partial volume effects but also interobserver differences. Nonetheless, ROI based approaches which require manual identification of brain regions which are labor intensive, are prone to poor inter- and intrarater reproducibility, and generate partial volume effects.

### 3.1.2 VBM-based approach

Voxel-based morphometry (VBM) analysis allows objective and automated detection of structural differences in brain tissue (e.g. atrophy) between subjects after normalizing for random shape differences[12]. Being an unbiased assessment, it can be used for exploratory analyses when no *a priori* knowledge of distribution in pathology is available. For example, atrophy in ALS may occur outside of motor regions, especially when patients have additional dementia, making VBM-based morphometry an ideal approach to studying this. Once the patient's brain is fitted to a common brain template (e.g., from normal controls) which normalizes for any random variation between brains shapes and sizes, it is smoothed and a statistical parametric map generated of grey and white matter from which significant differences in tissue amounts is identified between patient and control brain templates.

A VBM-based approach has been applied to DTI measures. Sach et al[13] and Thivard et al[14] generated statistical parametric maps of FA values and found reductions not only in CST and pyramidal tracts but also in the thalamus, corpus callosum and in

other extramotor regions of ALS brains when compared to controls. In contrast, Abe et al[15] found changes only in the CST and pyramidal tracts. The disparate results may be due to different patient phenotypes with varying degrees of involvement in non-motor brain regions supporting the notion that ALS is a multisystem disease[16].

Since our DTI data has large slice thickness contributing significantly to partial volume effects and anisotropic voxels leading to poor signal to noise ratio (SNR), VBM based approach will not be followed in this study.

### 3.1.3 Fiber Tractography

Virtual fiber tracts can be generated in 3D from quantitative DTI information (fiber tractography) providing a visual correlate to the data. Abe et al[15] first employed tractography in ALS to accurately localize the supratentorial CST. In their more extensive study, Wang et al[17] used color maps and fiber tracking in ALS to show a thinning of the CST in ALS compared to control brain. They also showed a reduction in CST fiber number in ALS patients compared to control individuals. Although mean CST volumes in right and left hemispheres were not different between affected and unaffected hemispheres, the total CST volume in both hemispheres was significantly lower in ALS patients compared to healthy volunteers.

Fiber tractography is sensitive to angular threshold, vector step length, and seed ROI; it also shows variability among subjects because of anatomical differences.

## 3.2 Limitations of current ALS DTI studies

Some of the limitations of the above mentioned studies are: a) manual ROI identification, b) Changes in FA values can result from either decrease in axial diffusivity or increase in radial diffusivity or could be due to both[18]. It is also demonstrated using an example that even if a patient and a control subject have same FA values their individual axial and radial diffusivities may vary greatly[18]. FA (equation 2) being calculated taking into account all the eigen values cannot show differences when one or more eigen values increase or decrease. In other words, FA can differentiate neither radial ( $\lambda_{\perp} = \frac{\lambda_2 + \lambda_3}{2}$ ) & axial ( $\lambda_{ll} = \lambda_1$ ) diffusivity figure 14, nor the tubular ( $\lambda_1 > \lambda_2 \approx \lambda_3$) & planar anisotropy ( $\lambda_1 \approx \lambda_2 > \lambda_3$) as shown in figure 15 below.

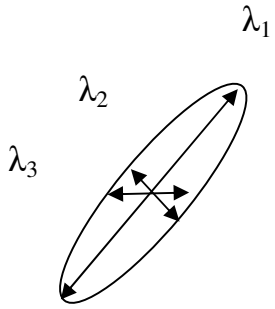


**Figure 14: Axial and radial anisotropies Lambda 1 (λ1) being along the fiber called as axial anisotropy and λ2 & λ3 being perpendicular to fiber orientation so their average named as radial anisotropy**

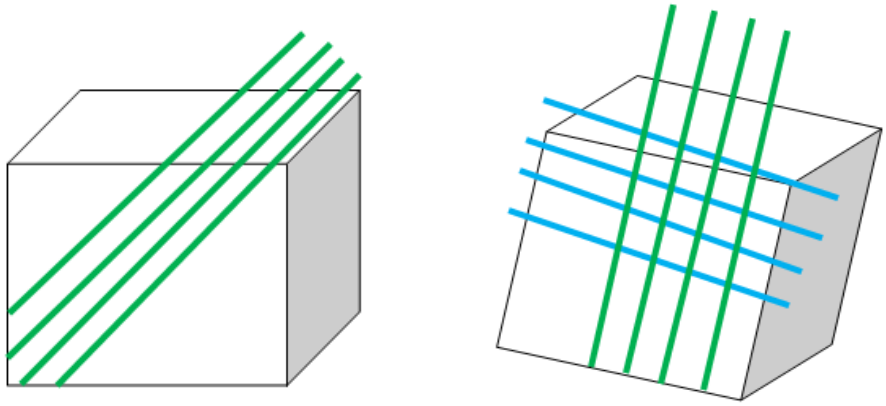


**Figure 15: Ilustration of Tubular anisotropy ( λ1 > λ2 ≈ λ3 ) A)and planar anisotropy ( λ1 ≈ λ2 > λ3) B). (where green and blue colors indicate different fiber populations)**

So in order to overcome the above drawbacks we propose to study radial and axial diffusivities, and Westin's CP = $(\lambda_2 - \lambda_3)/\lambda_1$ and CL = $(\lambda_1 - \lambda_2)/\lambda_1$ for tubular and planar anisotropy [19, 20]. As can be seen from the above definitions CL will be bright for tubular regions and dark for planar regions and CP on the other hand will be bright for planar regions and dark for tubular regions.

Other important issues that will be addressed in this work are: a) categorizing ALS patients into various subgroups and b) evaluating susceptibility artifacts in CST. Many DTI studies in ALS failed to categorize/classify ALS patients appropriately based

on their clinical symptoms thereby leading to inconclusive results[7, 17]. Since ALS patients manifest themselves with variable clinical symptoms (like predominant UMN, classic ALS, or predominant LMN symptoms) it is imperative to categorize them according to their clinical symptoms rather than pooling them under a single category of "ALS". Motivation to categorize ALS patients came from the observance of hyperintense signal along CST in T2-weighted images in some but not all of the ALS patients with predominant UMN signs[21, 22]. It is intriguing to know whether there is any difference in DTI metrics between UMN predominant ALS patients with and without hyperintensity along CST. We believe that categorization will enable us to better understand the pathophysiological mechanisms of ALS, for instance DTI measures will be used to determine whether the presence or absence of CST hyperintensities in UMN-predominant ALS patients results from (1) divergent pathologies in subcortical axons (if both groups show similar changes) or (2) degeneration of the perikaryon in motor cortex or extracranial CST (if differences are found between groups). Therefore, ALS patients were categorized into four different groups namely; a) predominant UMN ALS with hyperintense signal along CST (observed in their T2-weighted images), b) predominant UMN ALS without CST hyperintensity, c) ALS patients with mixed UMN and LMN signs (classic ALS), and d) ALS patients with frontotemporal dementia (FTD).

Most of the DTI studies in ALS employed single shot echo planar imaging (SS-EPI) sequence[7, 9, 10, 13, 15, 23-25]. SS-EPI suffers greatly from susceptibility artifacts at air-tissue-bone interfaces. Since most of the clinical DTI protocols are inherently devoid of field map acquisition scan we aimed to investigate the effects of susceptibility artifacts along

CST.

## 3.3 Aim

The goal of this study is to evaluate pathology in ALS using scalar DTI metrics like fractional anisotropy (FA) along the CST. We also aimed to explore the usefulness of indices namely; radial and axial anisotropy, Westin's CP and CL, which are yet to be studied in ALS.

## 3.4 Hypothesis

It is hypothesized that a) DTI metrics (FA, RA, MD, radial and axial diffusivities) will be significantly different in the CST among ALS subgroups and between ALS and control groups. b) If there is no difference in DTI metrics between CST hyperintense and non-hyperintense groups then there are divergent pathologies in subcortical axons. c) In classic ALS with mixed UMN and LMN findings, disease onset is more caudal when compared to UMN predominant ALS patients. d) CST will not be significantly affected by susceptibility artifacts.

## 3.5 Method

### 3.5.1 DTI Protocol

Clinically obtained MRI data and storage of de-identified images was approved by

the Institutional Review Board at the Cleveland Clinic as part of the "Neuroimaging Registry/Database for CNS Analysis in Patients with Motor Neuron Disease". DTI data of 8 control subjects (5 men, 3 women), 13 UMN predominant with CST hyperintensity ALS patients (C-group) (8 men, 5 women), 21 UMN predominant without CST hyperintensity ALS patients (B-group) (15 men, 6 women), 12 ALS patients with predominant LMN signs (E-group) (9 men, 3 women) and 14 ALS patients with dementia (D-group) (3 men, 11 women) was obtained using 1.5 T system (Siemens Symphony, Erlangen, Germany). DTI was performed using echo planar imaging (EPI) sequence along 12 diffusion weighted (b = 1000 s/mm$^2$) directions and one $b_0$ = 0 s/mm$^2$. Imaging parameters were: 30 slices, 4 mm thick, with 1.9×1.9 mm in-plane resolution; pulse sequence parameters were: TR = 6000 ms, TE = 121 ms, EPI factor = 128, number of averages = 6 and scan time = 7.54 minutes. Gradient-echo field map images were acquired to correct for geometrical distortion caused by susceptibility artifacts. Field map imaging parameters were: number of slices = 30, slice thickness = 4 mm, slice gap = 4 mm, TR=500 msec, TEs = 6.11 and 10.87 msec.

### 3.5.2 Data processing

DTI images were first corrected for distortion effects using FSL's FUGUE (http://www.fmrib.ox.ac.uk/fsl/)[26-28]. Undistorted DTI images were then processed using DTI Studio open software (https://www.mristudio.org/)[29].. DTI matrix for each voxel was calculated based on multivariate linear least square fit. The tensor matrix was then diagonalized to derive principal eigen values and eigen vectors. Maps of diffusion metrics namely Fractional anisotropy (FA), relative anisotropy (RA), mean diffusivity (MD),

parallel diffusivity ($\lambda_{||}$) radial diffusivity ( $\lambda_{\perp}$ ), Westin's linear (CL) and planar (CP) index were obtained. Virtual neuronal fibers were reconstructed using the fiber assignment by continuous tracking (FACT) algorithm[29] , described in detail elsewhere. Fiber tracking parameters were initiated from every voxel with FA = 0[32], threshold for termination was 0.2[32] and a bending angle of 41°.

After these preliminary processing steps, all subjects CST fiber tracts on both left and right sides were reconstructed after Wakana et al[32] by placing first ROI caudally in the cerebral peduncle (CP) and the second rostrally just below the primary motor cortex. Along the CST, four regions of interest (ROIs) were identified to evaluate the pathophysiological changes in ALS. These are cerebral peduncle (CP), internal capsule (IC), top of the lateral ventricle (LV) and subcortical motor cortex (MC). DTI metrics mentioned above were measured for each subject in these ROIs and were compared against controls and also between the patient subgroups. We randomly selected 19 of 68 subjects to study distortion effects caused by susceptibility artifacts along the CST. In these 19 subjects diffusion tensor matrix and the diffusion metrics were calculated for both conditions i.e. with and without field map corrections. ROIs of same size and shape were applied at CP and MC levels while reconstructing the CST in both with and without field map corrected images. The number of CST fibers, CST fiber volume and average FA along the entire CST were evaluated to determine the effects of susceptibility artifacts. Statistical comparisons for each of the DTI metrics across control and patient groups were carried out using SPSS 16.0. Based on data meeting the assumptions of ANOVA one of the following statistical methods was used with a significance level of $p < 0.05$; a)

one-way ANOVA followed by Tukey's post hoc test was carried out when the assumptions of both normality and equal variance were met. b) On the other hand only if the equal variance assumption was violated Welch ANOVA followed by Dunnett T3 post hoc test was employed. c) When both normality and equal variance assumptions were violated Kruskal-Wallis non-parametric approach followed by Bonferroni correction of Mann-Whitney test was used. The effects of susceptibility artifacts was evaluated by employing Student T-test or Mann-Whitney U test based on data meeting the assumptions of normality and equal variance.

## 3.6 Results

The statistical group comparison results along different levels of CST for FA, RA, MD, axial and radial diffusivities are given in Figures 16 to 20.

### 3.6.1 Fractional anisotropy

FA values were found to be reduced in all ALS groups when compared with the controls. FA values showed significant difference between control and the CST hyperintense, CST non-hyperintense and dementia groups at the level of IC. In addition to this, the ALS-dementia and CST hyperintense groups were significantly different from controls on the left CP. On the other hand FA values were significantly different between control and classic ALS groups only at the level of CP. Dementia patients were significantly different from the controls in CP and IC levels. Besides this, there was no significant difference among the ALS sub groups at any levels of the CST.

### 3.6.2 Relative anisotropy

Similar to FA results, RA values were found to be decreased in ALS patients when compared to controls. RA results were similar to FA values except that there was no significant difference between control and CST hyperintense and dementia groups on the left CP.

### 3.6.3 Axial and Radial diffusivities

In general, axial diffusivity values were reduced in ALS patients compared to controls. Axial diffusivity, on the other hand, showed significant differences between control and CST hyperintense, CST non-hyperintense and classic ALS groups mainly in the left IC; however with CST non-hyperintense group, the difference was significant on the right side too. Between ALS subgroups, axial diffusivity was significantly different between CST non-hyperintense group and dementia group at the level of IC. On the other hand, between classic ALS and ALS-dementia groups, significance was observed only in the right MC. Radial diffusivity values, on the other hand, were elevated in ALS patients compared to controls, and were almost identical to FA values at the IC level; at the CP level, radial diffusivity also reached significance between CST non-hyperintense and classic ALS groups. In addition, radial diffusivity was significantly different between control and ALS groups in the left LV, i.e. CST hyperintense and CST non-hyperintense, whereas significant differences were observed in both right and left LV levels between control and dementia patients.

### 3.6.4 Mean diffusivity

In general, MD values were elevated in ALS patients when compared to controls.

MD was significantly different between control and CST hyperintense and ALS-dementia groups in the left IC; the ALS-dementia group also showed significance at the LV level. Between ALS groups, comparisons resulted in significant differences between dementia and CST hyperintense, CST non-hyperintense and classic ALS groups in the right LV. In addition to this, the ALS-dementia group was also significantly different from CST non-hyperintense and classic ALS groups in the left IC.

### 3.6.5 Susceptibility artifact measures

Total number of CST fibers, fiber volume and average FA values along the entire CST were measured in order to evaluate susceptibility artifacts. These results are given in Table 3. No significant difference ($p>0.05$) was observed in any of the above measures obtained with or without field map correction.

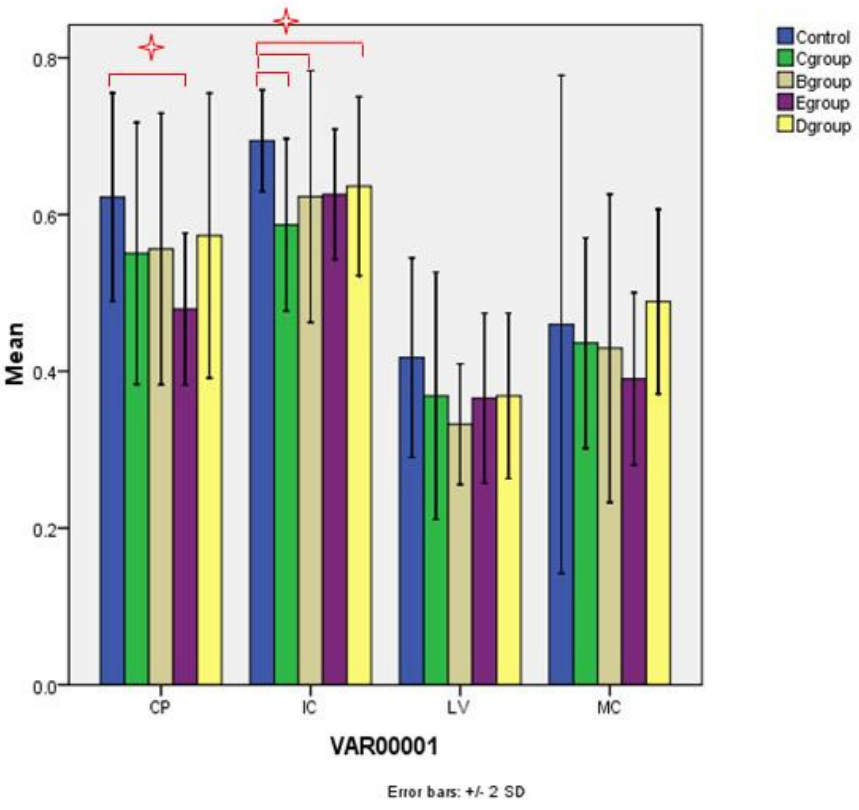


a)

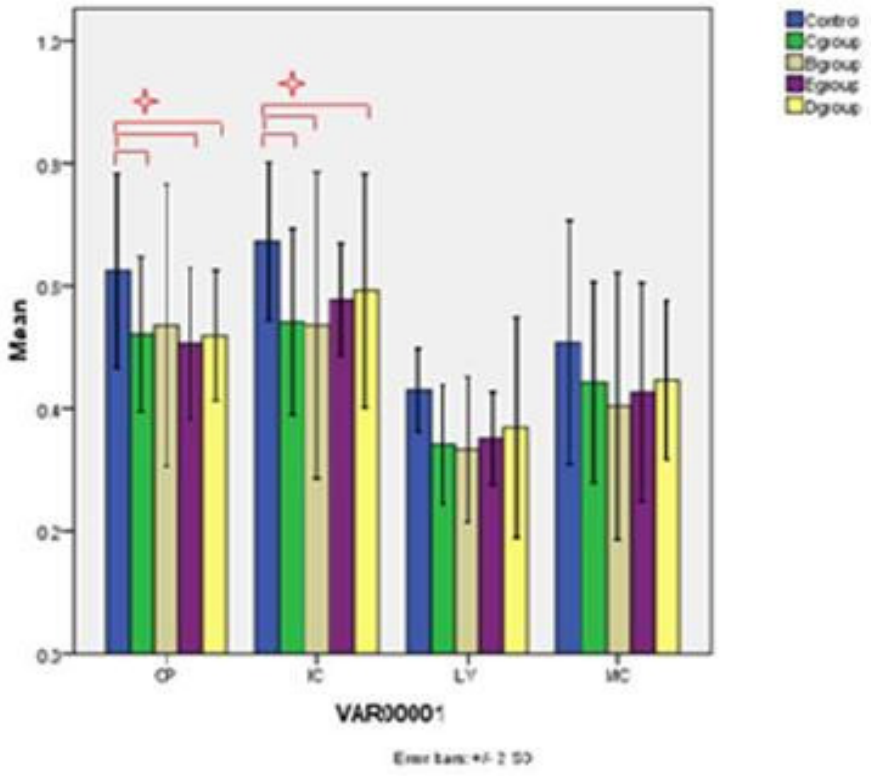


b)

Where CP- Cerebral peduncle, IC –Internal capsule, LV- Top of lateral ventricle, MC-Sub cortical motor cortex.

Significance at p<0.05

**Figure 16: FA results at various levels of CST a) Right CST and b)Left CST. revealing significant difference between groups at p<0.05**

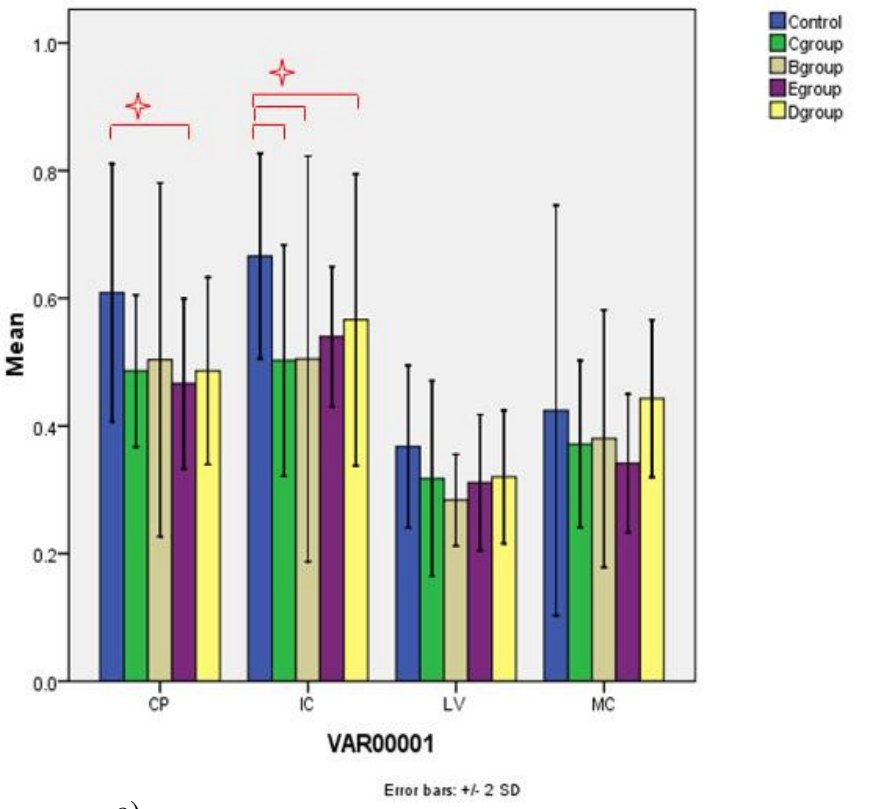
Control
Cgroup
Bgroup
Egroup
Dgroup
1.0
0.8
0.6
0.4
0.2
0.0
Mean
CP
IC
LV
MC
VAR00001
Error bars: +/- 2 SD

a)

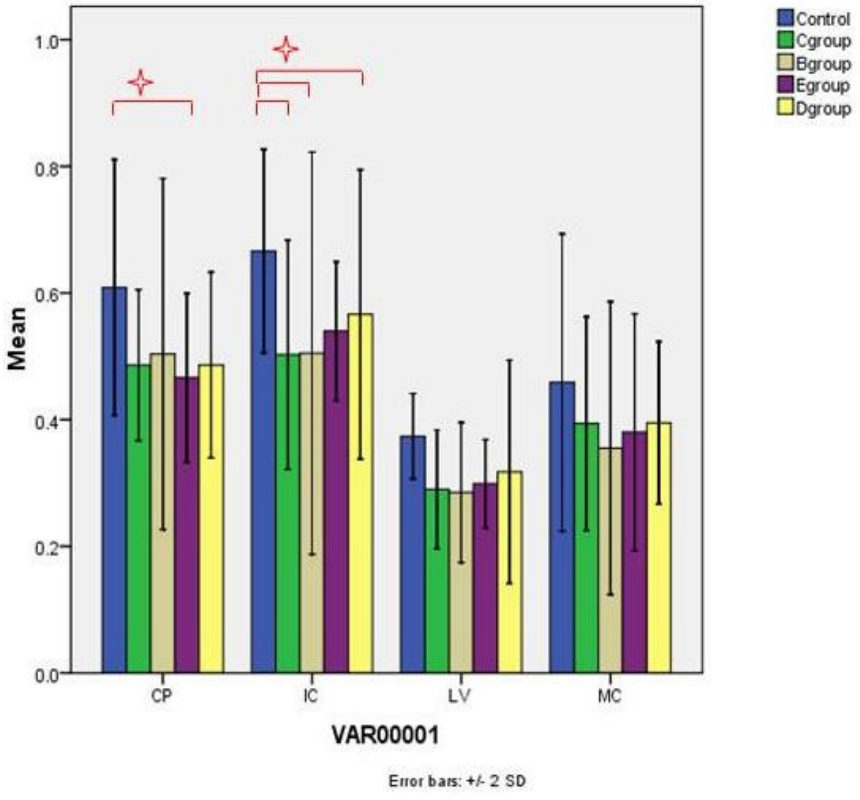
Control
Cgroup
Bgroup
Egroup
Dgroup
1.0
0.8
0.6
0.4
0.2
0.0
Mean
CP
IC
LV
MC
VAR00001
Error bars: +/- 2 SD

b)

Where CP- Cerebral peduncle, IC –Internal capsule, LV- Top of lateral ventricle, MC-Sub cortical motor cortex.

✧ Significance at p<0.05

**Figure 17: RA results at various levels of CST a) Right CST and b)Left CST revealing significant difference between groups at p<0.05**

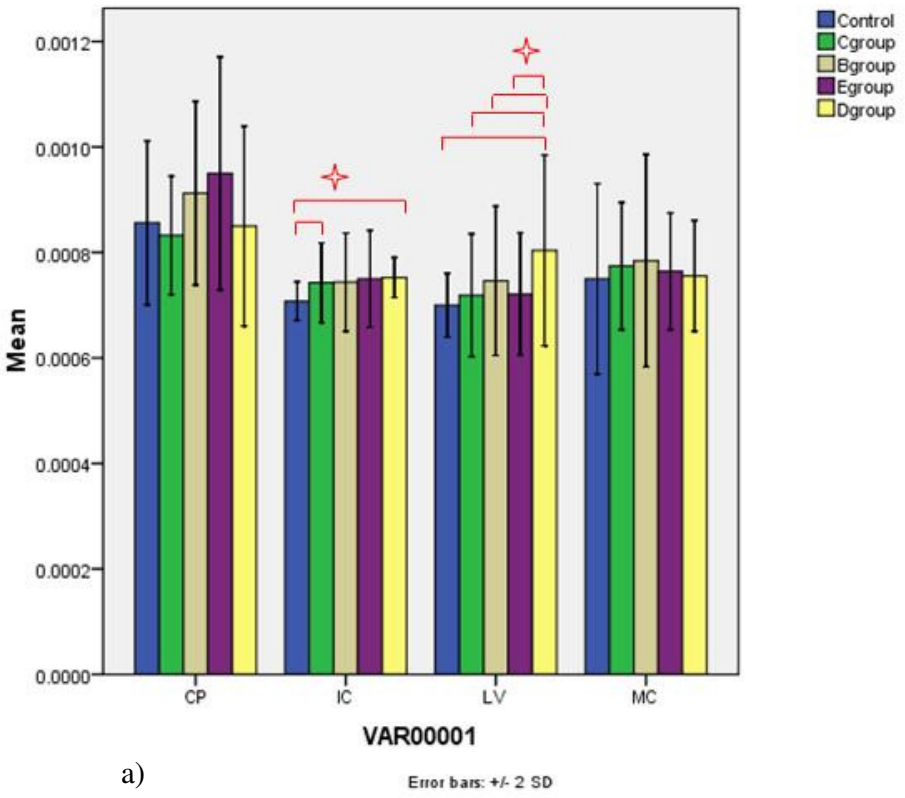


a)

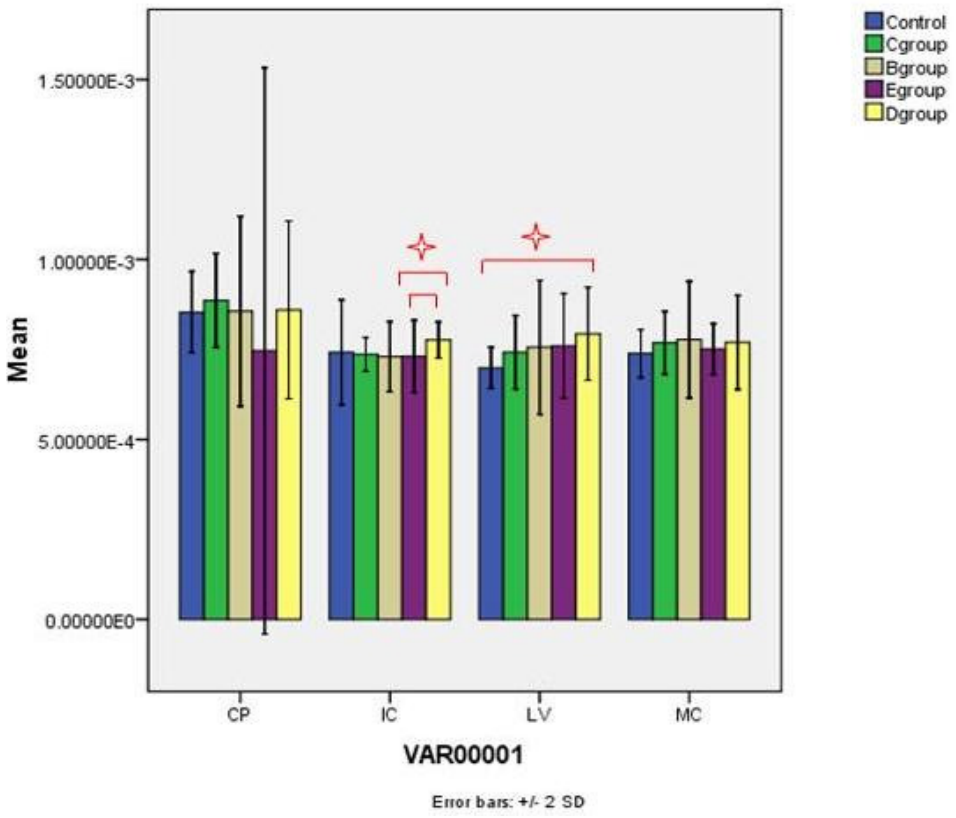


b)

Where CP- Cerebral peduncle, IC –Internal capsule, LV- Top of lateral ventricle, MC-Sub cortical motor cortex.

✧ Significance at p<0.05

**Figure 18: MD results at various levels of CST a) Right CST and b)Left CST revealing significant difference between groups at p<0.05**

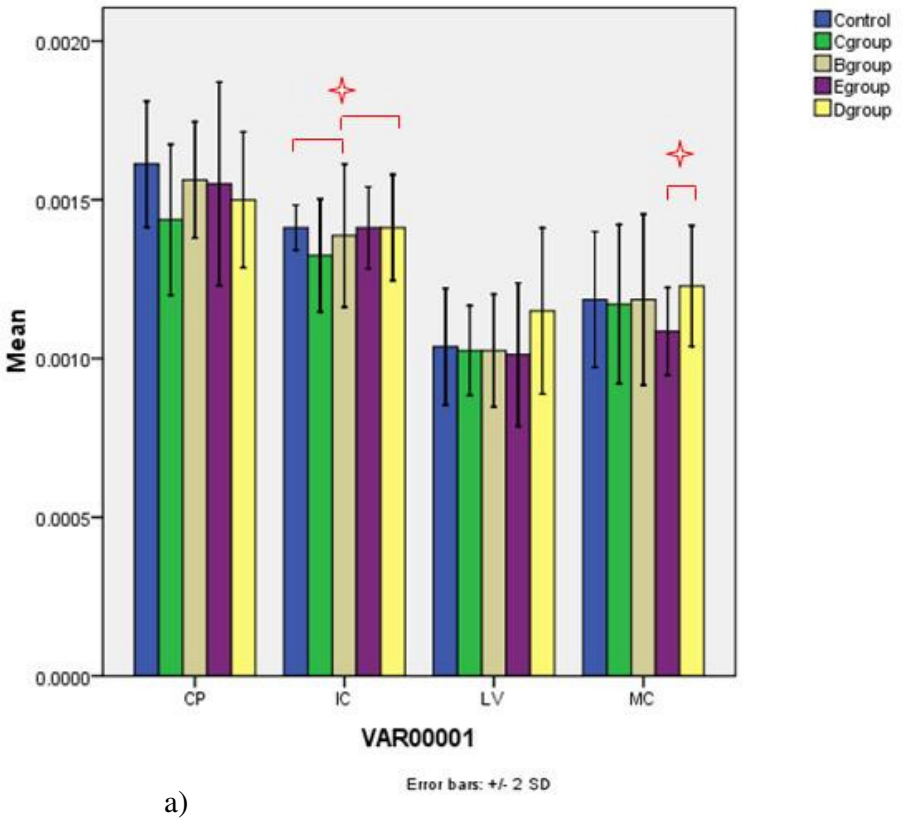
Control
Cgroup
Bgroup
Egroup
Dgroup
0.0020
0.0015
0.0010
0.0005
0.0000
Mean
CP
IC
LV
MC
VAR00001
Error bars: +/- 2 SD

a)

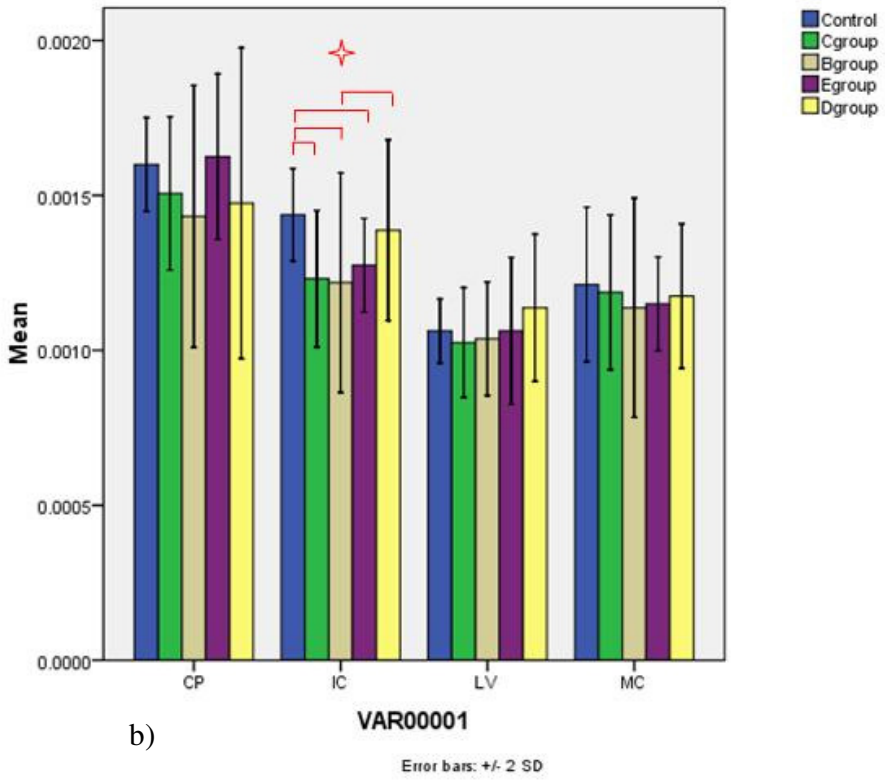
Control
Cgroup
Bgroup
Egroup
Dgroup
0.0020
0.0015
0.0010
0.0005
0.0000
Mean
CP
IC
LV
MC
VAR00001
Error bars: +/- 2 SD

b)

b)

Where CP- Cerebral peduncle, IC –Internal capsule, LV- Top of lateral ventricle, MC-Sub cortical motor cortex.

Significance at p<0.05

**Figure 19: Axial diffusivity results at various levels of CST a) Right CST and b)Left CST revealing significant difference between groups at p<0.05**

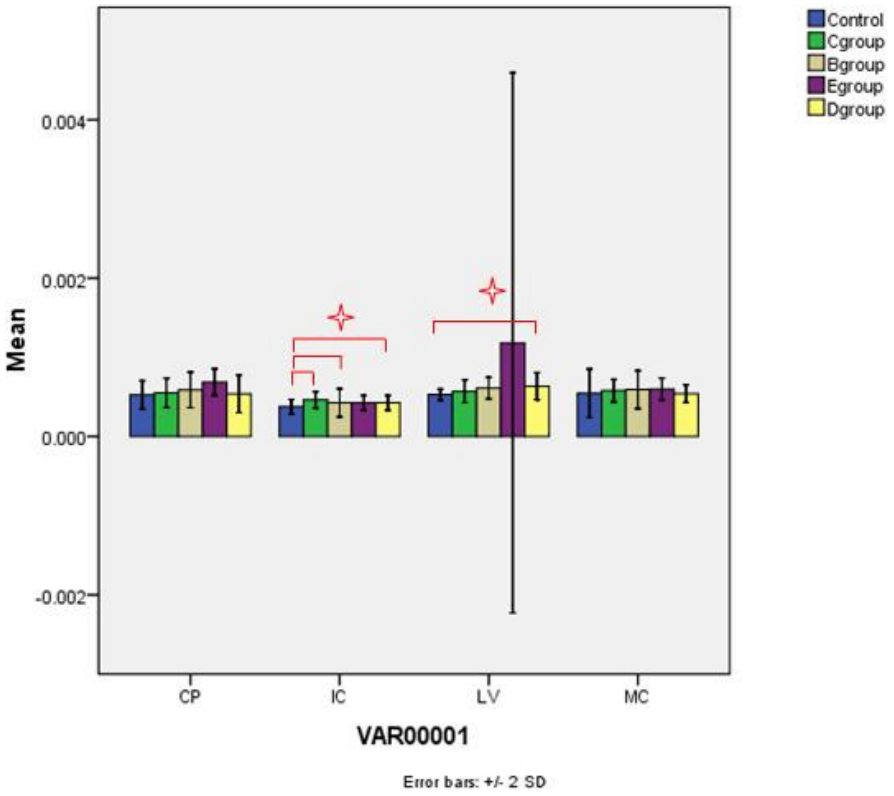


a)

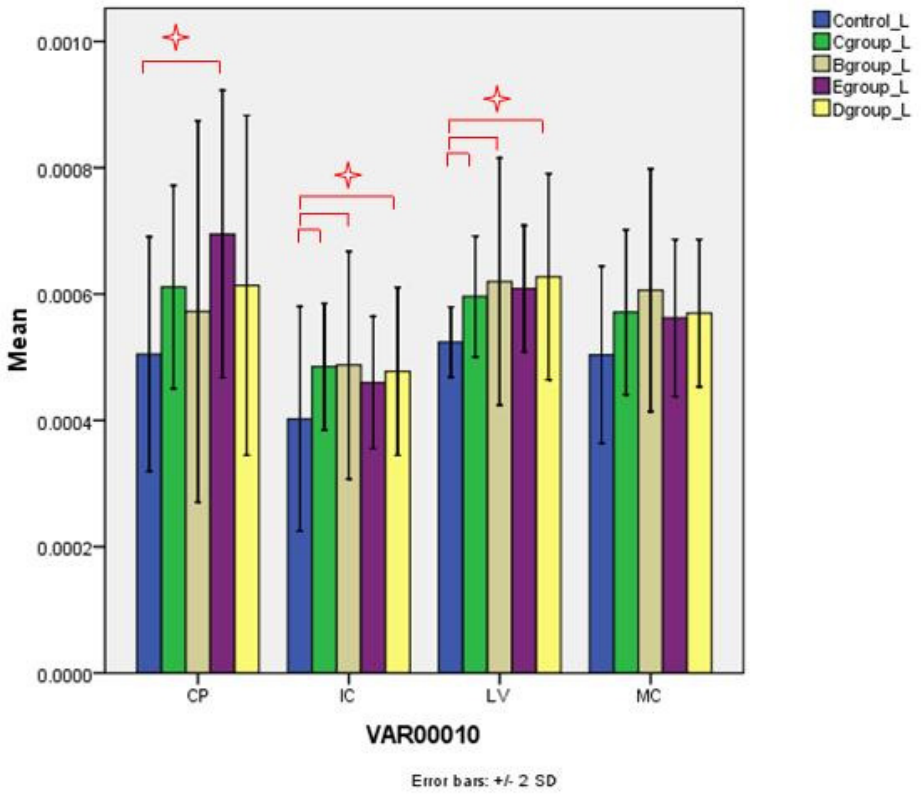


b)

Where CP- Cerebral peduncle, IC –Internal capsule, LV- Top of lateral ventricle, MC-Sub cortical motor cortex.

✧ Significance at p<0.05

**Figure 20: Radial diffusivity results at various levels of CST a) Right CST and b)Left CST revealing significant difference between groups at p<0.05**

## 3.7 Discussion

### 3.7.1 Fractional anisotropy

FA results seen in this study at the level of the IC agree well with previous ALS studies[8-10, 13, 15, 33]. Absence of significant differences between CST hyperintense and non-hyperintense groups in all the DTI metrics suggests that divergent pathologies may exist in the extracranial (e.g.spinal cord) axons of these two groups rather than degeneration of the perikaryon in motor cortex or extracranial CST. One of the reasons we didn't observe any significance at the MC level between CST hyperintense and non-hyperintense groups might have resulted from the truncation of CST below MC in 7 of 13 patients in the former group and **7** of 21 in the latter group. However, this was not observed in the ALS-dementia or in control subjects, however in the classic ALS group,only 2 of 12 subjects' left CST tracts were truncated below the MC level. Since acquisition and post-processing of images in all groups were performed identically, we believe the extent of CST degeneration is greater in these patients than in the others. Figure 21 a) shows the CST in a control subject and figure 21 b) shows absence of CST in MC in a UMN predominant CST hyperintensity patient. Further studies are required in order to validate these findings.

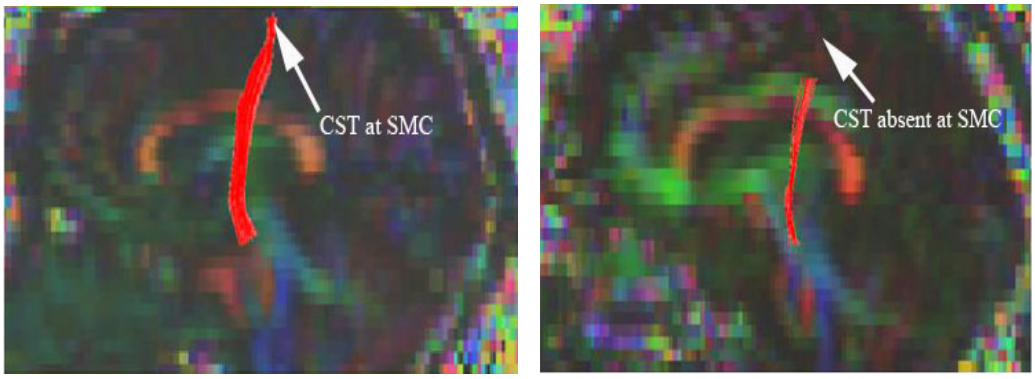


a) b)

**Figure 21: Sagittal view of FA color map shows localization of using subject's own tractography-derived CST a) control b) UMN predominant hyperintense patient**

### 3.7.2 Relative anisotropy

Jacob et al[33] observed reduction in RA values in the pyramidal tract in one UMN ALS patient before and after a 9 month follow-up, while no significant difference was reported in two patients with LMN and bulbar symptoms. In our study, RA values were significantly different between the classic ALS group and controls in the CP, whereas comparison between other ALS groups (CST hyperintense, non-hyperintense and dementia groups) and controls significance was reached only in the IC. Since the study paradigms are different and a very small population of ALS patients was studied by Jacob et al[33] the results are difficult to compare.

### 3.7.3 Axial and Radial diffusivities

Christian Beaulieu[18] showed that changes in FA values can result from either decreased axial diffusivity, increased radial diffusivity, or both. He also demonstrated that two subjects can have the same FA values but individual axial and radial diffusivity values may differ. Beaulieu[18] also shows some encouraging evidence from animal and human studies suggesting that axial diffusivity physiologically corresponds to axonal degradation and radial diffusivity to myelin degradation. However, these interpretations should be interpreted with caution because they are likely over-simplifications and further studies are warranted to confirm these above findings. Nonetheless, The above factors suggest that a more accurate physiological insight can be obtained by using axial and radial diffusivities.

Axial diffusivity values in our study reached significance only at the IC level between control and ALS groups whereas, Wong et al[34] showed significant increase only in corona radiata. In our study, we observed a decreasing trend in axial diffusivity values from the CP to MC in both control and ALS patients. Discrepancies in these results may be due to the following factors: a) ALS group studied by Wong et al included both bulbar- and limb-onset patients, b) small sample size (only 14 ALS subjects), c) less number of diffusion weighting directions in both studies (Wong et al employed 6 directions, ours 12 directions) whereas studies by Jones et al[35] and Ni et al[36] recommend 30 directions for robust estimation of individual eigen values $\lambda_1$, $\lambda_2$ and $\lambda_3$, d) significant partial volume effects from thicker slices (Wong et al's 5 mm thickness, ours 4 mm), e) compared to manual ROI tracing, tractography methods result CST identification which is more

accurate, more reproducible[37], free from operator bias, and less time intensive. Tractography methods on the other hand are sensitive to signal to noise ratio, anatomical variability between subjects[6] and resolution. An interesting finding in our study was that axial diffusivity revealed significant differences between the ALS subgroups which was not observed with FA or RA. Axial diffusivity values were significantly elevated in the ALS-dementia group at the IC level when compared with the CST hyperintense group, and at the right MC level when compared with classic ALS group.

Radial diffusivity values revealed some variation in our ALS patients when compared to controls, being elevated in the MC, reduced in IC and increased in CP. On the other hand, Wong et al showed a decreasing trend rostrocaudally from the corona radiata to the CP. They failed to observe significant differences between ALS patients and control subjects whereas in our study radial diffusivity not only showed significant difference between these groups, but we also found it to be significantly elevated in the classic ALS group when compared with UMN predominant CST non-hyperintense group. An interesting point here is that radial diffusivity values between control and UMN predominant CST hyperintense, UMN predominant CST non-hyperintense and ALS-dementia groups were not significantly different at CP level but were more rostrally, i.e. at IC and LV levels. In contrast, control and classic ALS groups showed significant radial diffusivity differences only at the CP level and not higher up along the CST. Values were significantly higher in the classic ALS group, when compared to UMN predominant CST non-hyperintense group suggesting a more pronounced CST degeneration in the classic ALS patients (who have prominent LMN degeneration) at the CP level when compared to

the UMN group. Diffusion metrics FA, RA also showed significant differences between control and classic ALS groups at the CP level but not rostrally along the CST. Taken together, our findings suggest that axon degeneration in classic ALS patients (who have prominent LMN signs) may be more caudal (e.g., at the spinal cord level) when compared with UMN group (who do not). To our knowledge, this is the first MRI study using tractography to evaluate axial and radial diffusivities along the CST in large subgroups of ALS patients.

### 3.7.4 Mean diffusivity

In general MD values in ALS patients were found to be elevated at all the levels of the CST when compared with controls. However, MD values reached significance more rostrally i.e. in LV and IC levels between control and ALS groups and also among ALS subgroups. Between group comparisons showed significant increases in MD values in the left IC of ALS-dementia patients when compared with classic ALS and UMN CST non-hyperintense groups. Our results at the IC level agree with other ALS studies[7, 38, 39]. However, Yin et al[39] in their study group of ALS patients (6 limb onset , 2 bulbar onset) found no significant differences in MD values at IC.

### 3.7.5 Westin's linear (CL) index and planar index (CP)

The values of DTI metrics along the CST at the LV level were found to be slightly different from those of the other 3 ROIs. In our control subjects, axial diffusivity values were lowest in LV region compared to those at CP, IC & MC levels, and radial diffusivity values were higher in LV region compared with other 3 ROIs. Since the LV ROI is in a

region where superior longitudinal fasciculus fibers cross with the CST, we explored this using Westin's linear index (CL) and planar index (CP)[19, 20]. Westin's index is a geometrical index which measures the shape of the diffusion tensor ellipsoid against scalar measures like FA. Westin's CL (where $\lambda_1 >> \lambda_2 \approx \lambda_3$) measures uniformity of tracts in a voxel whereas Westin's CP (where $\lambda_1 \approx \lambda_2 >> \lambda_3$) indicates fiber crossings. If there is fiber crossing, the planar index (CP) will have high values (close to 1) whereas the linear index (CL) will be low (close to 0). Table III gives Westin's CL and CP (left and right side combined) for all the 4 ROIs in control subjects. Average linear values (CL) were found to be lower in LV region when compared with other 3 ROIs, on the other hand planar values were comparatively elevated in LV. Figure 22 a) and (b) shows changes in CL values at the level of cerebral peduncle and in LV. Figure 23 (a) and (b) are the color maps of CL at cerebral peduncle and LV obtained by using CL map and first eigen vector. High linear index and low planar values in CP and IC agree well with the anatomical structure of CST in these regions (i.e. highly coherent and uniform), so reduced linear index and slightly elevated planar index in LV indicates that there may be more than one fiber population in this region.

**Table III: Average values of Westin's linear and planar indices at different levels of CST**

| Westin's Index | CP | IC | LV | MC |
|---|---|---|---|---|
| Linear index (CL) | 0.64 | 0.68 | 0.41 | 0.46 |
| Planar index (CP) | 0.09 | 0.12 | 0.19 | 0.15 |

CP-cerebral peduncle, IC-internal capsule, LV-top of lateral ventricle, MC-subcortical motor cortex

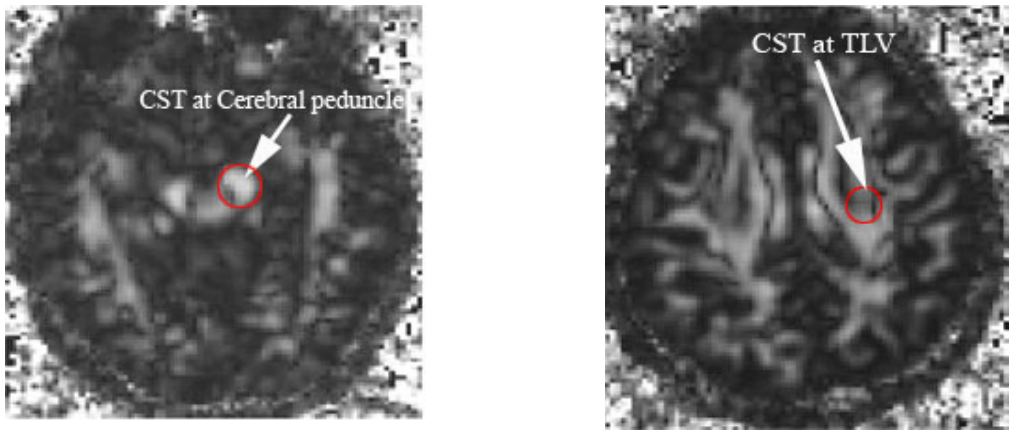


a) **b)**

**Figure 22: Transverse image of a control subject's CL map a) Cerebral peduncle level, b) top of lateral ventricle level**

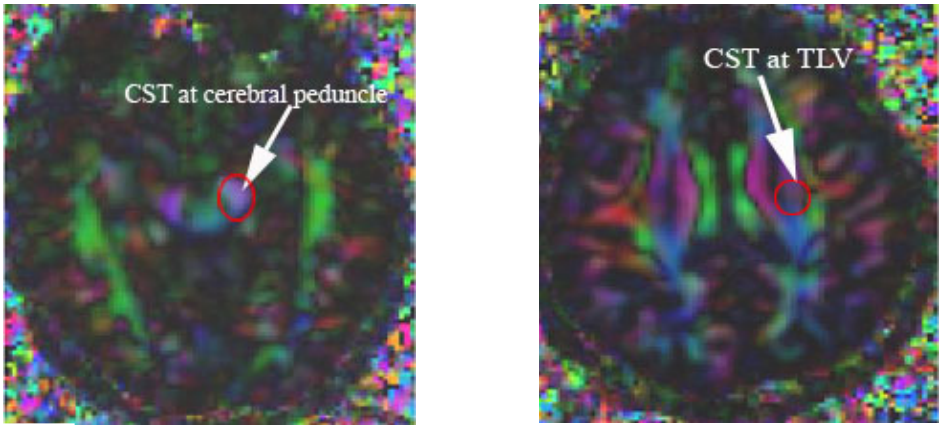


a) b)

**Figure 23: Transverse image of a control subject's CL color map a) Cerebral peduncle level, b) top of lateral ventricle level**

### 3.7.6 Evaluating susceptibility artifacts in CST

Figure 24 (a) and (b) shows DW images before and after field map correction. It can be seen from Table IV that parameters number of fibers, fiber volume and average FA values remain almost identical in CST between with and without field map correction procedures which suggests that CST is not affected by susceptibility artifacts. Under regular conditions, field maps were not acquired as part of clinical DTI protocols. Since most of the clinical studies employ SS-EPI sequence we believe that susceptibility artifacts need to be corrected before employing these images for any research purpose because to our knowledge there are no post-processing techniques available today to correct for these distortions. However, the results of this study indicate that if CST is the primary region of interest then field map acquisitions may not be required.

Table IV: Measures to evaluate susceptibility artifacts in CST

| Measure | Number of fibers | | Fiber volume (number of voxels) | | FA | |
|---|---|---|---|---|---|---|
| | With field map | Without field map | With field map | Without field map | With field map | Without field map |
| Mean±SD | 48.82 ±48.79 | 42.58±46.44 | 195.95 ±160.42 | 183.36 ±157.71 | 0.502±0.05 | 0.501±0.05 |
| Median | 34.5 | 23 | 158.5 | 149.5 | 0.497 | .499 |
| Quartiles ($1^{st}$, $3^{rd}$) | 14, 63.50 | 12, 63.50 | 101.25, 230.25 | 105.25, 191.75 | 0.465 0.530 | 0.474, 0.530 |
| Mann-Whitney U test / T-test | P=0.395 | | P=0.617 | | P=0.963 | |

SD- standard deviation

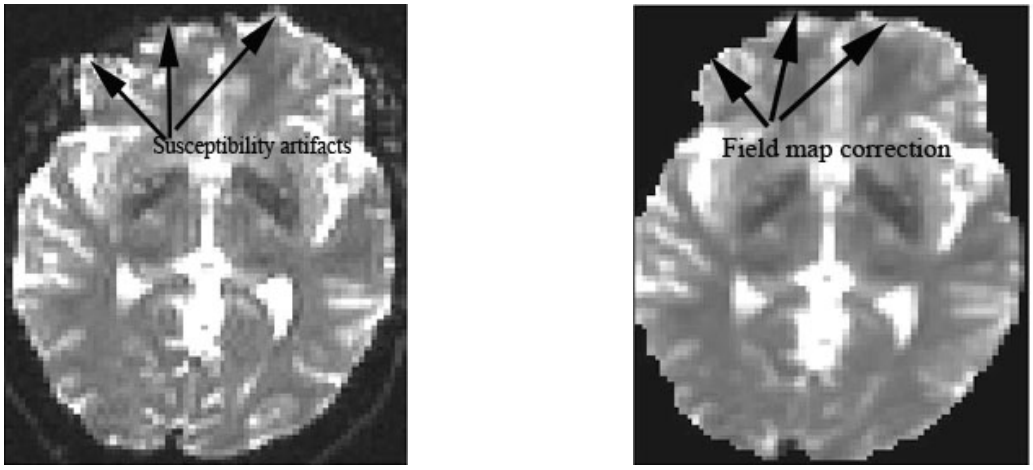


a). b).

**Figure 24: Transverse image showing susceptibility artifacts in frontal regions of the brain a) before correction, b) after correction in one of our subjects**

In essence, the discrepancies seen in results between our study and the ALS literature can be due to some of the following factors; a) tractography method is sensitive to signal to noise ratio, anatomical variability between subjects and resolution. According to Mori[6], tractography method gives 30% variability even when used within control subjects. b) On the other hand ROI approach suffers from operator bias, poor reproducibility and is time consuming. c) Studies[35, 36] have shown that at least 30 directional measurements are required for robust estimation of eigen values whereas only 12 directional DTI data was acquired in our study (due to scanner software constraints). d) Thicker slices of 4 mm in our study will contribute of partial volume effects and anisotropic voxels may affect tractography results.

## 3.8 Conclusion

One caveat is that comparing and contrasting results of this study with others may be inaccurate because of differences in used DWI schemes and sequences, number of gradient directions, and methods to process DTI images. However, similarities between results from this and previous DTI studies are changes in FA and MD values at the level of internal capsule in ALS patients compared to controls. This study shows that axial and radial diffusivities provide additional information when compared to anisotropy measures FA or RA. To our knowledge, this is the first study to assess diffusion metrics in a large group of ALS patients after being categorized into different subgroups, and to demonstrate that CST measures remain unaffected by susceptibility artifacts. This study also shows that subcategorizing ALS patients by clinical features (e.g., extent of UMN and LMN dysfunction) reveals group-specific differences in DTI metrics which suggests variance in ALS pathogenesis, increasingly considered a syndrome rather than a single disease. Finally, by showing that DTI measures along the CST are unaffected by susceptibility artifacts, additional field map correction sequences would not be necessary for clinical imaging protocols, thereby saving time and data storage space. However, future studies with larger sample sizes of subgroups and using robust DW acquisition schemes are warranted to confirm our findings.

## 3.9 Limitations and Future scope

The main limitation of this study is the low directional DTI data (12 directions), anisotropic voxels which result in suboptimal signal to noise ratio, and thicker slices contributing to partial volume effects. Future studies will utilize probabilistic tracking

instead of the deterministic approach (used in this study) to reconstruct the entire CST to assess the reason for its truncation rostrally in some ALS patient subgroups. This will reveal whether the truncation is due to differences in the disease process and provide novel insights into pathogensis. Adding more control subjects will increase the power of the statistical tests. Future comparisons of DTI and post-mortem histopathology in the same patient will allow radiopathologic correlation of tissue pathology underlying the radiographic changes, including CST hyperintensity.

Next study addresses assessment of neuronal integrity in ALS patients using high resolution T1 weighted images . Quantitative measurements techniques such as voxel based morphometry and cortical thickness were used to assess grey matter volume changes especially in ALS patients when compared to controls.

## 3.10 References


**1.** Lowe MJ, Horenstein C, Hirsch JG, et al. Functional pathway-defined MRI diffusion measures reveal increased transverse diffusivity of water in multiple sclerosis. *Neuroimage.* Sep 2006;32(3):1127-1133.

**2.** Filippi M, Cercignani M, Inglese M, et al. Diffusion tensor magnetic resonance imaging in multiple sclerosis. *Neurology.* Feb 13 2001;56(3):304-311.

**3.** Cosottini M, Giannelli M, Siciliano G, et al. Diffusion-tensor MR imaging of corticospinal tract in amyotrophic lateral sclerosis and progressive muscular atrophy. *Radiology.* Oct 2005;237(1):258-264.

**4.** Ulug AM, Grunewald T, Lin MT, et al. Diffusion tensor imaging in the diagnosis of primary lateral sclerosis. *J Magn Reson Imaging.* Jan 2004;19(1):34-39.

**5.** Pioro EP. Neuroimaging in ALS and ALS with Frontotemporal Dementia. In: Dementia and Motor Neuron Disease: Informa Healthcare 2006. MJ Strong, ed.

**6.** Mori S. Introduction to Diffusion Tensor Imaging. UK: Elsevier; 2007.

**7.** Toosy AT, Werring DJ, Orrell RW, et al. Diffusion tensor imaging detects corticospinal tract involvement at multiple levels in amyotrophic lateral sclerosis. *J Neurol Neurosurg Psychiatry.* Sep 2003;74(9):1250-1257.

**8.** Ellis CM, Simmons A, Jones DK, et al. Diffusion tensor MRI assesses corticospinal tract damage in ALS. *Neurology.* Sep 22 1999;53(5):1051-1058.

**9.** Graham JM, Papadakis N, Evans J, et al. Diffusion tensor imaging for the assessment of upper motor neuron integrity in ALS. *Neurology.* Dec 14 2004;63(11):2111-2119.

**10.** Schimrigk SK, Bellenberg B, Schluter M, et al. Diffusion tensor imaging-based fractional anisotropy quantification in the corticospinal tract of patients with amyotrophic lateral sclerosis using a probabilistic mixture model. *AJNR Am J Neuroradiol.* Apr 2007;28(4):724-730.

**11.** Hong YH, Lee KW, Sung JJ, et al. Diffusion tensor MRI as a diagnostic tool of upper motor neuron involvement in amyotrophic lateral sclerosis. *J Neurol Sci.* Dec 15 2004;227(1):73-78.

**12.** Ashburner J, Friston KJ. Voxel-based morphometry--the methods. *Neuroimage.* Jun 2000;11(6 Pt 1):805-821.

**13.** Sach M, Winkler G, Glauche V, et al. Diffusion tensor MRI of early upper motor neuron involvement in amyotrophic lateral sclerosis. *Brain.* Feb 2004;127(Pt 2):340-350.

**14.** Thivard L, Pradat PF, Lehericy S, et al. Diffusion tensor imaging and voxel based morphometry study in amyotrophic lateral sclerosis: relationships with motor disability. *J Neurol Neurosurg Psychiatry.* Aug 2007;78(8):889-892.

**15.** Abe O, Yamada H, Masutani Y, et al. Amyotrophic lateral sclerosis: diffusion tensor tractography and voxel-based analysis. *NMR Biomed.* Oct 2004;17(6):411-416.

**16.** Strong MJ. The syndromes of frontotemporal dysfunction in amyotrophic lateral sclerosis. *Amyotroph Lateral Scler.* Dec 2008;9(6):323-338.

**17.** Wang S, Poptani H, Bilello M, et al. Diffusion tensor imaging in amyotrophic lateral sclerosis: volumetric analysis of the corticospinal tract. *AJNR Am J Neuroradiol.* Jun-Jul 2006;27(6):1234-1238.

**18.** Beaulieu C, ed. *Diffusion MRI: From quantitative measurement to in vivo neuroanatomy.* First ed. ed. San Diego, CA,USA: Elsevier; 2009. Heidi J TEJB, ed.

**19.** Westin C- F, Peled S, Gudbjartsson H, et al. Geometrical Diffusion Measures for MRI from Tensor Basis Analysis. *ISMRM*; 1997.

**20.** Westin C- F, Maier SE, Mamata H, et al,. Processing and visualization for diffusion tensor MRI. *Med Image Anal.* Jun 2002;6(2):93-108.

**21.** Mitusmoto H, Chad DA, Pioro, EP. Amyotrophic Lateral Sclerosis Contemporary Neurology Series: Oxford University Press,Philadelphia; ; 1998.

**22.** Yagishita A, Nakano I, Oda M, et al. Location of the corticospinal tract in the internal capsule at MR imaging. *Radiology.* May 1994;191(2):455-460.

**23.** Ciccarelli O, Behrens TE, Altmann DR, et al. Probabilistic diffusion tractography: a potential tool to assess the rate of disease progression in amyotrophic lateral sclerosis. *Brain.* Jul 2006;129(Pt 7):1859-1871.

**24.** Roccatagliata L, Bonzano L, Mancardi G, et al. Detection of motor cortex thinning and corticospinal tract involvement by quantitative MRI in amyotrophic lateral sclerosis. *Amyotroph Lateral Scler.* Feb 2009;10(1):47-52.

**25.** Yin H, Cheng SH, Zhang J, et al. Corticospinal tract degeneration in amyotrophic lateral sclerosis: a diffusion tensor imaging and fibre tractography study. *Ann Acad Med Singapore.* May 2008;37(5):411-415.

**26.** Jenkinson M. Fast, automated, N-dimensional phase-unwrapping algorithm. *Magn Reson Med.* Jan 2003;49(1):193-197.

**27.** Jenkinson M. Improving the registration of B0-disorted EPI images using

calculated cost function weights. *Tenth IntConf on Functional Mapping of the Human Brain*; 2004.

**28.** Smith SM, Jenkinson M, Woolrich MW, et al. Advances in functional and structural MR image analysis and implementation as FSL. *Neuroimage.* 2004;23 Suppl 1:S208-219.

**29.** Jiang H, van Zijl PC, Kim J, Pearlson GD, Mori S. DtiStudio: resource program for diffusion tensor computation and fiber bundle tracking. *Comput Methods Programs Biomed.* Feb 2006;81(2):106-116.

**30.** Leemans A, Jones DK. The B-matrix must be rotated when correcting for subject motion in DTI data. *Magn Reson Med.* Jun 2009;61(6):1336-1349.

**31.** Sage CA, Van Hecke W, Peeters R, et al. Quantitative diffusion tensor imaging in amyotrophic lateral sclerosis: revisited. *Hum Brain Mapp.* Nov 2009;30(11):3657-3675.

**32.** Wakana S, Caprihan A, Panzenboeck MM, et al. Reproducibility of quantitative tractography methods applied to cerebral white matter. *Neuroimage.* Jul 1 2007;36(3):630-644.

**33.** Jacob S, Finsterbusch J, Weishaupt JH, Khorram-Sefat D, Frahm J, Ehrenreich H. Diffusion tensor imaging for long-term follow-up of corticospinal tract degeneration in amyotrophic lateral sclerosis. *Neuroradiology.* Sep 2003;45(9):598-600.

**34.** Wong JC, Concha L, Beaulieu C, Johnston W, Allen PS, Kalra S. Spatial profiling of the corticospinal tract in amyotrophic lateral sclerosis using diffusion tensor imaging. *J Neuroimaging.* Jul 2007;17(3):234-240.

**35.** Jones DK. The effect of gradient sampling schemes on measures derived from diffusion tensor MRI: a Monte Carlo study. *Magn Reson Med.* Apr 2004;51(4):807-815.

**36.** Ni H, Kavcic V, Zhu T, et al. Effects of number of diffusion gradient directions on derived diffusion tensor imaging indices in human brain. *AJNR Am J Neuroradiol.* Sep 2006;27(8):1776-1781.

# CHAPTER IV

# Voxel Based Morphometry and Cortical Thickness in ALS

## 4.1 Voxel Based Morphometry

### 4.1.1 Introduction

Although ALS has been traditionally regarded as purely a motor neuron disease, there is increasing awareness of extramotor involvement, especially of brain regions subserving cognition and behavior[1]. Unlike dementia in Alzheimer's disease, the cognitive impairment seen in some patients with ALS affects predominantly frontotemporal areas and is known as frontotemporal dementia (FTD). A recent discovery that nuclear TDP-43 protein is mislocalized to the cytoplasm in patients with ALS, FTD, or both is the first pathobiologic link between these two conditions[2].

2,3-FDG positron emission tomography (PET) studies of ALS patients with co-existent dementia have revealed reduced cerebral blood flow in frontotemporal regions which indicates neuronal hypometabolism, as shown in figure 25. When dementia is advanced, cerebral atrophy usually is detected on MRI.

In this study we aim to understand the extent of extramotor involvement in ALS patients by assessing the degree of atrophy in gray matter (GM) structures in different patient subgroups using 3D high resolution T1-w images.

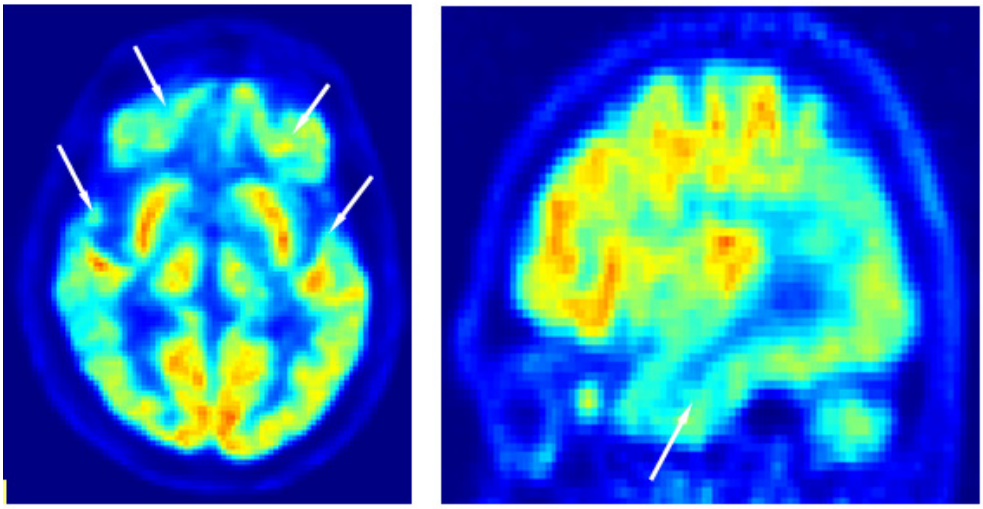

**Figure 25: [18F]2-fluoro-2-deoxy-D-glucose PET brain imaging of an ALS dementia patient showing reduced metabolism in both temporal lobes (arrowheads) and inferior frontal lobes (arrowheads).**

Conventional MRI of ALS patient brain usually shows little if any atrophy, although this is likely a misrepresentation because of the qualitative nature of these studies[3]. Quantitative assessment of high resolution 3D MR images will allow more precise measures of GM and white matter (WM) loss in ALS. Post mortem studies have revealed various forms of cortical pathology in ALS ranging from obvious neuronal loss to neuronal shrinkage but no loss or no obvious pathology, all in the setting of

proliferation and hypertrophy of neuroglia, which add to the complexity of the degrees of cortical atrophy in ALS.

Voxel-based morphometry (VBM) analysis allows objective and automated detection of structural differences in brain tissue (e.g. atrophy) between subjects after normalizing for random shape differences[4]. Being an unbiased assessment, it can be used for exploratory analyses when no *a priori* knowledge of distribution in pathology is available. For example, atrophy in ALS may occur outside motor regions, especially when patients have additional dementia, making VBM-based morphometry an ideal approach to studying this. Once the patient's brain is fitted to common brain template (e.g., study-specific template created from a sub-group of patients under study) which normalizes for any random variation between brains shapes and sizes, it is smoothed and a statistical parametric map generated of grey matter from which significant differences in tissue amounts are identified between patient and control brain templates.

Atrophy measures in ALS GM and WM throughout the brain will also assess the growing belief that ALS is a multisystem disease and not restricted to motor regions, even in patients without frontotemporal dementia (FTD)[1, 5, 6]. Ellis and colleagues were the first to apply VBM to ALS patient brains[6]. Their study using T2-weighted images showed significant differences in GM and WM volumes between ALS and control subjects and also between ALS with limb-onset and bulbar-onset groups. Using VBM, Chang and collaborators studied GM and WM changes in ALS patients with ($n$=10) and without ($n$=10) FTD when compared to control subjects ($n$=20)[7]. No WM volume

change was observed either between ALS subgroups or between ALS and controls subjects. Distribution of GM volume change was similar between ALS with and without FTD except that ALS-FTD patients had more atrophy in motor, premotor and frontal and posterior thalamus. Based on these observations, they concluded that a continuum of cortical atrophy exisits between these two ALS groups. Abrahams and colleagues studied GM and WM changes in ALS patients with and without cognitive impairment which was assessed based on verbal fluency test[5]. ALS patients with FTD were excluded from their study. ALS with cognitive impairment showed extensive atrophy changes in both motor and in extra- motor (frontal and temporal) WM structures when compared to both controls and unimpaired ALS patients. However, no significant change was observed in any of the GM structures. They also reported that the above changes were consistent with their PET studies suggesting that cognitive impairment may be more common in ALS patients and not restricted only to ALS patients with dementia. Mezzapesa and collaborators on the other hand, studied atrophy changes in 9 healthy and 16 ALS patients without any cognitive deficits[8]. VBM results showed significant ($p<0.001$, uncorrected) reductions in gray matter volume in temporal and frontal lobes of non-demented ALS patients compared to controls, although WM volume loss was not observed.

### 4.1.2 Limitations of previous studies

Large slice thickness (e.g., 3 mm in studies by Abrahams et al[5] and Chang et al[7]) contributes to partial volume effects; voxel resolution of 1×1×1 mm is highly recommended for VBM studies[7] . Absence of significant differences in clinical measures between ALS-FTD and ALS groups in the study by Chang and colleagues raises concerns

regarding criteria used to classify ALS patients into subgroups[7]. The study by Ellis and collaborators, on the other hand, employed T2-weighted images, which suffer from poor tissue contrast between GM and WM structures[6]. Inadequate information was provided by Abraham and colleagues regarding level of significance and multiple comparisons, making assessment of their methodology difficult[5]. In addition, Mezzapesa and collaborators identified $p<0.001$ but this was uncorrected for multiple comparisons[8]. This raises significant statistical concerns considering VBM tests the same hypothesis in every voxel and correcting for multiple comparisons is therefore mandatory. Furthermore, the aforementioned studies all employed Gaussian random field theory based statistical comparisons for which the analyzed data should have had Gaussian distribution. However, several studies[9-11] have shown that these criteria are difficult to verify and meet due to inherent noise in the data and so recommend non-parametric permutation based analyses for statistical comparisons. Therefore, the discrepancies seen in the above studies can be attributed to various factors, including: methodological differences (e.g., imaging parameters, statistical analyses) and combining patients with differing clinical presentations and stages of disease, assuming that they all manifest the same disease.

### 4.1.3 Aim

Earlier studies provide ample evidence that ALS is a multifactorial entity (i.e. processes like neuronal degeneration, gliosis) causing effective changes in cerebral (e.g., GM and WM) volumes. Therefore, we aimed to measure changes in volume of GM structures due to atrophy in our ALS-FTD patients primarily, but also in our other ALS patient subgroups.

### 4.1.4 Hypothesis

It is hypothesized that cerebral GM volume is significantly different between control individuals and ALS patients and also between the ALS subgroups themselves. We also hypothesize that if GM volume is lower in ALS patients compared to control subjects, onset of neurodegeneration in ALS is in the perikaryon (cell body), as a neuronopathy. If, on the other hand, no change is detected in cerebral GM volume of ALS patients compared to controls, the disease process is a "dying-back" (retrograde axonopathy) phenomenon.

### 4.1.5 Method

#### 4.1.5.1 Imaging protocol

Magnetization prepared rapid gradient echo (MPRAGE) sequence was used to acquire T1 weighted images on a 1.5 T system (Siemens Symphony, Erlangen, Germany) in 9 control subjects (6 men, 3 women), and 72 ALS patients: 13 UMN-predominant with CST hyperintensity (8 men, 5 women), 25 UMN-predominant without CST hyperintensity (16 men, 9 women), 14 typical ALS with mixed UMN and LMN signs (9 men, 5 women), and 20 with ALS-FTD (5 men, 15 women,). This high resolution 3D T1-weighted MPRAGE sequence provided good GM-WM contrast[14]. MPRAGE sequences are less sensitive to pulsation artifacts because of shorter TEs and saturation effects of flowing blood in the whole excitation volume[11]. The following MPRAGE parameters were used for pulse sequence: TR = 1970 ms, TE = 4.38 ms, number of averages = 1, flip angle =$10^{o}$, TI =1100 ms, scan time = 6.45 minutes, and imaging: number of slices = 160, contiguous, slice thickness = 1 mm, in-plane resolution = 0.9×0.9 mm.

#### 4.1.5.2 Data Processing

An optimized VBM approach of Good and colleagues was adopted[12] with all processing steps carried out using openware FSL (http://www.fmrib.ox.ac.uk/fsl/). Data processing was divided into four major steps: (1) Brain extraction in all the subjects using fsl_vbm_1_bet routine, with manual editing to remove any remaining non brain regions; brain extracted images were segmented into WM, GM and CSF probability maps. (2) Creation of a study specific GM template[13] by registering a subset of subjects from control and ALS groups into the MNI152 space (to avoid bias during the registration process). 3) GM template was created were registration of all subjects to the study-specific GM template using both linear and non-linear registration methods; GM volumes were concatenated and smoothed (to increase singal-to-noise ratio) using a Gaussian kernel of 3 mm with a full-width half-maximum (FWHM) of ~7 mm. (4) Application of permutation based non-parametric statistics to the data set to identify significant differences in GM volume between control subject and ALS groups. As mentioned above, non-parametric statistical approaches are recommended in the literature[8-10] because the data often violates Gaussian distribution. A general linear model (GLM) was adopted to compare differences in GM volume between 4 different ALS subgroups and the control group. A $p<0.05$ corrected for multiple comparisons using false discovery rate (FDR) was considered the level of significance.

### 4.1.6 Results

Significant differences were detected in motor and extra motor regions only between control and ALS-FTD subjects, as shown in figure 26 below. Cortical regions significantly atrophic in ALS-FTD patients compared to controls are shown in figure 26

to be: frontal and temporal lobes, occipital fusiform gyrus, lingual gyrus, lateral occipital cortex inferior division, inferior temporal gyrus temporooccipital part, temporal occipital fusiform cortex, lateral occipital cortex superior division and superior parietal lobule. The extra motor regions of inferior temporal gyrus, fusiform gyrus, and lingual gyrus have cognitive functions[30], including face recognition[30], word recognition, and color information processing. The hippocampus in the temporal lobe is primarily responsible for long-term memory[30]. Non-motor frontal and prefrontal areas are responsible for executive functions, behavioral and emotional regulation. GM volume changes in ALS-FTD supports our hypothesis that these patients exhibit early neurodegeneration in the perikaryon (as a neuronopathy) with early anterograde degeneration affecting the entire axon with wallerian degeneration . No other ALS subgroup showed GM volumes that were significantly different from control individuals, consistent with a "dying back" axonopathy of motor pathways and relative preservation of the perikaryon until later in the disease process. Like our findings, Sage et al[13] and Abrahams et al[5] also did not identify significant differences in GM volume between control subjects and ALS patients without dementia whereas other studies did[7,8]. Discrepancies in results between our study and the latter ALS studies may be due to the following: a) potential misclassification by Chang and collaborators[7] of ALS patients with and without dementia considering both groups had similar clinical symptoms; b) use of uncorrected statistics ($p<0.001$) by Mezzapesa and colleagues[8], which will lead to large Type I error; c) employment of Gaussian random field (GRF) theory based statistical analysis by both of these groups[7,8], while we used a non-parametric permutation based approach.

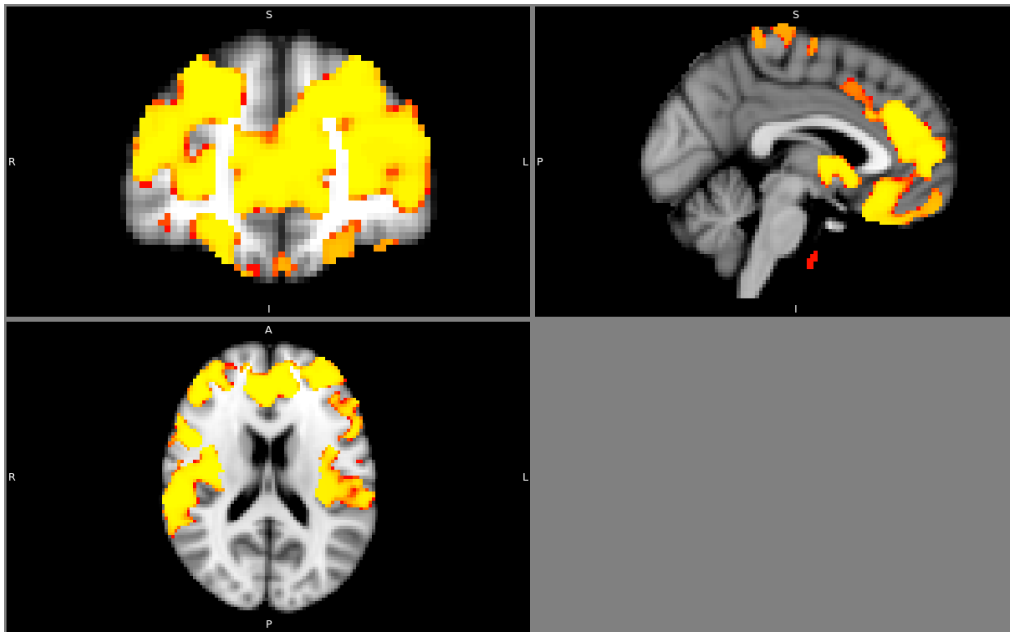


**Figure 26: Regions which showed statistical significance between control and ALS dementia were shown by superimposing them on MNI brain template**

### 4.1.7 Conclusion

Absence of GM changes in non-demented ALS patient subgroups supports our hypothesis that such patients may experience a "dying back"axonopathy of the UMN with only late perikaryon degeneration and loss. In contrast, GM loss in ALS-FTD patients suggests an early loss of perikaryon (neuronopathy) with resultant global anterograde wallerian degeneration.

### 4.1.8 Limitations and Future Scope

Since previously published ALS VBM studies widely employed GRF-based statistical analyses, a comparison of these and permutation based statistics in same sample of patients and controls would determine whether discrepancies between different studies are due to the statistical procedures utilized. A larger sample study, especially of the control group, would confirm our findings.

A better understanding of the pathophysiological mechanisms in ALS can be achieved by combining GM VBM results with brain 2,3-FDG PET data in order to correlate structural and functional changes. In addition, combination of VBM and DTI studies would help validate the dying-back axonopathy vs. early neuronopathy sites of degeneration in ALS patient subgroups. Confirmation and validation of our findings could be achieved by post-mortem histopathological studies of such patients showing the aforementioned VBM changes.

## 4.2 Cortical Thickness in ALS

### 4.2.1 Introduction

The human cerebral cortex has a complex organization of layers and columns: a) six horizontal layers (I-VI) each having a unique cellular organization and synaptic connections, b) multiple vertical columns (comprised of neurons and surrounding neuropil) for each single function and c) subdivision of each column into hypercolumns, which combine different functional columns. Therefore, pathological changes of cortical neurons (e.g. shrinkage or loss) and surrounding neuropil resulting in physiologic dysfunction may affect column length (e.g. reduction), which in turn alters cortical thickness (e.g. reduction). Therefore, a physical and functional change in the cortical neuronal circuitry is reflected by altered cortical thickness (usually reduced). Thinning of the cortex due to pathological changes has been widely reported in various neurological disorders namely; Alzheimer's disease[15], Huntington's disease[16] and multiple sclerosis[17]. Voxel based morphometry (VBM) described in the previous section quantitatively assesses GM volume changes in the brain using high resolution T1-weighted images. However, VBM provides only part of the information because volume change can result either from changes in cortical thickness or cortical surface area or both and differentiating between the two is not possible with VBM. In addition, estimation of GM volume by VBM includes both cortical thickness and cortical foldings (gyri and sulci) such that adjacent gyri can be mistaken as a single GM area, as shown in figure 27, resulting in erroneous high GM concentration[18]. Cortical thickness measurements overcome this error, as well as providing additional information on the possible pathophysiological changes in ALS, as discussed above.

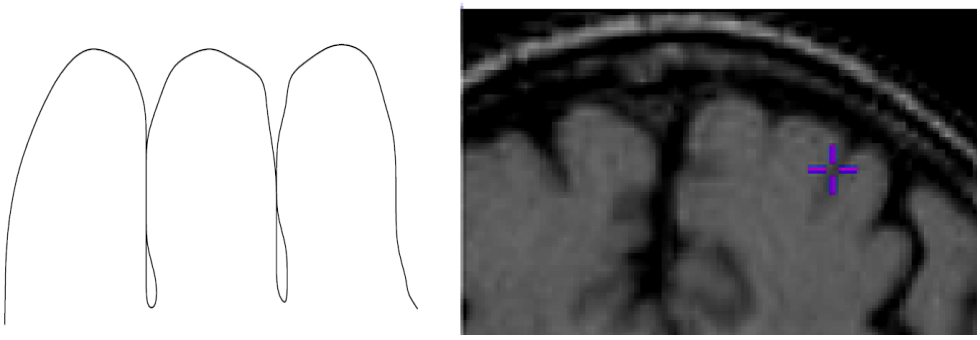

a) b)

**Figure 27: a) Cartoon of adjacent gyri appearing connected to each other, b) MR image in which this gyral foldings (adjacent gyri abutted) appears as a single large GM area (indicated by cross hair).**

**Adapted from Jason Lerch Master's thesis proposal**

An earlier study reported shrinkage in the surface area of precentral gyri of ALS patients although without significant differences between ALS and control subjects on group comparisons[3]. A stereological study surprisingly found no abnormalities in post mortem ALS brain tissue after estimating total number of cortical neurons, measuring cortical thickness, as well as surface area and volume of neocortex, white matter and central grey nuclei[19]. Measurements in the two aforementioned studies were performed manually which is not only time consuming but also introduces operator bias and poor reproducibility. Furthermore, huge errors in thickness measures will result if the image plane is not perpendicular to the cortical surface, as pointed out by Fischl and Dale[20] .As shown in figure 28 below, measuring cortical thickness in the same location (identified by green dot) but in two different planes will result in a higher value in the coronal view as compared to axial view. This discrepancy occurs because cortical thickness is measured

parallel to the imaging plane in the coronal view but perpendicular to it in the axial view. In their earlier study, Kiernan and Hudson identified six potential measurement errors of cortical surface area by MRI: partial volume, head tilt, plane of view, contiguous slices, intensity manipulation, and magnetic inhomogeneities[3].

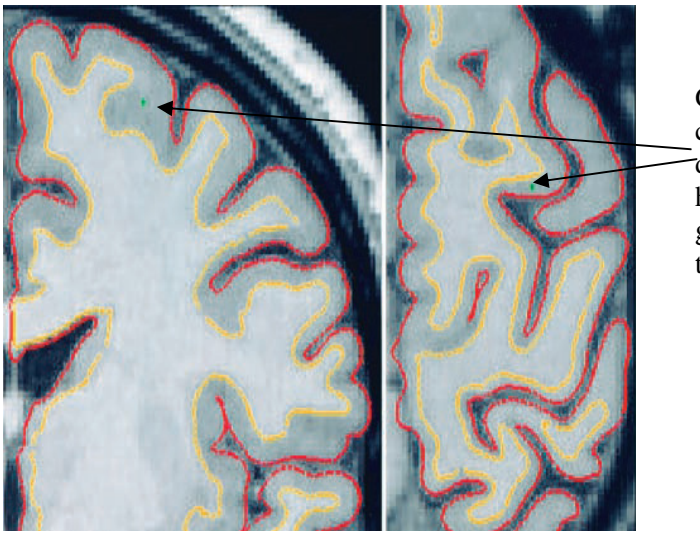


**Figure 28: Cortical thickness of the same cortical region is over estimated when measured in the coronal plane (a) compared to the axial plane (b) where it is more accurately represented**

**Adapted from Fischl, (2000).**

The aforementioned drawbacks of manual cortical thickness measurements can be essentially removed if automated image processing techniques are employed. Therefore, a fully automated cortical thickness measurement software (developed by Fischl and

Dale[20]) was used in this study to assess cortical thickness in our ALS patient subgroups.

Multiple earlier studies have amply demonstrated that ALS is a multicellular disorder (i.e. neuronal shrinkage and/or loss, gliosis) causing degenerative changes in GM structures

### 4.2.2 Aim

Our VBM study showed significant GM volume loss in only ALS-FTD dementia patients but not in the other ALS subgroups, compared to control individuals. Therefore, the present analysis of cortical thickness aims to determine whether the GM volume reduction by VBM is due to decreased cortical surface area, cortical thickness, or both.

### 4.2.3 Hypothesis

It is hypothesized that cortical thickness is significantly different between control and ALS patients, especially the ALS-FTD subgroup, and also within the ALS subgroups themselves. We also hypothesize that if significant changes in cortical thickness are observed between ALS patients and control subjects, then the neurodegeneration mechanism in the ALS subgroup may be a neuronopathy affecting the neuronal perikayon.

### 4.2.4 Method

#### 4.2.4.1 Imaging protocol

Magnetization prepared rapid gradient echo (MPRAGE) sequence was used to acquire T1-weighted images on a 1.5 T system (Siemens Symphony, Erlangen, Germany) in 11 control subjects (8 men, 3 women) and 72 ALS patients: 13 UMN-predominant

with CST hyperintensity (8 men, 5 women), 25 UMN-predominant without CST hyperintensity (16 men, 9 women), 14 typical ALS with mixed UMN and LMN signs (9 men, 5 women) and 20 with ALS-FTD (5 men, 15 women). This high resolution 3D T1-weighted MPRAGE sequence provided good GM-WM contrast[14]. MPRAGE sequences are less sensitive to pulsation artifacts because of shorter TEs and saturation effects of flowing blood in the whole excitation volume[12]. MPRAGE pulse sequence parameters were: TR = 1970 ms, TE = 4.38 ms, number of averages = 1, flip angle =10$^{o}$, TI =1100 ms and scan time = 6.45 minutes; imaging parameters were: number of slices = 160, contiguous, slice thickness = 1 mm, in-plane resolution = 0.9×0.9 mm.

#### 4.2.4.2 Data Processing

Cortical thickness measures were carried out using Freesurfer, an openware (http://surfer.nmr.mgh.harvard.edu/). Image processing steps begin with motion correction and skull stripping based on hybrid watershed /surface deformation procedure[21]. The images are then registered to a Talairach brain template, segmented for subcortical WM and GM structures[22], and intensity normalized for uniform intensity values across the WM and GM structures[23]. After intensity normalization, a tessellation step estimates the GM-WM boundary and subsequent automated topology correction[24,25]. The GM-WM and GM-cerebrospinal fluid (GM-CSF) boundaries are optimally placed using surface normalization and intensity gradients[20,26]. After cortical models are completed, deformable procedures are performed for further processing and analysis like surface inflation and registration to a spherical atlas[27]. Both intensity and continuity information from the entire 3D MR volume is used to produce representations of cortical thickness and thickness is measured as the closest distance from GM-WM to GM-CSF

boundary at each vertex on the tessellated surface[20] as shown in figure 29 below. Because the maps are not restricted to voxel resolution of the original data they are capable of detecting submillimeter differences between groups.

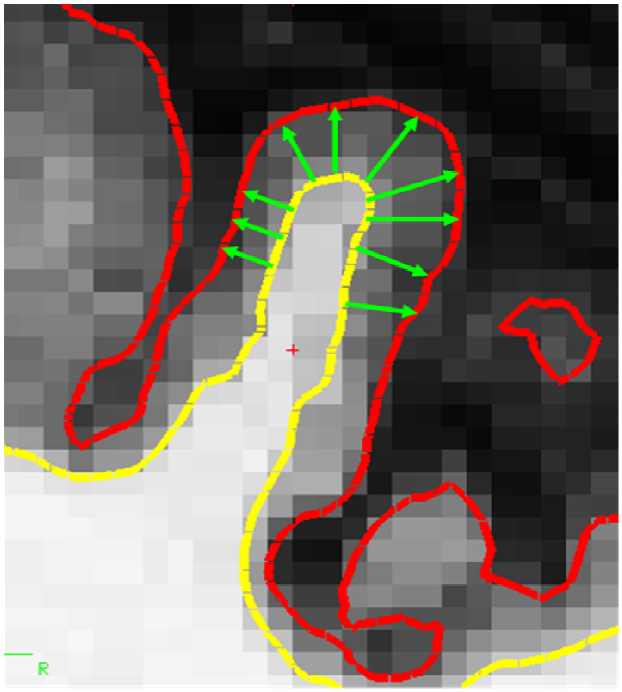

**Figure 29: MPRAGE image showing how cortical thickness (arrows) is determined between GM-WM (broken yellow line) and GM-CSF (broken red line) boundaries.**

**Adapted from Fischl, Tutorial slides.**

### 4.2.5 Results

High resolution 3D T1-weighted images from all control and ALS subjects were processed as described in the data processing section. This analysis provides additional

information on the changes in GM structures, as discussed previously (i.e. volume = area * thickness). Cortical thickness, surface area, and volume were compared between control and ALS subgroups using the GLM statistical model with FDR at $p< 0.05$ for multiple comparisons. Significant differences in cortical thickness were observed only between control subjects and the ALS-FTD subgroup, as shown below in figure 30. These regions were mapped based on the Desikan[28] atlas. Table V below gives the Talairach coordinates and corresponding cortical regions, which were significantly different between the control and ALS-FTD groups. No significant differences in cortical thickness were observed between control and any of the other ALS subgroups. Cortical surface area and volume were also compared between control subjects and ALS patients. No significant differences were observed in cortical surface area but cortical volume (Note that cortical volume here refers to volume of the cortex whereas in VBM study the volume measured has both cortical and sub cortical GM structures) was significantly different between control and only ALS-FTD groups, as shown in figure 31; no significant differences in cortical volume were observed between control individuals and any other ALS subgroups. Table VI below gives Talairach coordinates of regions which were significantly different between control and ALS-FTD groups for both cortical volume and thickness metrics. Therefore, these results indicate that decreased cortical volume in the ALS-FTD patients (found by VBM) is due to reduced cortical thickness and not reduced cortical surface area.

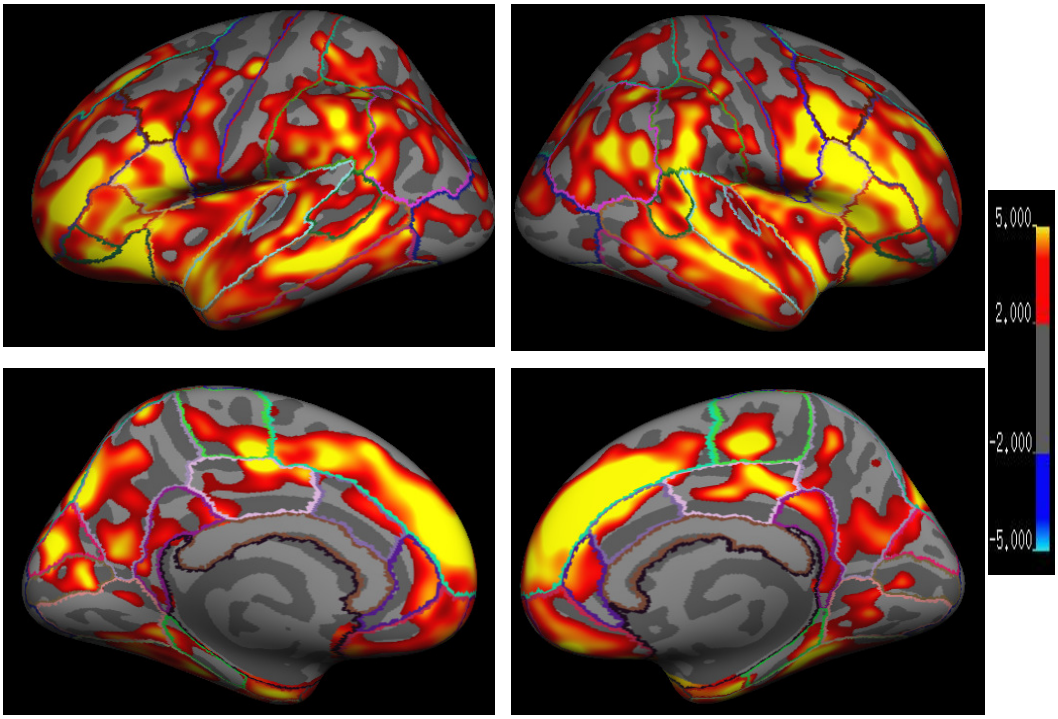


**Figure 30: Colored regions (heat map) indicate regions of statistical significance (p<0.01) superimposed on average inflated template showing cortical thinning in ALS-FTD patients relative to controls results are projected onto the left hemisphere, laterally (top left image), medially (bottom left image) and right hemisphere, laterally (top right image), medially (bottom right image). Color bar is scaled in units of log 10 (*p*)**

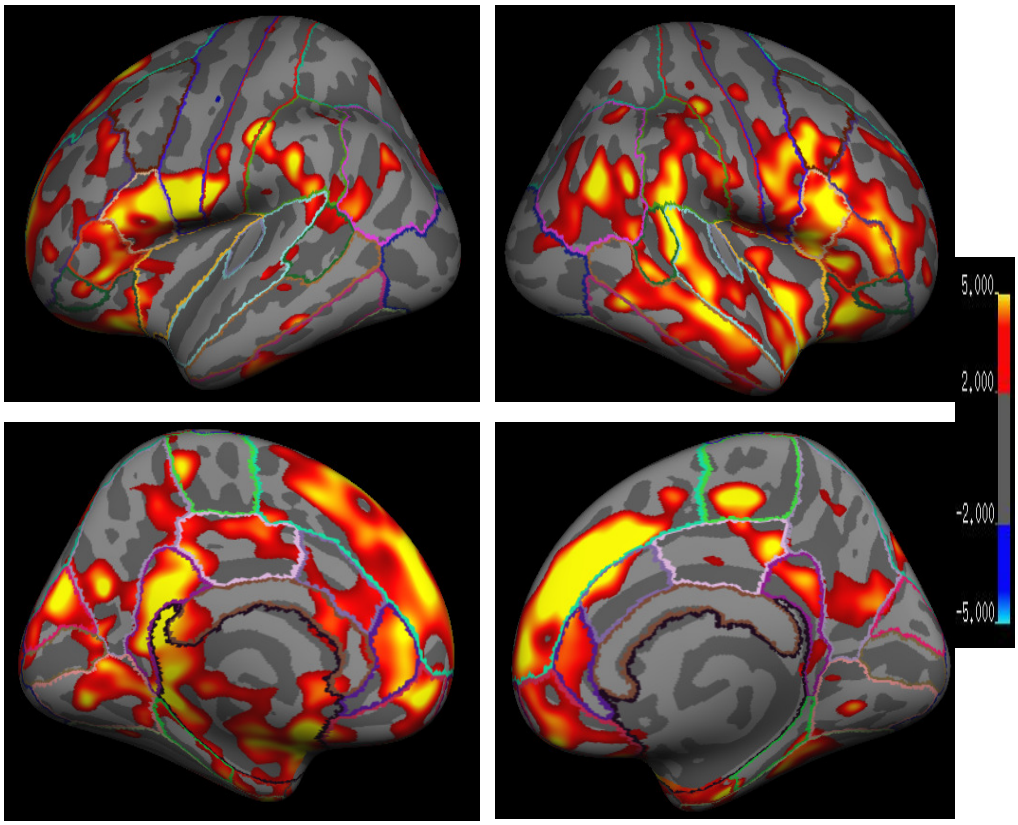


**Figure 31: Colored regions (heat map) indicate regions of statistical significance (p<0.01) superimposed on average inflated template showing reduction in cortical volume in ALS-FTD patients relative to controls results are projected onto the left hemisphere, laterally (top left image), medially (bottom left image) and right hemisphere, laterally (top right image), medially (bottom right image). Color bar is scaled in units of log 10 (*p*)**

**Table V: Talairach coordinates and regions which are significantly different between control and ALS dementia groups using cortical thickness measure**

| Talairach coordinates (vertex of cortical region) (X, Y, Z) | Cortical regions significantly affected in ALS dementia |
|---|---|
| -37.55, 42.61,4.82 | rostral middle frontal |
| -46.14, 30.35, -3.23 | lateral orbitofrontal |
| -40.43, 38.91, -12.20 | pars orbitalis |
| -32.81, 21.55, -17.09 | lateral orbitofrontal |
| -50.36, 15.76, 16.36 | pars opercularis |
| -34.99, 9.32, 31.24 | caudal middle frontal |
| -50.57, 3.39, 27.25 | precentral gyrus |
| -59.25, -15.11, 17.06 | postcentral gyrus |
| -20.47, 23.90, 39.84 | superior frontal |
| -33.22, 1.29, 5.70 | insula |
| -50.74, -0.23, -9.71 | superior temporal |
| -58.22, -10.57, -18.96 | middle temporal |
| -53.69, -26.93, -21.94 | inferior temporal |
| -54.28, -34.79, 31.34 | supramarginal |
| -35.83, -42.63, 50.00 | superior parietal |
| -42.60, -50.87, 22.47 | inferior parietal |
| -53.93, -43.88, 0.51 | banks of superior temporal sulcus |
| -47.48, -19.26 , 6.55 | transverse temporal |
| -42.24, -77.29, 4.81 | lateral occipital |
| -10.45, 47.28, 13.50 | superior frontal |
| -5.41, -10.39, 35.99 | posterior cingulate |
| -8.41, -31.26, 27.05 | isthmus cingulate |
| -6.69, -57.13, 17.09 | precuneus |

| | |
|---|---|
| -12.61, -77.93, 14.91 | pericalcarine |
| -4.18, -75.36, 23.06 | cuneus |
| -12.73, -23.40, 45.41 | paracentral |
| -7.84, 40.16, -0.64 | rostral anterior cingulate |
| -28.52, -5.33, -28.31 | entorhinal |
| -27.18, -49.98, -11.27 | fusiform |
| -25.83, -48.36, -2.05 | lingual |
| -26.83, -40.03, -6.55 | parahippocampal |
| -7.47, 16.15, -15.29 | medial orbitofrontal |
| -9.10, 21.47, 25.17 | caudal anterior cingulate |

**Table VI: Talairach coordinates and regions which are significantly different between control and ALS-FTD groups in both cortical thickness and in cortical volume (right side)**

| **Talairach coordinates (vertex of cortical region) (X, Y, Z)** | **Cortical regions significantly affected in ALS dementia** |
|---|---|
| -50.36, 15.76, 16.36 | pars opercularis |
| -37.55, 42.61,4.82 | rostral middle frontal |
| -34.99, 9.32, 31.24 | caudal middle frontal |
| -50.57, 3.39, 27.25 | precentral gyrus |
| -54.28, -34.79, 31.34 | supramarginal |
| -59.25, -15.11, 17.06 | postcentral gyrus |
| -35.83, -42.63, 50.00 | superior parietal |

| | |
|---|---|
| -42.60, -50.87, 22.47 | inferior parietal |
| -42.24, -77.29, 4.81 | lateral occipital |
| -58.22, -10.57, -18.96 | middle temporal |
| -53.93, -43.88, 0.51 | banks superior temporal sulcus |
| -50.74, -0.23, -9.71 | superior temporal |
| -33.22, 1.29, 5.70 | insula |
| -32.81, 21.55, -17.09 | lateral orbitofrontal |
| -40.43, 38.91, -12.20 | pars orbitalis |
| -20.47, 23.90, 39.84 | superior frontal |
| -7.47, 16.15, -15.29 | medial orbitofrontal |
| -7.84, 40.16, -0.64 | rostral anterior cingulate |
| -9.10, 21.47, 25.17 | caudal anterior cingulate |
| -12.73, -23.40, 45.41 | paracentral |
| -5.41, -10.39, 35.99 | posterior cingulate |
| -8.41, -31.26, 27.05 | isthmus cingulate |
| -6.69, -57.13, 17.09 | precuneus |
| -25.83, -48.36, -2.05 | lingual |
| -28.52, -5.33, -28.31 | entorhinal |

### 4.2.6 Discussion

We have found that cortical thickness and cortical volume are reduced not only in motor regions but also in non-motor frontal and temporal areas of ALS-FTD patients

compared to control subjects, as described above. Frontal and temporal lobes are mainly responsible for cognitive functions, including memory, object identification, facial recognition. Absence of significant differences between control subjects and other (non-demented) ALS patients suggests a subcortical axonal and not primarily perikaryal neurodegenerative process in the latter patients. Therefore, the significant reductions in cortical volume and thickness we identified in ALS-FTD patients support our hypothesis that primary neurodegeneration in these patients occurs in the perikaryon, as a neuronopathy. Little has been studied regarding cortical thickness in ALS patients. To our knowledge, only one study by Roccatagliata and colleagues (also using Freesurfer)[18] compared cortical thickness in 14 ALS patients and 12 control subjects over 3 regions of interest: precentral, postcentral and lateral occipital cortices. Cortical thickness was significantly reduced only in the precentral region and no correlations were observed between cortical thickness and clinical scores. Our study, on the other hand, found significant reductions in cortical thickness in precentral, postcentral (included both gyri and sulci) and lateral occipital cortices only in ALS-FTD patients, but not in ALS patients without dementia (i.e., in the other subgroups). It is difficult to determine the reason for the discrepant results between the two studies because we classified our patients based on the presence of prominent UMN signs, CST hyperintensities, or FTD, whereas the ALS patients of Roccatagliata et al examined ALS patients with a combination of UMN and LMN signs and either bulbar or spinal onset but no dementia[18] Nonethess, discrepancies in results of published VBM ALS studies arises when patients with differing clinical signs are included in the same group[5,7,14], as was the case in the study by Roccatagliata and colleagues[18]. Significant cortical thinning only in ALS-FTD patients and not in any

of the other ALS subgroups further emphasizes the need to categorize ALS patients based on their clinical phenotype. This will likely lead us to a better understanding of different pathophysiological mechanisms involved in ALS.

Use of cortical thickness analysis to identify significant decreases in cortical thickness and volume in ALS-FTD patients demonstrates the additional perspective/dimension obtained compared to VBM analysis. Cortical thickness analysis revealed that volume reduction (also seen by VBM) is due to decreased thickness and not by changes in cortical surface area. However, cortical surface area reductions have been observed in normal aging[29] and in Alzheimer's disease[15]. However, visual comparison of figures 30 and 31 shows more cortical regions showing thinning (30) than atrophy (31). Although the reason for this is unclear, one possibility is that cortical thinning may be a more sensitive change than obvious volume decrease (atrophy); since cortical area is unchanged, it may be masking cortical volume changes (since volume =thickness*area).

### 4.2.7 Conclusion

Our results clearly demonstrate that the decreased cortical volume (by VBM) is due to reduced cortical thickness and that this occurs in patients with ALS-FTD. This suggests primary pathology occurring at the cortical neuron cell body (perikaryon) as a neuronopathy in this ALS subgroup. Such cortical thinning occurs only in ALS-FTD patients but not in the other ALS patient subgroups in which neurodegeneration may be primarily subcortical, affecting axons as a "dying back" process. Our findings suggest differences in the underlying neurodegenerative processes in these subgroups of ALS

patients, and support the need for subclassification of patients based on clinical phenotype in further ALS research.

### 4.2.8 Limitations and Future scope

The major limitations of this study were the small control group size and the need for manual intervention to edit out non-brain regions not removed during the automated brain extraction step, and possibly introducing some operator bias. The latter possibility can be assessed by measuring intra-operator reliability in the future.

Results obtained from cortical thickness analysis can be combined with DTI metrics to evaluate the contribution of cortical degeneration (neuronopathy) and subcortical degeneration (axonopathy) in each of the ALS patient subgroups. A correlation map can be obtained between reductions of cortical thickness and cortical volume to better understand the relative interaction of these two measures. It would be worthwhile examining other cortical measures such as average convexity (which measures the depth/height of each point above an average surface), smoothed mean curvature and Jacobian matrix (amount of anatomical variability between subjects). These parameters may provide more information about the forms and complexity of cortical degeneration in ALS.

### 4.2.9 References


**1.** Strong MJ. The syndromes of frontotemporal dysfunction in amyotrophic lateral sclerosis. *Amyotroph Lateral Scler.* Dec 2008;9(6):323-338.

**2.** Neumann M, Sampathu DM, Kwong LK, et al. Ubiquitinated TDP-43 in frontotemporal lobar degeneration and amyotrophic lateral sclerosis. *Science.* Oct 6 2006;314(5796):130-133.

**3.** Kiernan JA, Hudson AJ. Frontal lobe atrophy in motor neuron diseases. *Brain.* Aug 1994;117 ( Pt 4):747-757.

**4.** Ashburner J, Friston KJ. Voxel-based morphometry--the methods. *Neuroimage.* Jun 2000;11(6 Pt 1):805-821.

**5.** Abrahams S, Goldstein LH, Suckling J, et al. Frontotemporal white matter changes in amyotrophic lateral sclerosis. *J Neurol.* Mar 2005;252(3):321-331.

**6.** Ellis CM, Suckling J, Amaro E, Jr., et al. Volumetric analysis reveals corticospinal tract degeneration and extramotor involvement in ALS. *Neurology.* Nov 13 2001;57(9):1571-1578.

**7.** Chang JL, Lomen-Hoerth C, Murphy J, et al. A voxel-based morphometry study of patterns of brain atrophy in ALS and ALS/FTLD. *Neurology.* Jul 12 2005;65(1):75-80.

**8.** Mezzapesa DM, Ceccarelli A, Dicuonzo F, et al. Whole-brain and regional brain atrophy in amyotrophic lateral sclerosis. *AJNR Am J Neuroradiol.* Feb 2007;28(2):255-259.

**9.** Arndt S, Cizadlo T, Andreasen NC, Heckel D, Gold S, O'Leary DS. Tests for

comparing images based on randomization and permutation methods. *J Cereb Blood Flow Metab.* Nov 1996;16(6):1271-1279.

**10.** Halber M, Herholz K, Wienhard K, et al. Performance of a randomization test for single-subject (15)O-water PET activation studies. *J Cereb Blood Flow Metab.* Oct 1997;17(10):1033-1039.

**11.** Nichols TE, Holmes AP. Nonparametric permutation tests for functional neuroimaging: a primer with examples. *Hum Brain Mapp.* Jan 2002;15(1):1-25.

**12.** Bluml S, Schad LR, Scharf J, et al. A comparison of magnetization prepared 3D gradient-echo (MP-RAGE) sequences for imaging of intracranial lesions. *Magn Reson Imaging.* 1996;14(3):329-335.

**13.** Smith SM, Jenkinson M, Woolrich MW, et al. Advances in functional and structural MR image analysis and implementation as FSL. *Neuroimage.* 2004;23 Suppl 1:S208-219.

**14.** Sage CA, Van Hecke W, Peeters R, et al. Quantitative diffusion tensor imaging in amyotrophic lateral sclerosis: revisited. *Hum Brain Mapp.* Nov 2009;30(11):3657-3675.

**15.** Dickerson BC, Feczko E, Augustinack JC, et al. Differential effects of aging and Alzheimer's disease on medial temporal lobe cortical thickness and surface area. *Neurobiol Aging.* Mar 2009;30(3):432-440.

**16.** Rosas HD, Liu AK, Hersch S, et al. Regional and progressive thinning of the cortical ribbon in Huntington's disease. *Neurology.* Mar 12 2002;58(5):695-701.

**17.** Sailer M, Fischl B, Salat D, et al. Focal thinning of the cerebral cortex in multiple sclerosis. *Brain.* Aug 2003;126(Pt 8):1734-1744.

**18.** Roccatagliata L, Bonzano L, Mancardi G, et al. Detection of motor cortex thinning and corticospinal tract involvement by quantitative MRI in amyotrophic lateral sclerosis. *Amyotroph Lateral Scler.* Feb 2009;10(1):47-52.

**19.** Gredal O, Pakkenberg H, Karlsborg M, et al. Unchanged total number of neurons in motor cortex and neocortex in amyotrophic lateral sclerosis: a stereological study. *J Neurosci Methods.* Feb 15 2000;95(2):171-176.

**20.** Fischl B, Dale AM. Measuring the thickness of the human cerebral cortex from magnetic resonance images. *Proc Natl Acad Sci U S A.* Sep 26 2000;97(20):11050-11055.

**21.** Segonne F, Dale AM, Busa E, et al. A hybrid approach to the skull stripping problem in MRI. *Neuroimage.* Jul 2004;22(3):1060-1075.

**22.** Fischl B, Salat DH, Busa E, et al. Whole brain segmentation: automated labeling of neuroanatomical structures in the human brain. *Neuron.* Jan 31 2002;33(3):341-355.

**23.** Sled JG, Zijdenbos AP, Evans AC. A nonparametric method for automatic correction of intensity nonuniformity in MRI data. *IEEE Trans Med Imaging.* Feb 1998;17(1):87-97.

**24.** Fischl B, Liu A, Dale AM. Automated manifold surgery: constructing geometrically accurate and topologically correct models of the human cerebral cortex. *IEEE Trans Med Imaging.* Jan 2001;20(1):70-80.

**25.** Segonne F, Pacheco J, Fischl B. Geometrically accurate topology-correction of cortical surfaces using nonseparating loops. *IEEE Trans Med Imaging.* Apr 2007;26(4):518-529.

**26.** Dale AM, Fischl B, Sereno MI. Cortical surface-based analysis. I. Segmentation and surface reconstruction. *Neuroimage.* Feb 1999;9(2):179-194.

**27.** Fischl B, Sereno MI, Dale AM. Cortical surface-based analysis. II: Inflation, flattening, and a surface-based coordinate system. *Neuroimage.* Feb 1999;9(2):195-207.

**28.** Desikan RS, Segonne F, Fischl B, et al. An automated labeling system for subdividing the human cerebral cortex on MRI scans into gyral based regions of interest. *Neuroimage.* Jul 1 2006;31(3):968-980.

**29.** Salat DH, Buckner RL, Snyder AZ, et al. Thinning of the cerebral cortex in aging. *Cereb Cortex.* Jul 2004;14(7):721-730.

**30.** Guyton A C, Text Book of Medical Physiology, A PRISM Indian ,W.B.Saunders Company, 8th edition, 1991.

# CHAPTER V

# CONCLUSION

The etiology and site of origin of ALS are unknown. Neurodegeneration can begin either in the upper motor neuron (UMN) or lower motor neuron (LMN), and even within an UMN origin, neurodegeneration can be an axonopathy or a neuronopathy. Based on preliminary data we hypothesize that ALS is predominantly an axonopathy, but, in ALS patients with frontotemporal dementia (FTD), it is neuronopathy. We also hypothesize that onset of neurodegeneration in patients with typical ALS is more caudal along the corticospinal tract (CST) when compared with UMN-predominant ALS.Axonal integrity will be investigated using T2 relaxometry and DTI, while neuronal integrity will be assessed by quantitative methods of voxel-based morphometry (VBM) and cortical thickness on qualitative T1-weighted images.

Study 1

Many clinical studies employ dual echo fast spin echo (FSE) sequence for measuring T2 relaxation times, although this is prone to high spatial frequency effects depending on the brain region of interest. Therefore in this study we evaluated the accuracy of T2 relaxation time measurements from dual echo FSE sequence relative to more robust multiple echo spin echo (SE) sequence prior to employing the former to evaluate pathologic changes in ALS. The results showed large systematic errors when using dual echo FSE sequence relative to multiple echo SE sequence. Therefore, we conclude that future T2 relaxometry studies employ multi-echo SE sequence or CPMG sequence for accurate and reliable results.

Study 2

Axonal integrity in ALS patients was evaluated using scalar DTI metrics. We also explored the usefulness of radial and axial diffusivities, Westin's linear and planar indices which are yet to be studied in ALS. We believed that axial and radial diffusivities, Westin's linear and planar indices provide additional information about pathophysiological changes in ALS when compared to the commonly used metrics of FA and MD.

1) All diffusion tensor metrics from DTI showed significant differences between ALS patients compared to control sunjects. Notably, subgroup of classic ALS patients showed abnormalities at more caudal levels of CST, supporting our hypothesis that site of maximal neurodegeneration (and possibly origin) in these patients is more caudal than in the UMN-predominant ALS subgroup.

2) Absence of significant differences in any DTI metrics of CST hyperintense and CST non hyperintense ALS groups, supporting our hypothesis that divergent pathologies occur in the subcortical axons (e.g. spinal cord).

3) Axial and radial diffusivities provided novel information about pathophysiology of ALS in that they showed not only significant differences between ALS subgroups but also showed significant difference at more rostral levels of CST which were not observed with FA metrics. Westin's linear and planar indices identified fiber crossings which were otherwise not distinguished with FA.

In general DTI metrics revealed group specific differences which clearly supported our view that better insight into the pathophysiological mechanisms of ALS will be obtained by categorizing ALS patients into subgroups based on clinical phenotypes.

Study 3

Neuronal integrity in grey matter structures was evaluated by measuring changes in grey matter volume, using voxel-based morphometry (VBM) method, and cortical thickness in ALS patients and control subjects. Since volume change could result from changes in cortical thickness, cortical surface area, or both, cortical thickness measurements were employed to investigate this. Both VBM and cortical thickness results showed significant reduction in grey matter volume (by VBM) and thinning of cerebral cortex occurred only in ALS dementia group when compared to controls. This supported our hypothesis of early perikaryal degeneration (neuronopathy) in this ALS subgroup and resultant global anterograde wallerian degeneration. Absence of significant reductions in cortical volume and thickness in other ALS patient subgroups supports our hypothesis that neuronal degeneration in these patients is primarily an axonopathy. Lack

of cortical surface area reductions clearly demonstrates that volume changes found by VBM are due to decreased cortical thickness and not cortical surface area. This provides additional insight into pathological changes in ALS brain.

To our knowledge, this is the first clinical study in ALS with a sufficiently large sample size that allows subcategorizing of ALS patients by clinical features to reveal subgroup specific differences in brain pathology using DTI metrics, VBM and cortical thickness measures. These findings suggest that ALS pathogenesis is variable among patients and support the notion that ALS is not a single disease but rather a syndrome.

# APPENDIX

Histograms of T2 relaxation error values along CST and in whole brain grey matter (GM) and white matter (WM) structures in all 8 subjects under study (Chapter 2)

Subject 1

CST Left

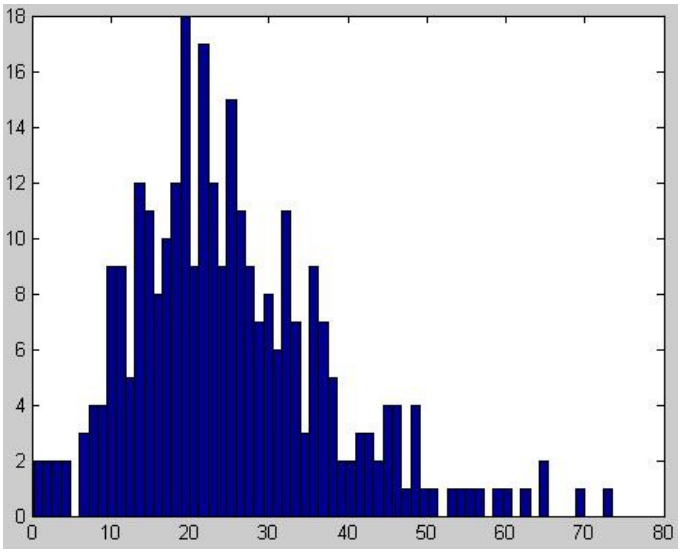


CST Right

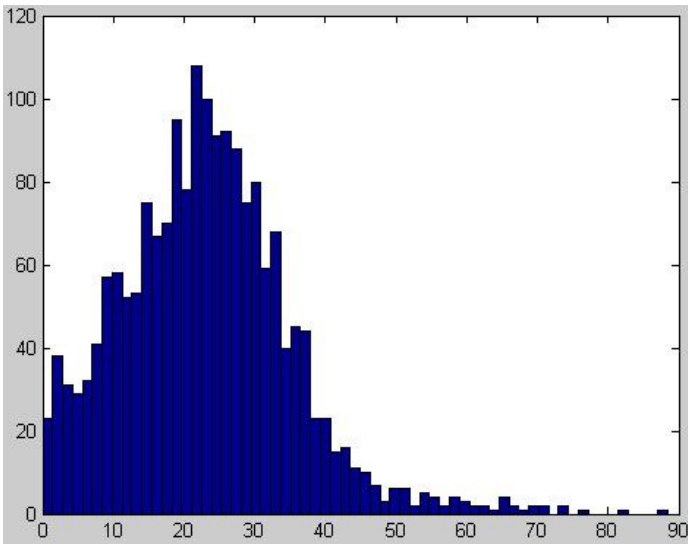

GM

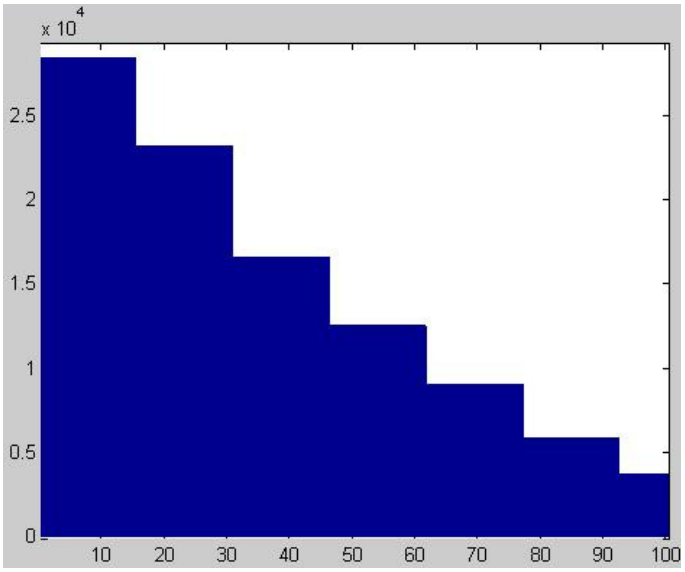
x 10^4
2.5
2
1.5
1
0.5
0
10
20
30
40
50
60
70
80
90
100

WM

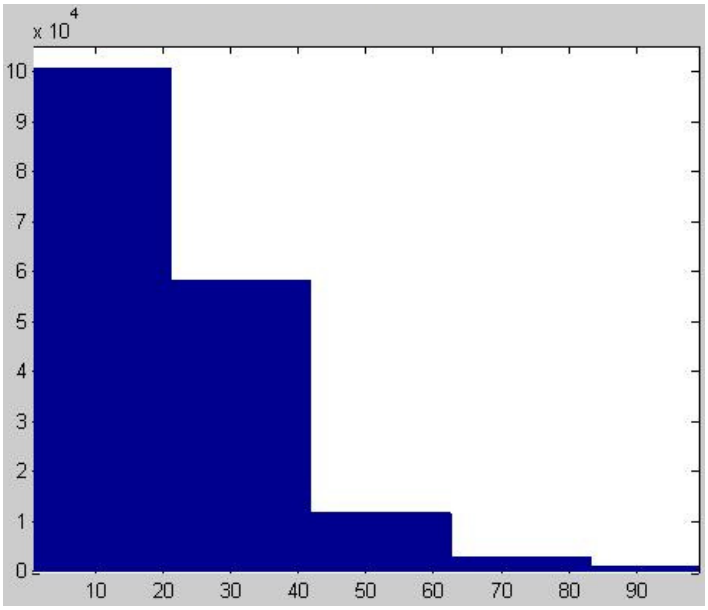
x 10^4
10
9
8
7
6
5
4
3
2
1
0
10
20
30
40
50
60
70
80
90

Subject 3

CST left

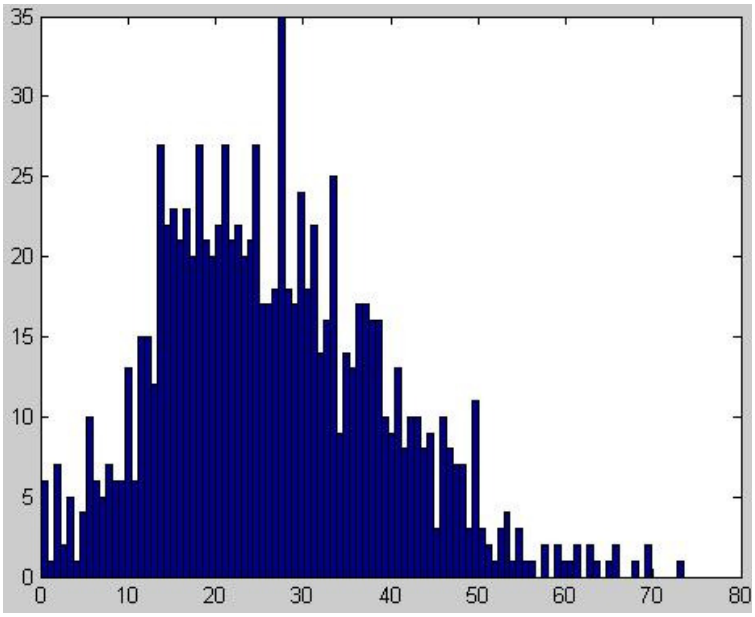


CST right

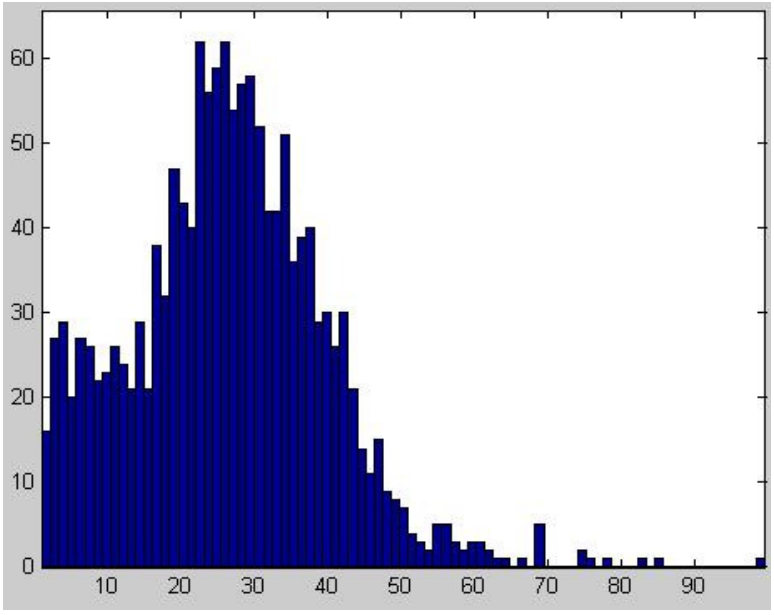

GM

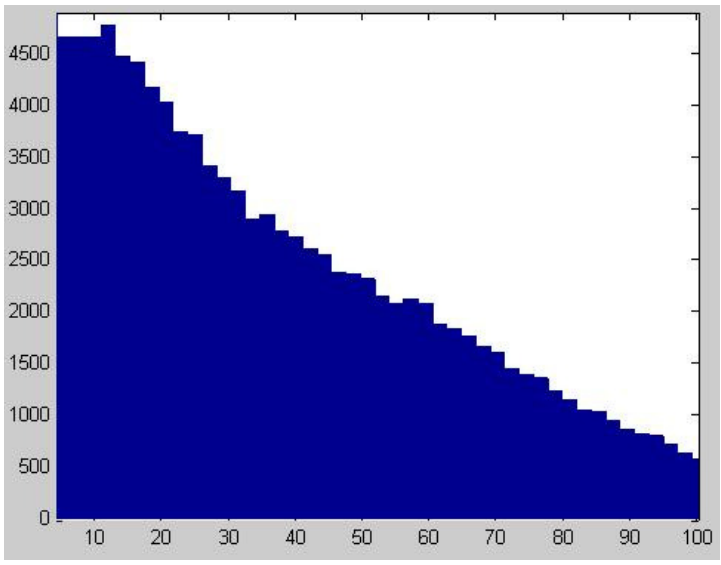
4500
4000
3500
3000
2500
2000
1500
1000
500
0
10
20
30
40
50
60
70
80
90
100

WM

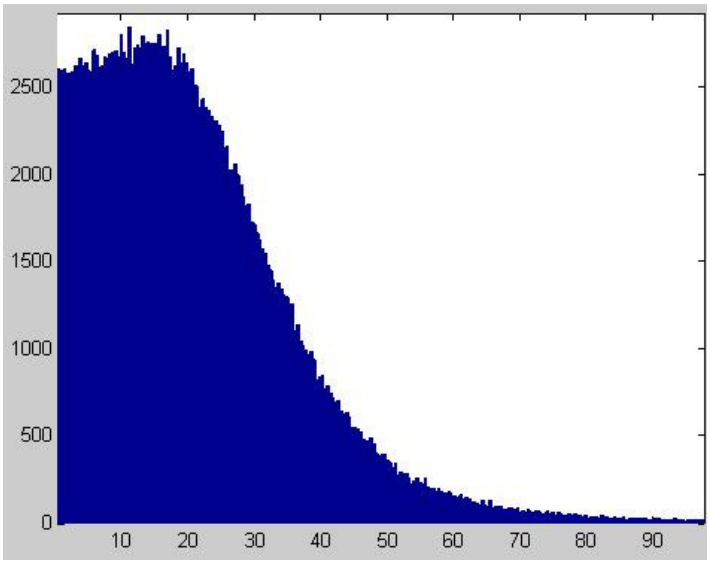
2500
2000
1500
1000
500
0
10
20
30
40
50
60
70
80
90

Subject 4

CST left

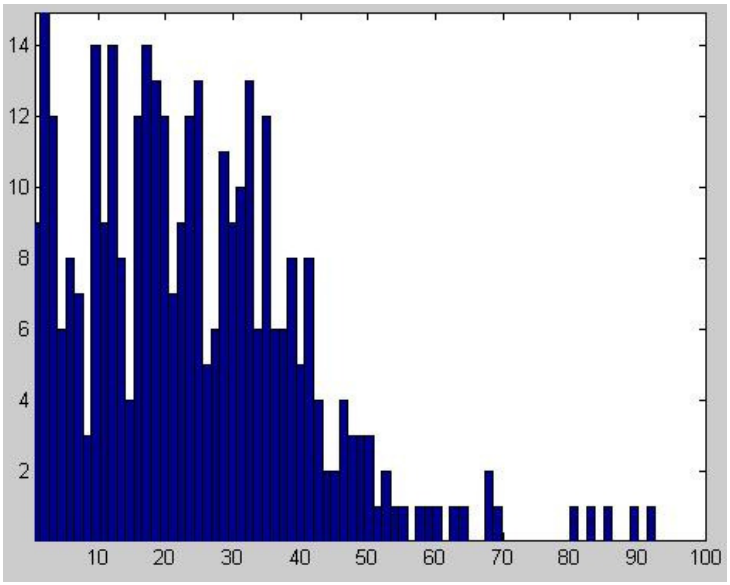


CST right

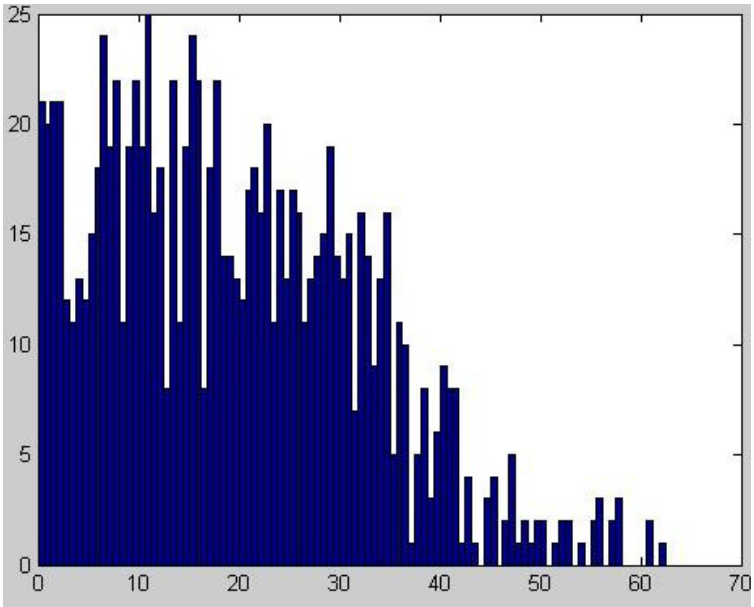

GM

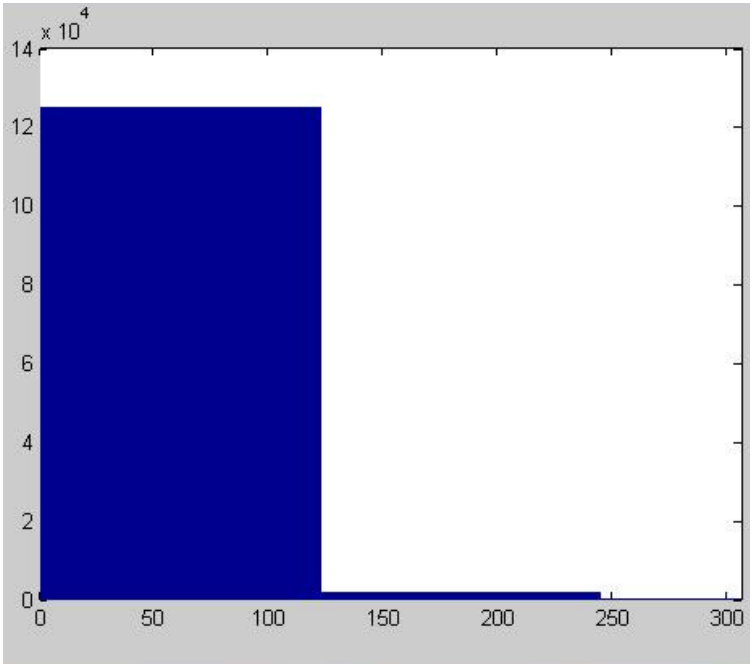
x 10^4
14
12
10
8
6
4
2
0
0
50
100
150
200
250
300

WM

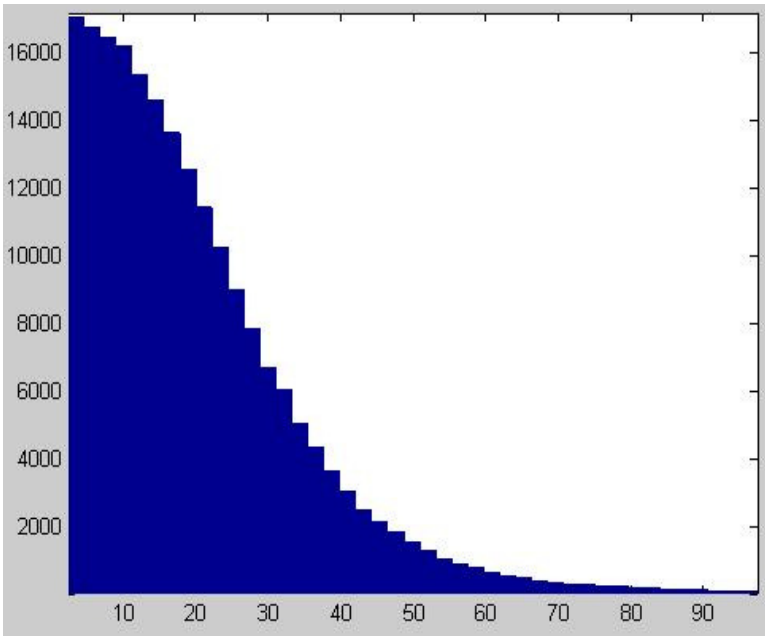
16000
14000
12000
10000
8000
6000
4000
2000
10
20
30
40
50
60
70
80
90

Subject 5

CST left

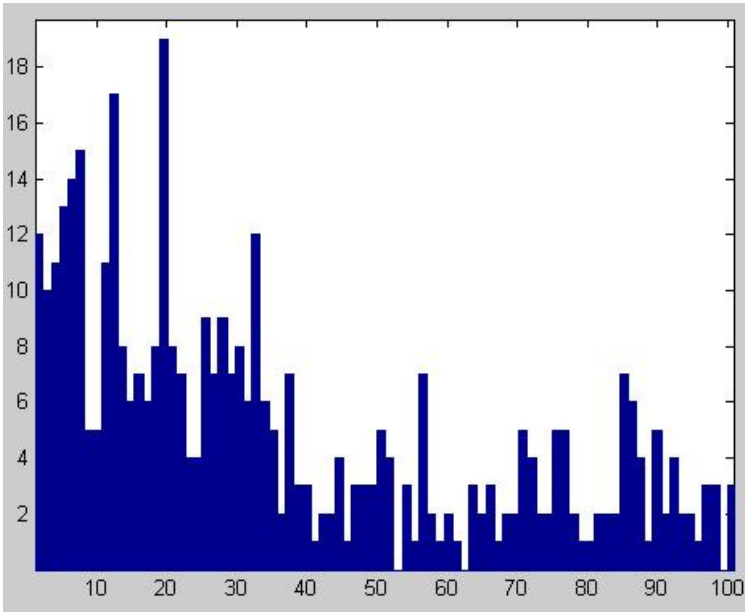


CST right

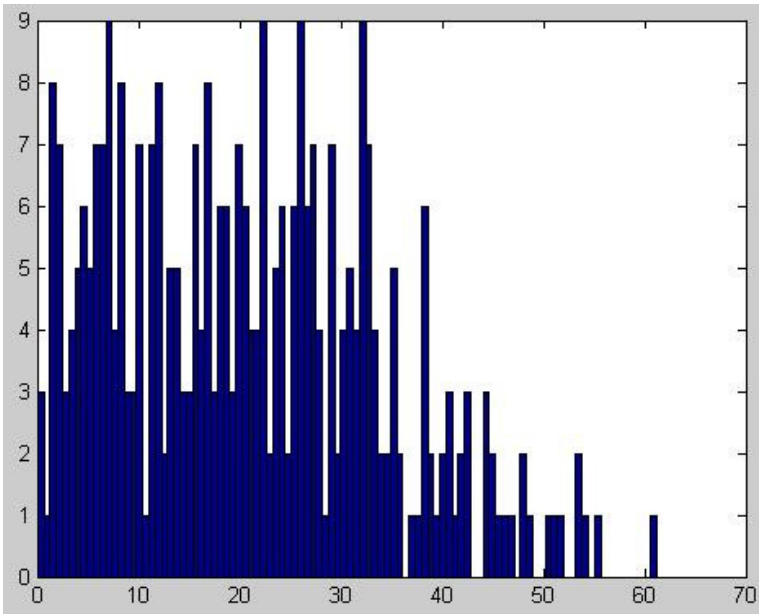

GM

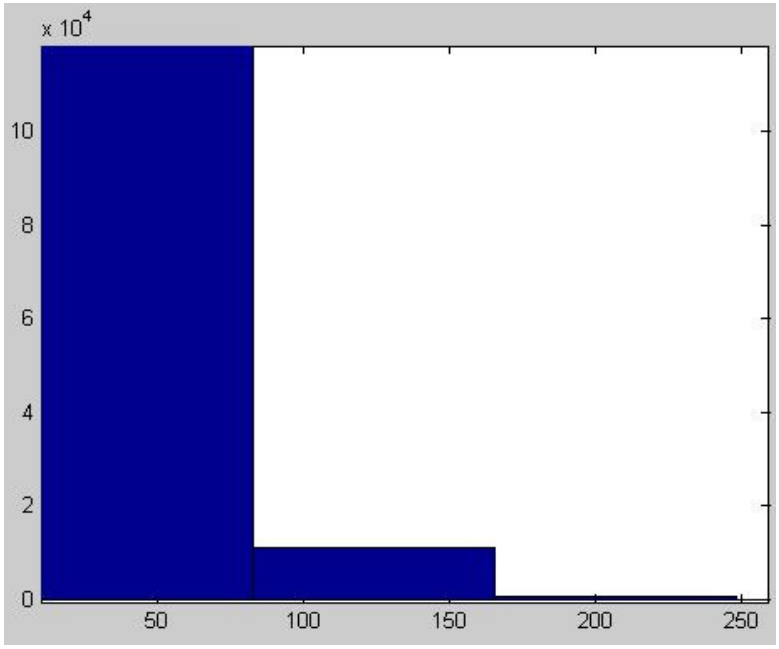
x 10^4
10
8
6
4
2
0
50
100
150
200
250

WM

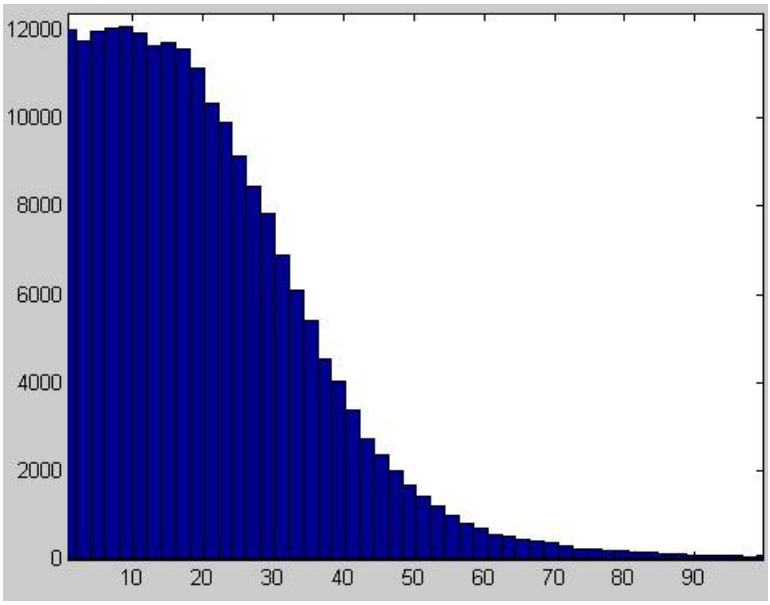
12000
10000
8000
6000
4000
2000
0
10
20
30
40
50
60
70
80
90

Subject 6

CST left

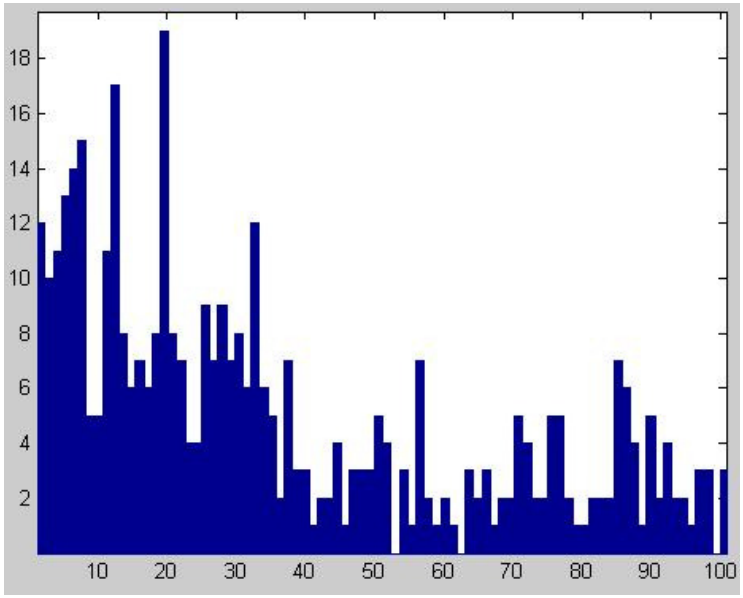


CST right

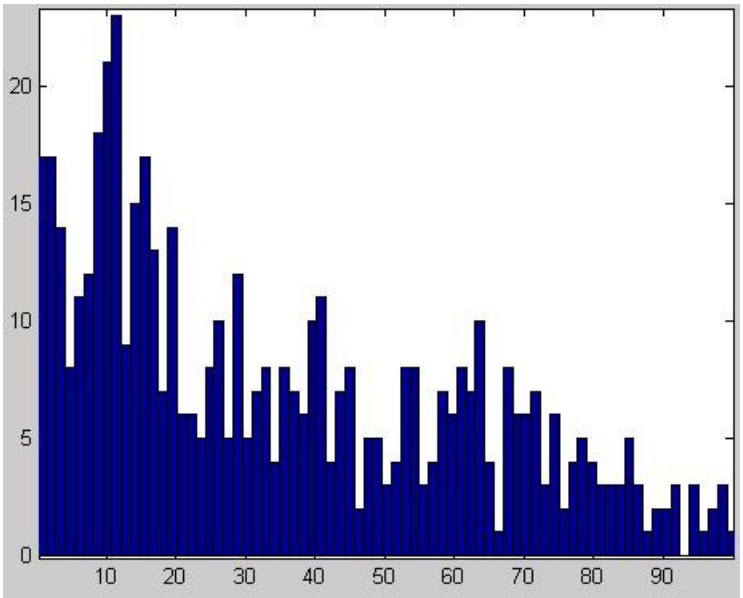

GM

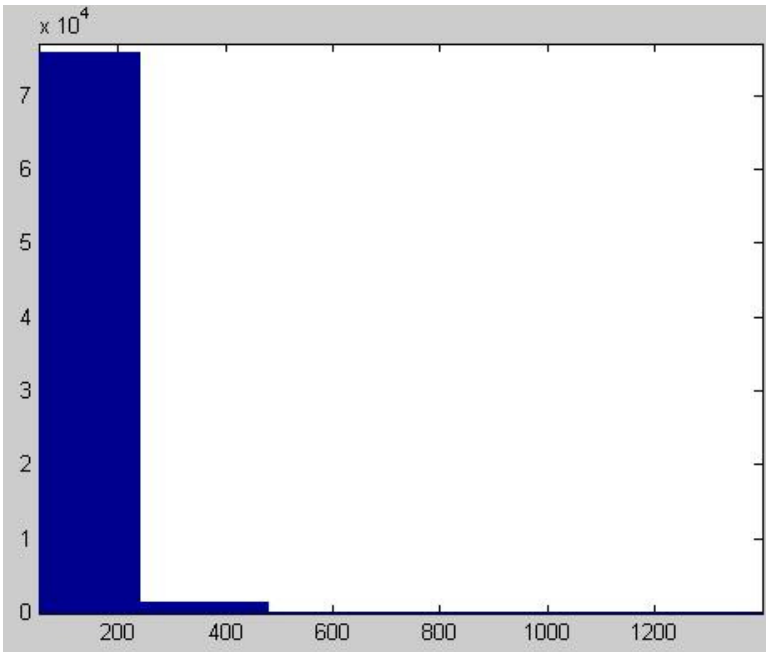
x 10^4
7
6
5
4
3
2
1
0
200
400
600
800
1000
1200

WM

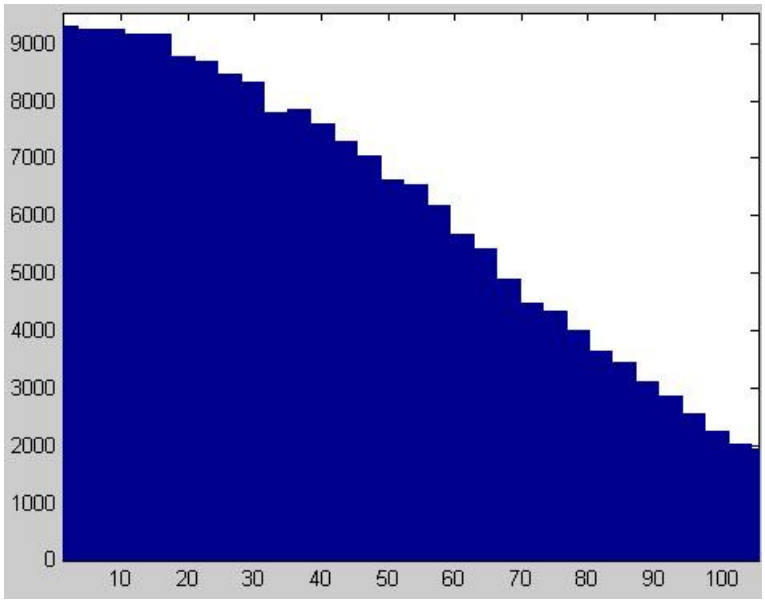
9000
8000
7000
6000
5000
4000
3000
2000
1000
0
10
20
30
40
50
60
70
80
90
100

Subject 7

CST left

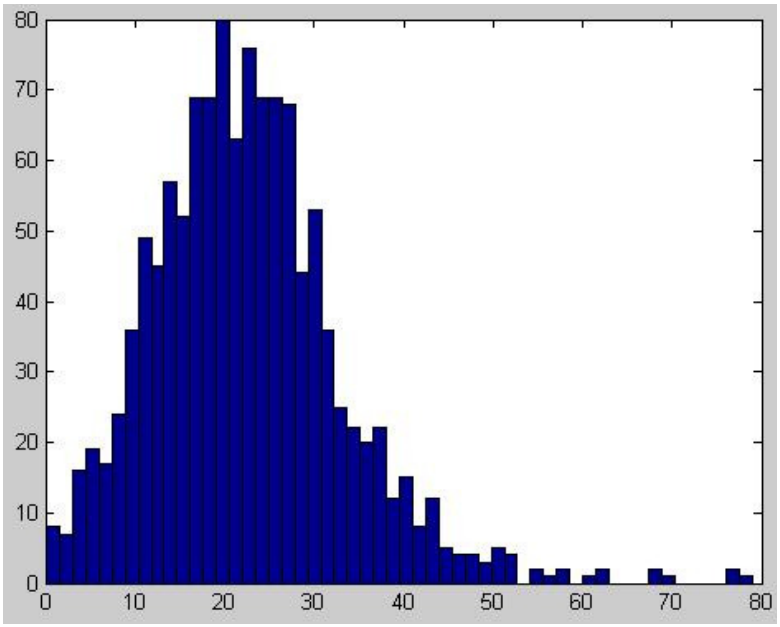


CST right

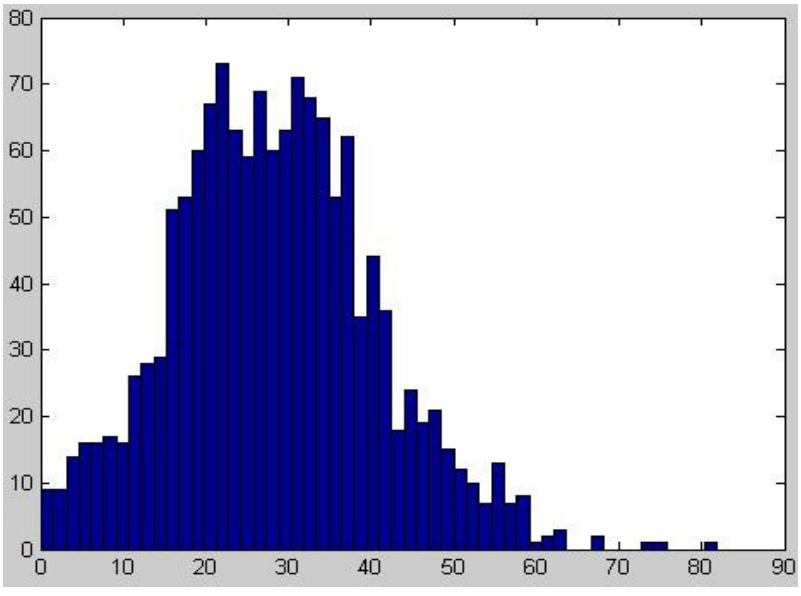

GM

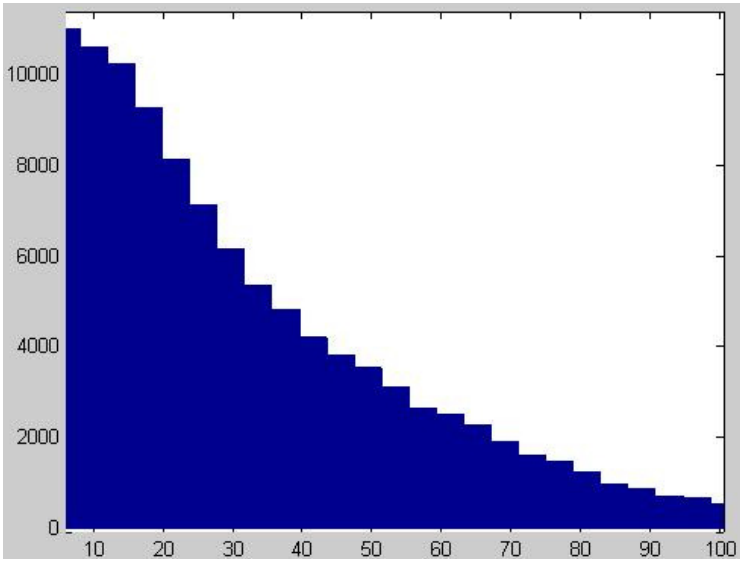
10000
8000
6000
4000
2000
0
10
20
30
40
50
60
70
80
90
100

WM

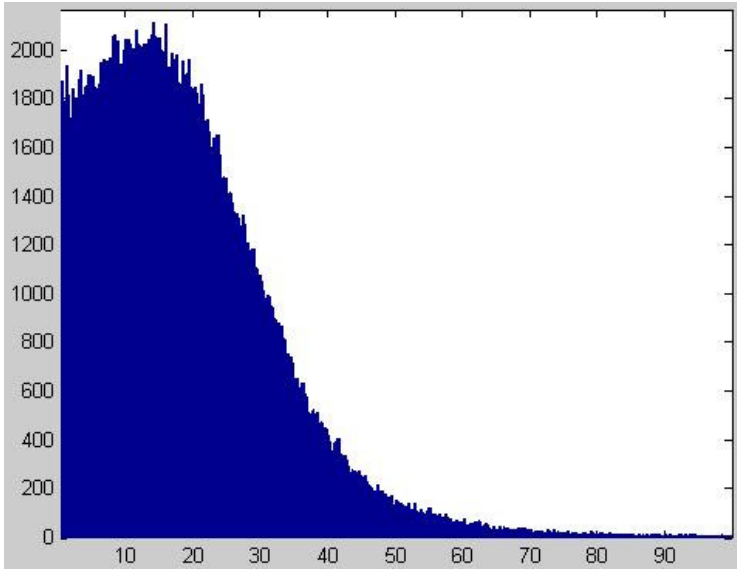
2000
1800
1600
1400
1200
1000
800
600
400
200
0
10
20
30
40
50
60
70
80
90

Subject 8

CST left

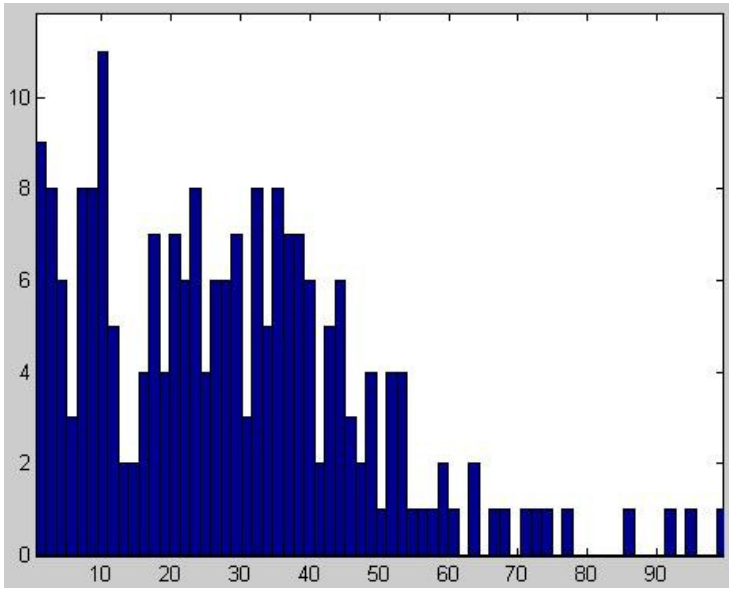


CST right

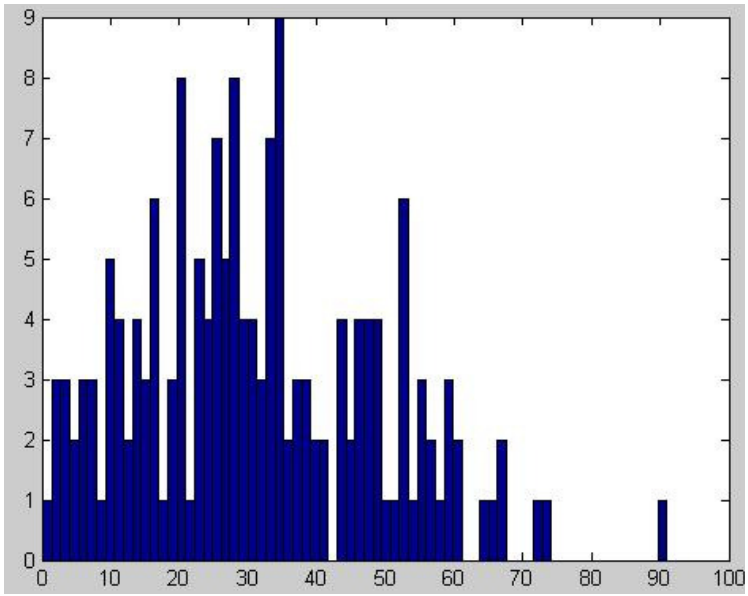

GM

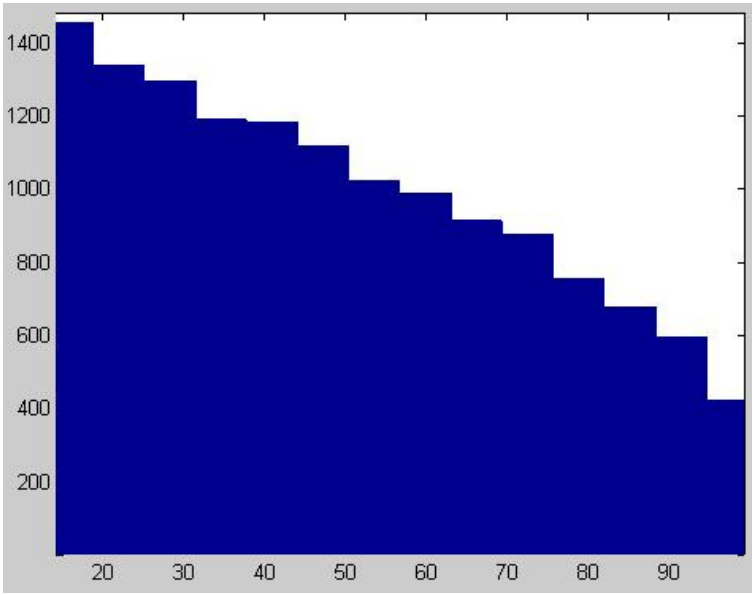
1400
1200
1000
800
600
400
200
20
30
40
50
60
70
80
90

WM

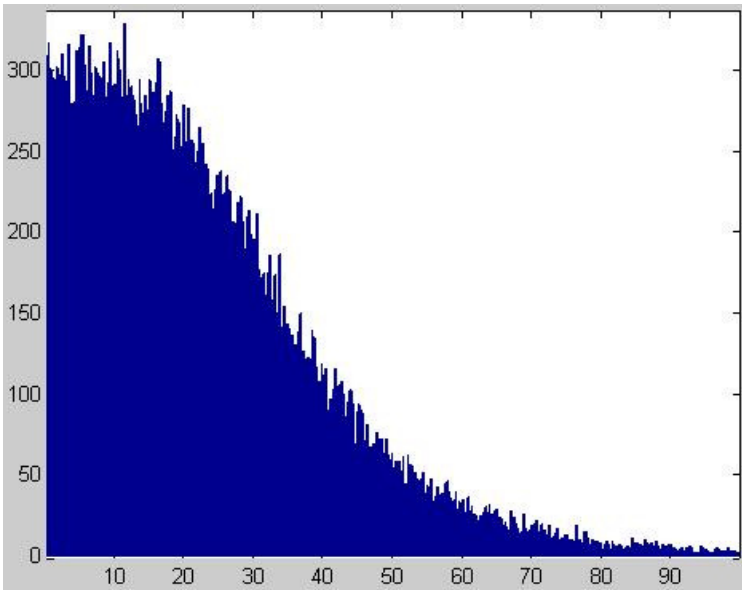
300
250
200
150
100
50
0
10
20
30
40
50
60
70
80
90

# Copyright Permission

| | | | |
|---|---|---|---|
| From: | Jason Lerch [jason@phenogenomics.ca] | Sent: | Sat 6/19/2010 10:38 AM |
| To: | Rajagopalan, Venkateswaran | | |
| Cc: | | | |
| Subject: | Re: Permission to use figures from your thesis proposal | | |
| Attachments: | | | |

Greetings,

no problem, of course, though one of the figures you mention actually comes from a book and is not my original.

Jason

On 10-06-17 12:28 PM, Rajagopalan, Venkateswaran wrote:

Dear Dr. Lerch,

I am in the process of writing my thesis. I am hoping that you would permit me to use the following figures from your thesis proposal

1) Figure 2.1 and 2.4 from your Thesis Proposal “Measuring cortical thickness” (file attached)

Please let me know if this is a possibility. I thank you for your kind consideration.

Regards
venkateswaran

==========

| | | | |
|---|---|---|---|
| From: | Bruce Fischl [fischl@nmr.mgh.harvard.edu] | Sent: | Thu 6/17/2010 12:15 PM |
| To: | Rajagopalan, Venkateswaran | | |
| Cc: | | | |
| Subject: | Re: Permission to use figures from manuscripts | | |
| Attachments: | | | |

sure, it's fine with me, although you may need to get approval from the
publishers for figures from papers.
On Thu, 17 Jun 2010, Rajagopalan,
Venkateswaran wrote:

> Dear Dr. Fischl,
>
>
>
> I am in the process of writing my thesis. I am hoping that you would permit me to use the following figures from your article and tutorial slides of freesurfer
>
>
>
> 1) Figure 1 from  Measuring the Thickness of the Human Cerebral Cortex from Magnetic Resonance Images <https://surfer.nmr.mgh.harvard.edu/ftp/articles/fischl00-cortical-thickness.pdf> , Fischl, B., and Dale, A.M., (2000). Proceedings of the National Academy of Sciences, 97:11044-11049.
>
>
>
> 2)  A Figure from your tutorial slides (file attached) tutorial topic "Introduction to Freesurfer"
>
> Please let me know if this is a possibility. I thank you for your kind consideration.
>
>
>
> Regards
>
> venkateswaran

| | | | |
|---|---|---|---|
| From: | PNAS Permissions [PNASPermissions@nas.edu] | Sent: | Thu 6/24/2010 2:37 PM |
| To: | Rajagopalan, Venkateswaran | | |
| Cc: | | | |
| Subject: | RE: Permission to use figures from manuscript | | |
| Attachments: | | | |

Dear Venkateswaran,

Permission is granted for your use of the figure as described in your message below. Please cite the full journal references and "Copyright (2000) National Academy of Sciences, U.S.A."

Please let us know if you have any questions.

Thank you!

Best regards,
Kelly Gerrity for
Diane Sullenberger
Executive Editor
PNAS

**From:** Rajagopalan, Venkateswaran [mailto:rajagov2@ccf.org]
**Sent:** Thursday, June 17, 2010 12:41 PM
**To:** PNAS Permissions; PNAS
**Subject:** Permission to use figures from manuscript

Dear Sir/Madam,

I am in the process of writing my thesis. I am hoping that you would permit me to use the following figure from an article published in your conference

Figure 1 from *Measuring the Thickness of the Human Cerebral Cortex from Magnetic Resonance Images Fischl, B., and Dale, A.M., (2000). Proceedings of the National Academy of Sciences, 97:11044-11049.*

Please let me know if this is a possibility. I thank you for your kind consideration.

Thanks

Regards
venkateswaran

PS: For your kind information I obtained permission to use the figure from the author of this article. Please see below.